Aspects of BSM theories in the Early Universe



Hannah Tillim

Balliol College

University of Oxford

A thesis submitted for the degree of

Doctor of Philosophy

Trinity 2022

Abstract

The Standard Model (SM) of particle physics is a tremendously successful explanation of the nature we observe, both in Earth-based experiments and cosmological observations of the past history of the universe. However its failure to account for gravity, dark matter and dark energy, as well as for various hierarchy and naturalness problems, motivates the formulation and investigation of Beyond-the-Standard-Model (BSM) theories.

In this thesis we will first review the evidence for and current understanding of dark matter (DM), including the mechanisms of freeze-out and freeze-in, before discussing the idea of 'secluded' dark matter without non-gravitational interactions with the SM. This will form the motivation for chapter 2, where we consider the emission of such secluded DM from an early population of primordial black holes, and for chapter 3, where we present a new mechanism by which an initially underpopulated secluded DM population may account for the observed DM in the universe today.

We will also discuss the hypothetical axion particle, which arises from an elegant solution to one of the problems with the SM (the Strong CP problem), and its generalisation, the Axion-Like-Particle (ALP). We will also introduce the one-dimensional topological defects called cosmic strings, and show how they can arise from ALP fields. ALPs serve as a candidate DM particle, and, further, are expected to appear in great numbers in the 4-dimensional effective theories arising from string theory (ST), a multiplicity known as the 'string axiverse'. We shall review the foundations of ST with a focus on the creation of the string axiverse by the compactification of extra dimensions; finally in chapter 4 we construct global cosmic string solutions arising from string axiverse ALPs and analyse aspects of the resulting physics. In particular, we include the physically-crucial presence of a stabilising potential.

Statement of originality

This thesis is wholly the work of the author except where stated. No part of this thesis has been submitted for any other qualification. Chapters 2, 3 and 4 are based on collaborative work in, respectively:

Black Hole Genesis of Dark Matter (2018) *JCAP* 04, arXiv number 1712.07664, by O. Lennon, J. March-Russell, R. Petrossian-Byrne and H. Tillim,

Reproductive Freeze-In of Dark Matter (2020) *Phys.Rev.D* 102 8, arXiv number 2007.14688, by J. March-Russell, H. Tillim and S. West

On the Nature of Axiverse Cosmic Strings (2021), arXiv preprint number 2109.14637, by J. March-Russell and H. Tillim

Acknowledgements

First and forever, to my supervisors John March-Russell and Stephen West.

John, thank you for being my teacher. Your trademark mixture of crackling curiosity and profound insight is an inspiration. Your compassion is a gift. I hope to always live up to your projections.

I quite seriously would not be here without Stephen, the first to push me to tackle a problem beyond my limits and force me into growth, who spent untold hours giving me help with physics, academia and applications, not to mention valuable Star Trek discussions. You were a dedicated mentor and champion and finally a wonderful friend.

Olivier Lennon, you were a kind and enlightening voice in a crazy town. I will never cease to be amazed at your incisive perception and your bottomless well of empathy.

I want to thank Adam Keilthy, for always being at the end of a line when I had emergency mathematical questions, no matter how ill-posed. Thank you also for your excellent pep talks. The respect of a good mathematician is beyond rubies.

Callum Brodie, finest of travelling companions, thank you for the days, and the love, and the mountains.

At Balliol I was fortunate to meet some extraordinary people without whose friendship the time would have ground on indeed - thank you especially to Rebecca Duke, Milla Jackson, Thomas Hancock, Lois Ogunlana, Ingvild Comfort Hvinden, Natalie Hill, Søren Gammelgaard, Brett Parris, Angharad Jones-Buxton and my comrade-in-arms Rudin Petrossian-Byrne.

In the Beecroft, thanks go in particular to John Wheater and Ard Louis for helping me find the optimal path, and to Michelle Jose for her tireless competence and friendly aid from the moment I walked in as an intern all those years ago.

In Cape Town I was fortunate enough to be drawn into the circles of many kind and fascinating friends. Luke – I'd have been lost without your support and love. Thank you also for teaching me to play chess, for your expert driving and most of all for the summer days at the farm. Here's to the power and the glory.

Most importantly of all, thank you Mum and Fa for telling me I could go anywhere I wanted, and then helping me get there. I stand on your shoulders.

Contents

1 Introduction **1**

1.1 The Standard Model and Beyond . . . 1
1.2 The Standard Cosmological History . . . 3
1.3 Dark Matter . . . 7
1.3.1 Evidence . . . 7
1.3.2 Early universe thermodynamics . . . 10
1.3.3 Constraints on dark sectors . . . 13
1.3.4 Freeze-Out . . . 17
1.3.5 Freeze-In . . . 19
1.3.6 Secluded sectors . . . 20
1.4 Axions . . . 22
1.4.1 The Strong CP problem . . . 23
1.4.2 Axion-like particles . . . 24
1.5 Cosmic strings . . . 27
1.5.1 Axionic cosmic strings . . . 33
1.5.2 Phenomenology . . . 34
1.6 String theory phenomenology . . . 34
1.6.1 Axiverse strings . . . 46

2 Production of secluded sectors by Primordial Black Holes **48**

2.1 Introduction . . . 48
2.2 Dark Matter Yield . . . 49
2.2.1 Light Dark Matter . . . 51
2.2.2 Heavy Dark Matter . . . 53
2.3 Observational Constraints and Possible Signatures . . . 54
2.4 Comments, Generalisations, and Future Work . . . 58

3 Reproductive Freeze-In **63**
3.1 Introduction . . . 63
3.2 RFI Setup . . . 64
3.3 The Yield Equations . . . 67
3.4 Essential behaviours . . . 70
3.5 Phenomenology . . . 75
3.5.1 Observational constraints . . . 77
3.5.2 Damping scales . . . 78
3.5.3 Plots . . . 83
3.6 Remarks . . . 84

4 Axiverse strings **88**
4.1 Introduction . . . 88
4.2 Basics . . . 88
4.3 The axiverse string tension . . . 92
4.4 Gravity and the core . . . 93
4.5 General axiverse strings . . . 95
4.6 Phenomenology . . . 97

A Homology and cohomology **99**

Bibliography **106**

Chapter 1
Introduction

1.1 The Standard Model and Beyond

The Standard Model (SM) is the most comprehensive and robust explanation of our reality ever formulated. It comprises, in essence, a list of particles - quarks, leptons, gauge bosons and the Higgs boson - together with rules about how they interact with each other, all encoded in an expression called the SM Lagrangian, given[1] by:

$$\begin{aligned}\mathcal{L}_{\text{SM}} = &-\frac{1}{4}B_{\mu\nu}B^{\mu\nu} - \frac{1}{4}\text{tr}W_{\mu\nu}W^{\mu\nu} - \frac{1}{4}\text{tr}G_{\mu\nu}G^{\mu\nu} \\ &+ |D\phi|^2 + \mu^2|\phi|^2 - \lambda|\phi|^4 \\ &+ i\overline{L}_L \not{D} L_L + i\overline{e}_R \not{D} e_R - \lambda_e \overline{L}_L \phi e_R \\ &+ i\overline{Q}_L \not{D} Q_L + i\overline{u}_R \not{D} u_R + i\overline{d}_R \not{D} d_R - \lambda_d \overline{Q}_L \phi d_R - \lambda_u \overline{Q}_L (i\sigma_2 \phi^\dagger) u_R,\end{aligned} \tag{1.1}$$

where

- B, W and G are the field strengths of the electroweak and strong gauge bosons with the traces running over Lie algebra indices,
- ϕ is the Higgs doublet, with μ and λ its quadratic and quartic couplings,
- Q_L is a weak doublet of left-handed quarks, u_R and d_R are the singlet up-type and down-type quarks respectively; these should be understood to be summed over all generations,
- similarly for the lepton doublet L_L and the electron singlet e_R,
- $\lambda_{e,u,d}$ are the Yukawa couplings for leptons, up and down quarks respectively,

[1] Note that the expression given in eq. (1.1) depicts the state of affairs before electroweak symmetry breaking, when the (local) gauge group is $SU(3) \times SU(2)_L \times U(1)_Y$.

- $\not{D} = \gamma^\mu D_\mu$, and each covariant derivative operator $D_\mu = \partial_\mu + i \sum_j g_j A^j_\mu$, where the sum runs over all gauge fields in the representations appropriate to the field the operator acts on, with coupling g_j. In the $U(1)$ case this includes the charge of the field, while for $SU(2)$ and $SU(3)$ gauge fields, acting on doublets etc., the gauge field will take values in a matrix Lie algebra.

However, despite its staggering success, the SM falls short of a complete explanation in some very important respects, of which three (in order of appearance) are relevant to this thesis.

First, the SM fails to explain the observed density of dark matter in our Universe (see section 1.3); that is to say, dark matter cannot be composed entirely (or even mostly) of the matter contained in the SM.

Second, there are *hierarchy* or *naturalness problems*, such as the electroweak hierarchy and cosmological constant problems. These centre in various ways on the wide separation between fundamental scales (for example, the electroweak and Planck scales differ by 17 orders of magnitude) and on the sensitivity of quantum corrections to 'new physics' in the UV (high energy regime). Very related and often overlapping are 'small parameter problems', where a parameter is measured to be extremely small, with the SM providing no explanation for, or even producing calculations which violate its smallness[2]. In section 1.4 we examine a particular solution to small parameter problem, the *Strong CP problem*, and the particles (*axions*) which arise from it.

Third, it fails to say anything about gravity, accounting only for the electroweak and strong forces. Our current best-supported theory of gravity is General Relativity, which is a classical (non-quantum) theory. We certainly live in a gravitational and quantum world, thus we naturally demand that a complete description of nature will be one of quantum gravity. Attempts to introduce gravity into the SM lead to inconsistencies; leading alternative quantum gravity theories such as string theory rely on an entirely new high energy structure. In section 1.6 we provide a lightning tour of those aspects of string theory relevant to the phenomenology of interest to us.

Beyond the Standard Model (BSM) theories are those that try to provide a more complete description for the observed universe, either through straightforward extensions of the SM such as introducing additional fields or symmetries (e.g. supersymmetry, many

[2] A parameter whose quantum corrections are proportional to the parameter itself are said to be 'technically natural', in that, if the parameter starts small, its quantum corrections will also be small. This occurs when taking the parameter to zero enhances the symmetry of the system [1]. It may still fail to be 'natural' in the broader sense if there is no explanation for the original smallness.

dark matter models, axions), or by positing an entirely different structure (e.g. string theory), of which the SM is a low-energy effective theory.

In this introduction, we will present a review of the origin and attempts at resolving some of these questions. First, we will look at the history of the early universe and what it can tell us about DM, as well as some of the popular DM models. In chapters 2 and 3 we will investigate new models of DM production and evolution respectively.

We will next introduce two hypothetical objects: axion-like-particles and cosmic strings, as well as their marriage in the axionic cosmic string. Then we will present a brief account of string theory compactifications and their relation to axions and axionic cosmic strings. In chapter 4 we will examine these axionic cosmic strings arising from string theory in detail.

1.2 The Standard Cosmological History

A general universe can be flat or either positively or negatively curved. The amount of curvature is determined by the energy density of the universe, with the amount needed for a flat universe called the *critical density* ρ_c. We measure a universe which is flat to within a 2% error [2] - yet the amount of matter and radiation (both SM and DM) forms only about $0.25\rho_c$. The missing energy density is known as *dark energy*, vacuum energy or the *cosmological constant* Λ (for reasons mentioned below).

Figure 1.1 shows a schematic of the most widely-accepted history of a ΛCDM[3] universe with the major milestones indicated. As time evolves, the universe expands, and the rate of expansion also depends on the type of energy density that dominates the universe.

The metric of a flat[4], homogenous, isotropic expanding universe, as we measure ours to be within high accuracy at very large scales, is given by the Friedmann-Lemaître-Robertson-Walker (FLRW) metric with zero curvature:

$$ds^2 = dt^2 - a^2(t)\left\{dr^2 + r^2 d\Omega^2\right\}, \tag{1.2}$$

where $a(t)$ is the *scale factor*, a quantity that accounts for the expansion of the universe and its effect on distances and is determined by a differential equation depending on the energy densities of radiation, matter and vacuum energy, the *Friedmann equation*:

$$H(t)^2 \equiv \left(\frac{\dot{a}}{a}\right)^2 = \frac{8\pi}{3M_{\rm Pl}^2}\left(\rho_{\rm rad}(t) + \rho_{\rm m}(t) + \rho_\Lambda(t)\right), \tag{1.3}$$

[3] A ΛCDM universe is one with vacuum energy and cold dark matter (see section 1.3) in addition to SM matter and radiation components, and no curvature.

[4] We will assume a flat universe throughout this thesis.

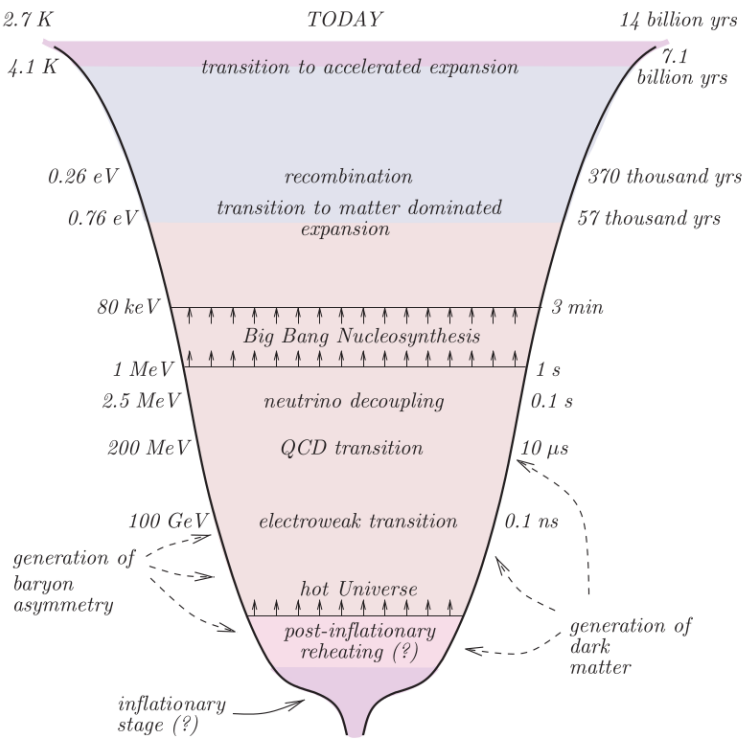


Figure 1.1: The story so far? Taken from [2]

where H is called the *Hubble parameter* and M_{Pl} is the Planck mass. In many epochs of the universe's history the total energy density was dominated by one form of energy or another. Because $\rho_{\text{rad}}, \rho_{\text{m}}$ and ρ_Λ all vary differently with time, the dependence of $\dot{a}/a$ on time (i.e. the acceleration of expansion) depends strongly on which element is dominant. A domination by matter or radiation (i.e. non-relativistic and relativistic particles respectively) cause the rate of expansion to decelerate, while domination by vacuum energy[5] causes expansion to accelerate. The rate of expansion today and into the past can be measured from the extent to which light emitted at a given time in the past - by a galaxy of a known distance away - is redshifted when it reaches Earth[6]. We see that in recent times we have entered a period of accelerated expansion, which is another (independent) argument for the existence of dark energy[7].

A quick review of cosmological highlights in chronological order follows.

[5] Λ has a constant energy density $\rho_\Lambda = \text{const}$. This means that its energy density doesn't decrease with universal expansion - it doesn't get diluted. We then have $\dot{a} \propto a$, so $a \sim \exp(\text{const} \times t)$.

[6] By the same token, measuring the redshift z of a galaxy tell us how long ago its light was emitted, given a model of the pattern of past expansion - this is known as the 'lookback time'. Redshift often serves as a clock in cosmology, reflecting as it does a physical measurement, since the conversion to actual time in seconds will depend on the expansion history and may thus change depending on the model.

[7] Additional sources of evidence for dark energy include effects on structure formation, CMB anisotropies and others [2].

Inflation: At very early times, it is widely thought the universe underwent a period of extreme accelerating expansion called *inflation*, driven by an 'inflaton' field, whose energy density dominated eq. (1.3) until a point known as 'reheating', at which point the various SM and non-SM sectors were injected with the inflaton's potential energy and heated to a high temperature. The inflationary paradigm was formulated to solve some major problems which otherwise exist in the standard history, in particular a series of initial value problems which ask why our universe today is so "large, warm, spatially flat and isotropic" [2]. Importantly for this thesis, inflation can be used to generate the Gaussian, near-scale-invariant spectrum of energy density perturbations that we require for correct structure formation (see the discussion below on structure formation in section 1.3.1). In addition, inflation can be used to explain the non-observance of inconvenient things like super-heavy GUT magnetic monopoles which might exist in the pre-inflationary epoch. Similarly, black hole relics and topological defects arising after pre-inflationary processes are diluted away sufficiently that we would not expect any in our observable universe.

Reheating: Inflation ends and the energy of the inflaton field is injected into the SM and DM sectors; in some scenarios there could be an intermediate stage where black holes form and then decay into the SM and DM - see chapter 2. In any case, SM and DM particles are created at some reheat temperature, $T_{RH} \gtrsim 3$ MeV (this lower limit is required for successful BBN, see below). However, in the standard story it is assumed that T_{RH} lies above all the known phase transitions - those of electroweak symmetry breaking (~ 100 GeV) as well as QCD confinement (~ 200 MeV). At this stage, the energy density of the universe is dominated by radiation.

Baryogenesis: One major unsolved cosmological problem is the predominance of matter over antimatter in our universe. It is thought that matter was initially produced with some small imbalance of baryons to antibaryons (perhaps 1 in $\sim 10^{-9}$); after matter-antimatter annihilation, the remaining balance formed the matter we observe today. However, the SM does not contain a mechanism to explain the original imbalance - to do so we require processes which violate baryon number, charge conjugation symmetry (C) and charge-conjugation-parity symmetry (CP), as well as some period of departure from thermal equilibrium (these are known as the Sakharov conditions [3]). The SM doesn't satisfy these conditions[8].

[8] At least, to the degree required.

Big Bang Nucleosynthesis (BBN): Around 1 MeV, temperatures fall below the binding energy of deuterium, and neutrons are captured into nuclei; nucleons also start teaming up into helium and lithium. The ratios of these elements is sensitive to the density of SM baryons in the universe at this time, as well as to the 'effective number of neutrino families'[9] N_{eff} (see section 1.3.3). BBN represents the earliest epoch of the universe we can probe with any confidence[10].

Matter-radiation equality: As the temperature of a given particle falls below its mass, it will become non-relativistic. The energy density of relativistic particles scales as $\rho_{\text{rad}} \sim 1/a^4$, while that of non-relativistic particles only goes as $\rho_{\text{m}} \sim 1/a^3$. At some point, the total energy density will become dominated by matter. This is measured to be at ~ 0.8 eV [2] by tracking the evolution of ρ_m and ρ_{rad} backwards in time and asking when they are equal. It is at this point that density perturbations in the DM - provided it is not too relativistic - can begin to grow quickly (see section 1.3.1)[11].

Recombination: Up to this point, the mean free path of photons is very short due to scattering off the sea of free electrons. Recombination begins after the temperature falls below the hydrogen binding energy, and electrons and protons can combine to form hydrogen nuclei without being immediately blasted apart by high-energy photons. In fact, due to the vastly greater number density of photons versus nucleons and leptons, even after the electron binding energy of ~ 10 eV is passed there are still sufficient numbers of photons at the high-energy tail of their distribution to ionize the nuclei, so that the recombination effectively took place in a slightly later epoch, at ~ 0.3 eV. Photons now have a chance to travel freely - many do, and are still travelling to this day, forming the Cosmic Microwave Background[12] (CMB), also known as the 'surface of last scattering'. The temperature of the CMB has been redshifted to about 2.7 K on average, but there are *CMB anisotropies* (variations) across the sky. By analysing the spectrum of these anisotropies, one can derive much information about the universe, including the ratio of the total energy density to the critical density, the fraction of that supplied by the various constituents (matter, radiation, vacuum energy) and the proportion of matter vested in baryons as opposed to

[9] As well as to many other things - for example, BBN tells us that the 'photon-to-baryon ratio' is very large, $\sim 10^{10}$.

[10] At least, by using SM measurements. Gravitational wave detection can allow us to probe earlier times, since the coupling of the metric to the radiation bath is so weak.

[11] Prior to this, although the DM does not interact much (or at all) with the SM, the curvature of the universe responds to and is smoothed out by SM radiation. Since the curvature tells the DM how to move, clumping is slow - though not static, there is a logarithmic growth - before matter-radiation equality.

[12] Universal expansion has redshifted them into the microwave region.

Parameter	WMAP value
Ratio of total energy density to critical density $\Omega = \rho_{\text{tot}}/\rho_c$	$0.71^{+0.04}_{-0.03}$
Matter density ratio $\Omega_m = \rho_m/\rho_c$	0.27 ± 0.04
Baryon density ratio $\Omega_b = \rho_b/\rho_c$	0.044 ± 0.004
Vacuum density ratio $\Omega_\Lambda = \rho_\Lambda/\rho_c$	0.73 ± 0.04

Table 1.1: Energy fractions today, found by the WMAP experiment for a ΛCDM model [4].

dark matter - see table 1.1. It is after recombination that the SM matter, freed from the radiation pressure of the photons, can fall into the gravitational wells of the DM and start to quickly form structure.

Vacuum energy domination: In recent (at redshift $z \sim 0.5$ [2]) times, the energy density of the universe has apparently become dominated by vacuum energy, leading to an accelerated expansion.

1.3 Dark Matter

It is now widely accepted that ∼ 85% of the matter content of the Universe is made up of a non-luminous component un-accounted for by Standard Model physics [5]. The name 'dark matter' (DM) is used to refer to matter content which does not emit or reflect sufficient photons to be visible to astronomical instruments on Earth. This could be as simple as a planet too far away to be measured with current telescopes but whose existence can be deduced from its effect on the orbits of other bodies (as was the case with Neptune), but today the phrase is usually meant to indicate non-SM particles. The identity and origin of dark matter is one of the greatest open questions in cosmology - even in all modern physics - but despite decades of model-building and experiment its nature remains obscure. A DM candidate must be cosmologically long-lived, cold (or possibly warm), with a dominant component(s) having mass(es) in the range: $10^{-22}\,\text{eV} \lesssim m_{\text{dm}} \lesssim 10^{68}\,\text{eV}$. Further, we know the DM has very weak interactions with the SM (if any); we also have upper bounds on its self-interaction strength (on which more below).

1.3.1 Evidence

The first indications that the universe was in fact mostly composed of non-luminous matter (as opposed to luminous stars) came as early as the 1920s, but a vast body of evidence

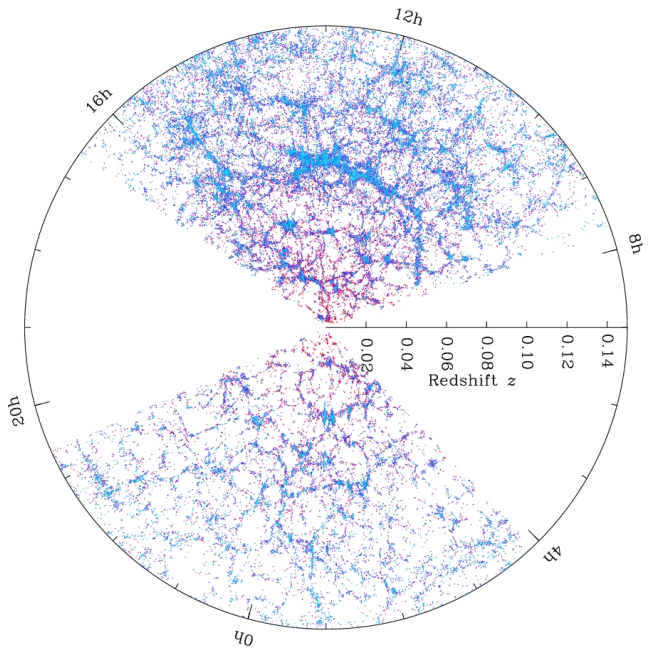


Figure 1.2: Map from the Sloane Digital Sky Survey showing the 'cosmic web' of galaxy clusters surrounding voids. At the centre is Earth, increasing radius corresponds to greater distance and further back in time, measured by the light's redshift z. Taken from [9]

(for an historical review see [6]) from widely different sources has accumulated in the years since, of which the following is an incomplete list.

Cluster velocities: In 1933 Fritz Zwicky [7], while measuring galactic orbital velocities in the Coma galaxy cluster, found them to be so high that the luminous mass was too small by a factor of 10 to hold the cluster together, and speculated that the cluster must contain a large amount of DM[13].

Galactic velocity curves: The velocity curve of a galaxy is a plot of the orbital velocities of stars about the galactic centre against their distance from the centre. In a spiral galaxy containing only luminous matter (concentrated in the central bulge) the velocity curve ought to follow a 'Keplerian' curve, dropping off with distance. Instead, it tends to a constant. In the 1960s and 70s, Vera Rubin made the most accurate measurements yet of spiral galaxy velocity curves [8], and found a non-Keplerian curve which was consistent with the majority of the galaxies' mass being vested in vast haloes of DM which dwarf the galactic discs.

[13] '*Dunkle Materie*'.

Structure formation: We live in a universe with a great deal of structure - that is to say, we are very far from being a homogeneous soup. This is obvious on the human, planetary and even galactic scale, however it wasn't until the 1970s [10–12] that it was realised that the arrangement of the galaxies themselves exhibits structure. Galaxies, galaxy clusters and superclusters are not randomly distributed, but instead adhere to vast cosmic filaments (see fig. 1.2) surrounding voids. While such patterns will naturally form from gravitational clustering, the amount of structure we observe today would require density perturbations at the time of recombination (when SM perturbations start to grow quickly) that were two orders of magnitude higher than those measured from the CMB [13]. This can be accounted for by a DM component which begins forming structures long before - the weak coupling of the DM to the SM means that perturbations will escape being slowed by radiation pressure before recombination, and they can start forming structures quickly from the time of matter-radiation equality. We still require some initial perturbations which are then amplified by gravitational clumping - this is a matter of initial conditions arising from, e.g. quantum fluctuations in the inflaton field. The DM is also required to be 'cold' (non-relativistic) or at the least 'warm' (semi-relativistic) at the time of structure formation commencement, since high velocities would allow particles to escape their mutual gravitational attraction and smear out the required perturbations on smaller scales. We present more quantitative constraints arising from structure formation in section 1.3.6.2.

Gravitational lensing: Photons travelling through the universe are bent by the gravitational curvature of large masses. We can use the amount of deviation to measure the amount of mass in a region, and gravitational lensing around galaxies shows much more mass than can be explained by their luminous matter. One spectacular example is that of the Bullet Cluster (see fig. 1.3) - two galaxy clusters in the process of colliding. We can use light and gravitational lensing to examine how various components of the galactic matter have been disrupted by the collision. Visible and X-ray measurements show the luminous stars have mostly passed undisturbed, but the interstellar gas which comprises most of the non-DM matter has experienced substantial slowing due to electromagnetic interactions. Turning to gravitational lensing, however, we can see large clumps of invisible mass have passed on relatively unscathed from the collision. This can be explained by each galaxy possessing a large DM halo, with halos having low enough interactions with each other and the other matter to be relatively unaffected by the collision [14]. This allows us to put an upper limit on the self-interaction strength of the DM, given in section 1.3.6.2.

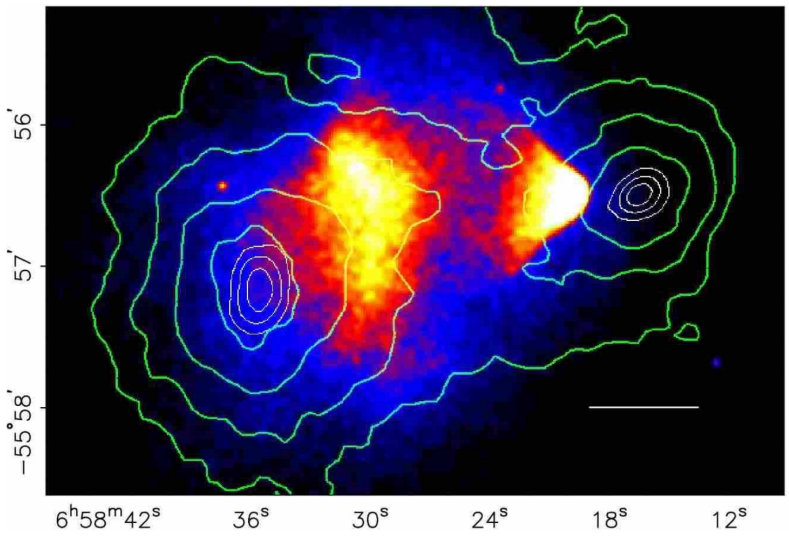


Figure 1.3: Image of the Bullet Cluster of colliding galaxy clusters, with the interstellar gas shown in false colour X-ray, and the contours of gravitational lensing indicating the position of the DM halos. Taken from [14].

The sources of evidence for DM mentioned above all involve no interaction other than gravity. For decades the dominant class of DM models has been that of the Weakly Interacting Massive Particle (WIMP) [15, 16]. In these models, there is some weak non-gravitational interaction between the SM and DM, whether through one of the known SM forces or some other medium, of sufficient size that WIMPs are produced in the early universe through thermal production from the SM (see the discussion of freeze-out in section 1.3.4). This would in principle allow measurements of the DM via its interactions with the SM - either in 'direct detection' experiments in Earth laboratories, or 'indirect detection' through cosmological and astrophysical observations. However, to date there have been no positive results of these types. The upshot of this is either to push the upper bound on DM-SM interaction strength lower and lower, and/or to shift the favoured mass ranges of the DM. Feebly Interacting Massive Particles (FIMPs) [17] are characterised by even lower non-gravitational interaction strengths with the SM, and are produced via the freeze-in mechanism (section 1.3.5). In section 1.3.6 we consider the possibility of a vanishing non-gravitational DM-SM interaction, which will form one of the main assumptions for the investigations in chapters 2 and 3.

1.3.2 Early universe thermodynamics

We want to constrain the parameter space of our DM models by comparing to the observational data described above. To do this, it is crucial to understand how the DM interacts

with itself and with the SM, and thereby how it influenced and was influenced by events in the early universe. The nature and strength of interaction couplings, as well as the DM mass and other fundamental parameters, will not only determine how much DM exists today, but also leave their imprint on structure formation, BBN, CMB and other observations.

We assume in this introduction and in chapter 3 that all particles follow a thermal distribution, i.e. that the number of particles per infinitesimal volume of momentum space is given (at least in a homogeneous and isotropic background) by the Bose-Einstein/Fermi-Dirac distribution

$$f(E,t) = \frac{e^{\mu/T}}{e^{E/T} \pm e^{\mu/T}}, \tag{1.4}$$

where $E^2 = m^2 + |\mathbf{p}|^2$, T is the temperature, μ is the *chemical potential* and $+1$ (-1) applies to fermions (bosons). A species whose distribution follows eq. (1.4) is said to be in *kinetic equilibrium* - in particular, it has a well-defined temperature[14]. The distributions above maximise the system entropy for a fixed total energy and particle number. Given a box of particles with random momenta not following a thermal distribution, and thus an ill-defined temperature, their elastic interactions will exchange momenta in such a way as to drive the system towards kinetic equilibrium, increasing the entropy of the system.

An important fact to reiterate here is that, as the universe expands and the scale factor a increases, the temperature T of a given species will (in the absence of interactions) go down. For relativistic particles, the relationship is $T \sim 1/a$, while for non-relativistic it is $T \sim 1/a^2$.

For a collection of particles $\{S_i\}$ with chemical potentials $\{\mu_i\}$, given any process $\sum_{\text{in}} S_i \rightarrow \sum_{\text{out}} S_j$, if the system is in *chemical equilibrium* then we will have $\sum_{\text{in}} \mu_i = \sum_{\text{out}} \mu_j$. For a species χ which has efficient number-changing interactions with itself, for example $\chi\chi \rightarrow \chi\chi\chi$, this implies $\mu_\chi = 0$. Therefore in this scenario μ is a measure of how far the system is away from chemical equilibrium. While kinetic equilibrium is associated with distribution of momenta, chemical equilibrium is associated with particle number. For a given temperature, there is some maximally entropic number of particles, and, if inelastic (number-changing) interactions are possible[15], they will occur in such a way as to drive the system towards that number, either via creation (when initially underpopulated, $\mu < 0$) or annihilation (when overpopulated, $\mu > 0$) of particles. When the number is reached, $\mu = 0$ and the particle is in chemical equilibrium.

[14] In the sense that a temperature is defined as the quantity which enters eq. (1.4) such that the distribution is correct.

[15] Note that for particles with particle-antiparticle asymmetry, μ-changing processes are C-violating, as they involve a net change in the number of particles without a corresponding increase in the number of antiparticles.

In general, the evolution of the particle species is determined by the *Boltzmann equation*, whose illuminating expression is

$$L[f] = C[f]. \tag{1.5}$$

Here, L is called the Liouville operator; its action on our distribution function eq. (1.4) in a FLRW universe is given by

$$L[f] = E\frac{\partial f}{\partial t} - H|\mathbf{p}|^2\frac{\partial f}{\partial E}. \tag{1.6}$$

The RHS of eq. (1.5) is called the *collision operator*, and it accounts for the effects on momenta and particle number of all elastic and inelastic interactions the particle species in question may be involved in. If there are no interactions, the RHS is zero and the evolution is determined by universal expansion. If the particle is in full equilibrium, the collision operator also vanishes because the equal rates of forward and backwards processes cancel.

For the purposes of this thesis, we are not interested in the evolution of f directly, but rather of integrated quantities: the number density n and the energy density ρ,

$$\begin{aligned} n(t) &\equiv \frac{g}{(2\pi)^3}\int d^3p\ f(E,t) \\ \rho(t) &\equiv \frac{g}{(2\pi)^3}\int d^3p\ f(E,t)\ E, \end{aligned} \tag{1.7}$$

where g is the number of *internal degrees of freedom* of the particle species, including helicity/polarisation states and gauge charges such as colour. For example, an uncharged real scalar has $g = 1$; photons have two polarisations $g_\gamma = 2$, weak gauge bosons have $g_{W,Z} = 3$ polarisations, charged leptons have 2 helicity states $g_e = 2$ for example, as do their antiparticles $g_{\bar{e}} = 2$. Each neutrino has $g_{\nu_e} = 1$ because our universe only has left-handed neutrinos (and right-handed antineutrinos). An up quark has 2 helicity states and 3 colour states, $g_u = 6$ and the same for an anti-up quark, and so on.

We can obtain useful explicit expressions in certain limits (for particle species in equilibrium):

$$\begin{aligned} T \gg m, T \gg |\mu| :&\qquad n = qg\frac{\zeta(3)}{\pi^2}T^3, &&\qquad \rho = qg\frac{\pi^2}{30}T^4, \\ T \gg m, T \ll |\mu| :&\qquad n = \frac{g}{\pi^2}e^{\mu/T}T^3, &&\qquad \rho = \frac{3g}{\pi^2}e^{\mu/T}T^4, \\ T \ll m :&\qquad n = g\left(\frac{mT}{2\pi}\right)^{3/2} e^{-(m-\mu)/T}, &&\qquad \rho = mn, \end{aligned} \tag{1.8}$$

where $q = 1$ for bosons and $7/8$ for fermions. The $T \gg m, T \ll |\mu|$ case corresponds to the phase space distribution eq. (1.4) reducing to the Maxwell-Boltzmann form $e^{-(E-\mu)/T}$.

Note also the exponential suppression in the non-relativistic case, which we will explain in the course of discussing freeze-out below.

The 'thermal bath' refers to those particles which are in thermal equilibrium with the photons of the SM, and this defines what we call the SM temperature $T_{\rm sm}$ - it is really T_γ. In hot early times, the entirety of the SM is in thermal equilibrium with itself; this status quo is maintained by interactions. When forward and backward elastic interactions between photons and some other particle are equal, energy is redistributed so that both species maintain the same temperature - i.e. they are in kinetic equilibrium. However, as the universe expands, a particle species which was in thermal equilibrium can fall out, as the density decreases and the rates of certain processes become too inefficient to maintain equilibrium. This can occur for SM particles (e.g. neutrinos) or for dark sectors (see section 1.3.4).

1.3.3 Constraints on dark sectors

In the following we focus on a dark matter sector, which we shall assume for simplicity is composed of a single species called χ, initially relativistic and in kinetic equilibrium, with temperature $\tilde{T}$.

In DM model-building, the quantity usually tracked is the *yield* Y:

$$Y \equiv \frac{n_{\rm dm}}{s_{\rm tot}}, \tag{1.9}$$

where s is the the total *entropy density* of the universe. During the radiation-dominated era, this is expressed as

$$s_{\rm tot} = \frac{2\pi^2}{45} g_{*S} T_{\rm sm}^3, \tag{1.10}$$

where g_{*S} is a certain weighted sum over the relativistic degrees of freedom of the relativistic particles [16].

In the physical situations of interest to us - when the universe is dominated by relativistic SM states in thermal equilibrium[17] and $s_{\rm tot} \approx s_{\rm sm}$ - the yield enjoys independence of universal expansion. This is because $g_{*S} T_{\rm sm}^3$ will scale as $1/a^3$, which is precisely the diluting effect of volume expansion on the number density of any species. In this way the yield gives us a measure of the 'number density per comoving volume', where a comoving

[16] The analogous parameter for the energy density is g_*, discussed below. Both the total energy density and the total entropy density of the universe are dominated by relativistic species in our epochs of interest, hence the inclusion only of relativistic degrees of freedom. If a species is not in kinetic equilibrium, it also contributes but its expression in g_{*S} will be of more complicated form than simple weighting.

[17] Though not necessarily in thermal equilibrium with each other.

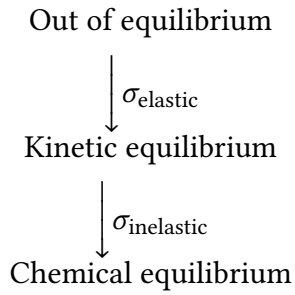


Figure 1.4: Possible evolution of a self-interacting sector initially out of equilibrium, in the case that elastic processes start out stronger than inelastic.

volume is to be thought of as a cube of space which expands purely with the scale factor. Variations in the yield are due entirely to the effects of number-changing interactions.

The *rate* Γ_P of a particular interaction P is the average number of such interactions taking place per unit time per unit volume, given by

$$\Gamma_P = n\langle\sigma_P v\rangle, \tag{1.11}$$

where n is the average number density of target particles in the universe, σ_P is the cross section for P, and the angular brackets indicate *thermal averaging* - i.e. averaged over a population of particles following a thermal distribution.

As mentioned previously, the relative efficiency of interactions vs universal expansion can change over time. A rough criterion is to compare Γ_P to the Hubble rate H. When

$$\Gamma_P \gg H, \tag{1.12}$$

the process P is considered 'efficient'. Broadly speaking, if SM-DM elastic processes (e.g. $P = \chi\gamma \to \chi\gamma$) are efficient, our particle species is in kinetic equilibrium with the SM; if elastic DM-DM processes (e.g. $P = \chi\chi \to \chi\chi$) are efficient, then it is at least in kinetic equilibrium with itself; if inelastic processes (e.g. $P = \chi\chi \to \gamma\gamma$ or $P = \chi\chi \to \chi\chi\chi$) are efficient, the species is in chemical equilibrium as well - see fig. 1.4. We shall see that whether or not a particle species is in kinetic or chemical equilibrium is extremely important for its own evolution and that of the universe as a whole.

However, interaction rates depend on number densities. As universal expansion continues, the number density decreases as $1/a^3$, until eventually a given particle is unlikely to pass close enough to others to induce an interaction. This occurs roughly when

$$\Gamma_P \sim H. \tag{1.13}$$

After this point, the yield will no longer change due to process P. Any model we describe needs to predict the correct density ratio of DM today $\Omega_{\rm dm}$, which can be expressed in terms of *relic abundance* Y_∞ (the abundance today, equal to the abundance after all number-changing interactions have ceased) and the DM mass:

$$Y_\infty m_{\rm dm} = 0.434 \text{ eV}. \tag{1.14}$$

This equivalent to $\Omega_{\rm dm} \approx 0.23$ (see table 1.1).

The minimal ΛCDM model assumes the DM is collisionless. However, though not necessitated by present observations it is entirely possible that there exist non-gravitational dark sector *self*-interactions, in the presence of which new phenomena can occur which may relieve a number of astrophysical or cosmological tensions [18–25]. The Bullet cluster itself imposes a limit of $\sigma_{\rm elas}/m_{\rm dm} \lesssim 1.25 \text{cm}^2/\text{g}$ [19], while mildly stronger constraints $\sigma_{\rm elas}/m_{\rm dm} \lesssim 0.5 \text{cm}^2/\text{g}$ arise from the other observations, including halo ellipticity [19,25–27], although there is in principle a considerable uncertainty in these limits [20–23, 27], with some claims that there exists positive evidence for DM self-interactions.

An important quantity which will enter our equations is the *effective number of relativistic degrees of freedom* g_*. This is defined as

$$g_* = \sum_{\substack{\text{relativistic} \\ \text{bosons}}} g_i \left(\frac{T_i}{T_{\rm sm}}\right)^4 + \frac{7}{8} \sum_{\substack{\text{relativistic} \\ \text{fermions}}} g_i \left(\frac{T_i}{T_{\rm sm}}\right)^4, \tag{1.15}$$

where the appearance of T_is accounts for the contributions of relativistic species with a thermal distribution at a different temperature than that of the thermal bath (i.e. the photons), such as neutrinos after they decouple from photons.

The importance of g_* is due to its correlation with the expansion rate during radiation domination. It appears in expressions for the total SM energy density

$$\rho_{\rm sm} = \frac{\pi^2}{30} g_* T_{\rm sm}^4, \tag{1.16}$$

where strictly speaking one should sum over all degrees of freedom, but in this epoch the sum is dominated by relativistic particles. As the temperature of the thermal bath falls, particle species become non-relativistic and their contribution to g_* drops out. This can also occur at phase transitions - for example, when quarks and gluons become confined at $T_{\rm sm} \approx 200$ MeV, the resultant nucleons (with masses ~ 1 GeV) are non-relativistic. In what follows, we assume the SM is initially relativistic and in full thermodynamic equilibrium with itself. This is usually a solid assumption at early times: relativistic temperatures are common in many reheating mechanisms like inflaton or black hole decay, and SM

couplings are so strong that they are likely to reach equilibrium rapidly after reheating [28].

Another source of constraints on the DM is the bounds on *dark radiation*. Since the expansion of the universe in the radiation-dominated era is driven by the amount of relativistic energy density, extra ('dark') relativistic degrees of freedom contributing to $\rho_{\rm rad}$ will have measurable effects. It is conventional to write this contribution to $\rho_{\rm rad}$ as a perturbation to N_ν, the number of neutrino families: $N_\nu^{\rm tot} = N_\nu^{\rm sm} + \Delta N_{\rm eff}$ and place constraints on $\Delta N_{\rm eff}$.

Explicitly, we have

$$\begin{aligned}
\rho_{\rm rad} &= \rho_{\rm sm} + \rho_{\rm dr} \\
&= \frac{\pi^2}{30} T_{\rm sm}^4 \left(g_{*,\rm sm} + g_{*,\rm sm} \frac{\rho_{\rm dr}}{\rho_{\rm sm}} \right) \\
&= \frac{\pi^2}{30} T_{\rm sm}^4 \left(\sum_{i \in {\rm SM}\setminus\nu} g_i \left(\frac{T_i}{T_{\rm sm}} \right)^4 + \frac{7}{8} (2 N_\nu^{\rm sm}) \left(\frac{T_\nu}{T_{\rm sm}} \right)^4 + g_{*,\rm sm} \frac{\rho_{\rm dr}}{\rho_{\rm sm}} \right) \\
&\equiv \frac{\pi^2}{30} T_{\rm sm}^4 \left(\sum_{i \in {\rm SM}\setminus\nu} g_i \left(\frac{T_i}{T_{\rm sm}} \right)^4 + \frac{7}{8} 2 (N_\nu^{\rm tot}) \left(\frac{T_\nu}{T_{\rm sm}} \right)^4 \right),
\end{aligned} \tag{1.17}$$

so

$$\Delta N_{\rm eff} = \frac{4}{7} g_{*,\rm sm} \left(\frac{T_{\rm sm}}{T_\nu} \right)^4 \frac{\rho_{\rm dr}}{\rho_{\rm sm}}. \tag{1.18}$$

After the neutrino thermally decouples from the photons, it has a different temperature, $T_\nu = (4/11)^{1/3} T_{\rm sm}$; the expression for $\Delta N_{\rm eff}$ is then

$$\Delta N_{\rm eff} = \frac{4}{7} \left(\frac{11}{4} \right)^{4/3} g_{*,\rm sm} \frac{\rho_{\rm dr}}{\rho_{\rm sm}}. \tag{1.19}$$

Around the time of BBN, of the SM particles only the photon, electron and neutrinos are relativistic, so $g_{*,\rm sm} = 10.75$. The value of $\rho_{\rm rad}$, and therefore the expansion rate, affects the temperature at which the processes which convert neutrons to protons become inefficient; this in turn affects the abundance of helium and deuterium, which can be measured. The precise bound depends on the details of one's model of cosmological history; in this thesis we use the rough bound drawn from [29]:

$$\Delta N_{\rm eff}(t_{\rm BBN}) < 0.1, \tag{1.20}$$

so we have the constraint

$$\frac{\rho_{\rm dr}(t_{\rm BBN})}{\rho_{\rm sm}(t_{\rm BBN})} \lesssim 0.004. \tag{1.21}$$

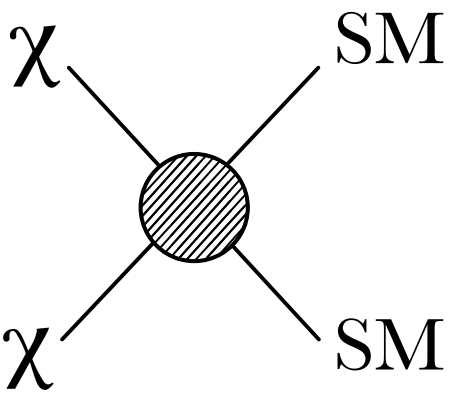


Figure 1.5: DM-SM interactions which help maintain thermal equilibrium.

Later on, at the time of CMB, $g_{*,\mathrm{sm}}$ receives contributions only from photons and neutrinos, $g_{*,\mathrm{sm}} = 3.36$. The bound we will use (from PLANCK2015 data [5]) is:

$$\Delta N_{\mathrm{eff}}(t_{\mathrm{CMB}}) < 0.3, \tag{1.22}$$

giving us

$$\frac{\rho_{\mathrm{dr}}(t_{\mathrm{CMB}})}{\rho_{\mathrm{sm}}(t_{\mathrm{CMB}})} \lesssim 0.05. \tag{1.23}$$

Dark radiation may be comprised of gravitons, non-SM relativistic particles, or a blend of different components.

Throughout this thesis, we are always assuming the non-SM *hidden sector* (i.e. excluding the graviton possibility) provides a small perturbation to the total energy density before matter-radiation equality, i.e.

$$r(t < t_{\mathrm{EQ}}) \equiv \frac{\rho_{\mathrm{dm}}(t)}{\rho_{\mathrm{sm}}(t)} \lesssim 0.1. \tag{1.24}$$

1.3.4 Freeze-Out

Consider the scenario in which the DM sector is initially in full equilibrium *with the SM* - there are efficient interactions (see fig. 1.5) between the two sectors, and they share a temperature - and relativistic. The yield passes through three phases, illustrated in fig. 1.6.

1. *Initially constant:* The number density follows the first expression in eq. (1.8). The yield will be constant, since both numerator and denominator have the same power of the same temperature.

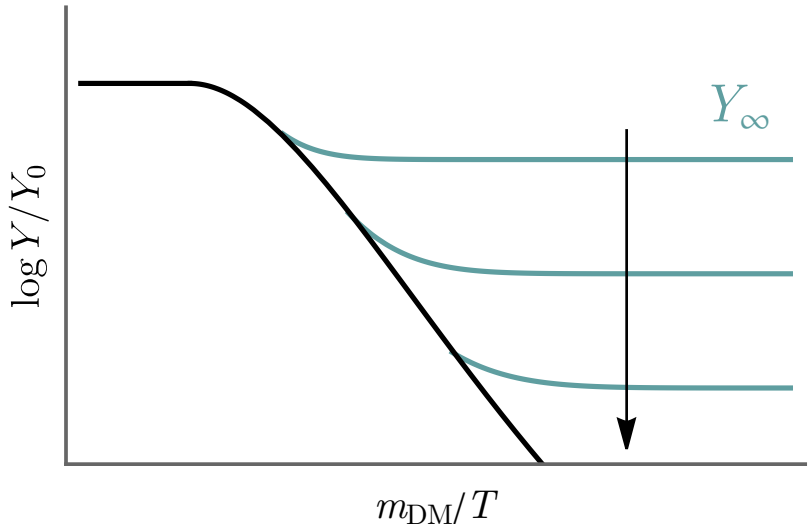


Figure 1.6: The evolution of the ratio of yield Y to initial yield Y_0 of a DM species initially in thermal equilibrium with the SM, undergoing freeze-out. The x-axis goes as $1/T$, increasing with time. The teal lines labelled Y_∞ denote possible values of the relic (final) abundance; the arrow indicates the effect on Y_∞ of increasing the DM-SM coupling.

2. *Exponential suppression:* The equilibrium number density of a non-relativistic particle species in thermal equilibrium is suppressed by the *Boltzmann factor* $e^{-(m-\mu)/T}$ (see eq. (1.8)).

3. *Freeze-Out:* Eventually, the number density becomes so low that even the DM-to-SM $\chi\chi \rightarrow$ SM processes that maintain equilibrium become inefficient at around eq. (1.13). The SM can no longer steal away χ particle number, and the number density of χs, out of equilibrium now, then scales only with universal expansion, so that Y is constant - we say the abundance *freezes out* and it is now known as the 'relic abundance'. Note from fig. 1.6 that the stronger the coupling between the DM and SM sectors, the longer they remain in thermal equilibrium after the DM goes non-relativistic, and the more exponential suppression takes place before freeze-out, leading to a lower relic abundance.

Freeze-out has probably been historically the most popular mechanism for explaining DM abundance [30, 31], and applies to dark sectors which have sufficiently strong couplings to the SM to be in thermal equilibrium at some point in the past, i.e. WIMPs.

An expression for the final yield will depend on the details of the dominant SM-DM interaction - in particular, whether the interaction is 's-wave' (angular momentum $l = 0$) or 'p-wave' ($l = 1$). For example, for fermionic DM going to a scalar, one would expect p-wave to dominate. The thermally-averaged $\langle\sigma v\rangle$ that enters the interaction rate in

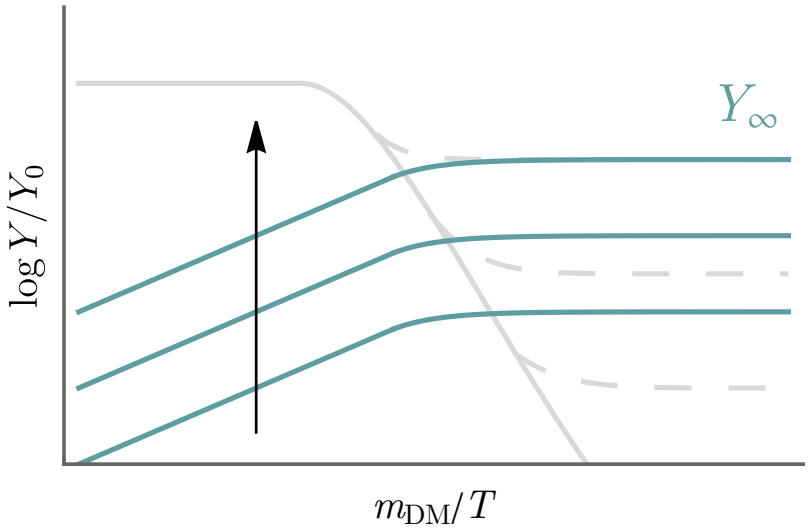


Figure 1.7: The evolution of the yield of a DM species beginning with negligible yield and thermally decoupled from the SM, undergoing freeze-in (teal lines). In gray the freeze-out evolution is shown for comparison. The arrow indicates the effect on Y_∞ of increasing the DM-SM coupling.

eq. (1.11) is expanded as $\langle\sigma v\rangle \equiv \sigma_0 x^{-l}$, where $x \equiv T/m_{\rm dm}$. The relic abundance in this parameterisation[18] is [13]

$$Y_\infty^{FO} m_{\rm dm} = \frac{3.79(l+1)x_f^{l+1}}{(g_{*S}/g_*^{1/2})M_{\rm Pl}\sigma_0}, \tag{1.25}$$

where $x_f \equiv m_{\rm dm}/T_f$, T_f is the temperature at freeze-out and σ_0 is a prefactor encoding the details of the interaction. For $m_{\rm dm}$ of order of the electroweak scale, the correct relic abundance is reproduced for a typical weak-type interaction cross-section $\sigma \sim G_F^2 T^2$ (where G_F is the Fermi constant). This is known as the *WIMP miracle*, and made a compelling case for WIMPs before experiments ruled out electroweak-scale DM [32].

1.3.5 Freeze-In

An alternative mechanism was put forth in [17] which applies to FIMPs; in this scenario the DM begins thermally decoupled from the SM and with a low yield, which then rises due to particle production from the SM.

1. *Initial conditions:* The DM is assumed to be out of thermal equilibrium with the SM, and with a negligible yield[19].

[18] Assuming a single dominant interaction channel.
[19] Due for example to exponential dilution of any initial population by inflation.

2. *Freeze-In:* Some production of χ takes place through the feeble interaction with the SM; for renormalisable interactions, production is most efficient when $T \lesssim m$.

3. *Die-off:* The temperature of the SM, redshifted by universal expansion, passes through the mass threshold of the DM and makes these feeble interactions kinetically forbidden.

In contrast to freeze-out, here the yield starts low and increases, and the relic abundance goes up with increasing interaction strength - see fig. 1.7. The details again depend on the interaction type, which could be $2 \longrightarrow 2$, $1 \longrightarrow 2$ and so on; for example, DM frozen-in from the decay process $B \longrightarrow \chi\chi$, with rate Γ_B, where B is a particle of the thermal bath with mass m_B, has a relic abundance which goes like

$$Y_\infty^{FI} m_{\rm dm} \sim \frac{M_{\rm Pl}\Gamma_B m_{\rm dm}}{m_B^2} \tag{1.26}$$

where λ is a dimensionless coupling entering the dominant interaction cross-section. All freeze-in situations share the quality that the relic abundance increases with increased interaction strength.

1.3.6 Secluded sectors

As discussed, we so far have no indication that the DM has any non-gravitational interactions with the SM. In this thesis we will be interested in the case where those interactions are absent - sometimes referred to as the 'secluded sector' scenario. The DM therefore cannot be produced in either the freeze-out or freeze-in mechanisms, neither can it ever be in thermal equilibrium with the SM. Instead, it may arise directly from inflaton reheating, or from purely gravitational production mechanisms, such as black hole evaporation or gravitational production from the SM via graviton exchange.

In chapter 2 we will consider a purely-gravitational production mechanism - Hawking radiation from a population of primordial black holes. Then in chapter 3 we will examine the subsequent evolution of a secluded sector with self-interactions.

1.3.6.1 Production from primordial black holes

It has long been thought that processes in the early Universe could have formed a population of primordial black holes (PBHs) [33] - for example from the relativistic collision of early domain walls, or overdense inflaton-induced density perturbations. By Hawking's

famous result [34], these PBHs emit[20] all states (due to gravitational universality) and, if they are sufficiently small, can completely evaporate in the early Universe, contributing to the primordial radiation density. As a subcomponent of this Hawking radiation will necessarily be the DM particles, PBHs can source some, or all, of the DM relic abundance. For earlier work in this direction, see [35–39].

In this thesis we consider Hawking evaporation of a single, Schwarzschild black hole (BH), motivated by the fact that BHs with charge and angular momentum very quickly radiate these away (e.g., [40]). The instantaneous temperature of a BH of mass M is given in gravitational natural units ($\hbar = c = k_{\rm B} = 1$) by an inverse relationship with its mass [34]:

$$T_{\rm BH} = \frac{M_{\rm Pl}^2}{8\pi M}. \tag{1.27}$$

For highly relativistic final states (which will be our case of interest in chapter 2), the rate of BH mass-loss due to emission of state i of spin s, degrees of freedom $g_{s,i}$ is [41]

$$\frac{\partial M}{\partial t} = -\frac{M_{\rm Pl}^4}{M^2} e_{s,i} g_{s,i}, \tag{1.28}$$

where $e_{s,i}$ are dimensionless grey-body 'power-factors', discussed in chapter 2.

For solar mass black holes, the rate of energy loss is tiny, and leads to a BH lifetime larger than the age of the universe - however, for very small BHs the rate can be substantial, and accelerates exponentially as M approaches $M_{\rm Pl}$. At $M \sim M_{\rm Pl}$, Hawking's calculation breaks down - we are now in the realm where a full quantum gravity calculation is needed - and it is not known for certain what the ultimate end of the PBHs are - they may continue to evaporate to extinction, as we assume in our work. On the other hand, they may leave behind stable relics which can cause tension with observations if too high in number, but which have also been proposed as a candidate for dark matter (see for e.g. [42]).

Concretely, the emission rate of a species i of spin s, and mass μ, and with energy in a range $(\omega, \omega + {\rm d}\omega)$ from a BH with temperature T is [41]

$${\rm d}\left(\frac{{\rm d}N_{s,i}}{{\rm d}t}\right) = \sum_{\ell,h} \frac{(2\ell+1)}{2\pi} \frac{\Gamma_{i,s,\ell,h}(\omega)}{\exp(\omega/T(t)) + (-1)^{(2s+1)}} {\rm d}\omega, \tag{1.29}$$

where $N_{s,i}$ is the total particle number, ℓ is the spherical harmonic, h the helicity or polarisation of the emitted particle, and $\Gamma_{i,s,\ell,h}(\omega)$ is the absorption probability for that mode, which encodes the grey-body factor.

In our chapter 2 we apply these formulae to a case of secluded sector DM.

[20] Hawking radiation is the process by which a BH transfers its mass energy into particle states outside the horizon, shrinking in size thereby.

1.3.6.2 Damping scales

Recall that one of our original motivations for the existence of DM was that it should form the seeds of structure in the early universe. In particular, the DM cannot be too relativistic ('hot') at the time structure formation begins, or it would have sufficient energy to overcome gravitational attraction, leading to density perturbations being 'smeared out' over large distances by the *free streaming* particles. In addition, in the presence of self-interactions, we must consider *collisional* or *diffusion damping*, which arises from elastic particle collisions, forcing clumps to expand just as a gas will diffuse into a box.

We characterise this smearing by a 'damping scale' l, indicating the scale over which perturbations have been smeared by time of matter-radiation equality t_{EQ}. In fact, the scales for free-streaming and collisional damping are uncorrelated and therefore are to be combined in quadrature [43] with the total damping length at t_{EQ} required to be less than ~ 100 kpc to compare favourably with numerical structure formation simulations [44, 45] i.e.:

$$l_{\mathrm{tot}} = \sqrt{l_c^2 + l_{\mathrm{FS}}^2} \lesssim 100 \text{ kpc}. \tag{1.30}$$

The length scale squared associated with collisional damping between particles of the same species, which is active until particle interactions become inefficient, is given by [46]

$$(l_c)^2 = \int_{t_0}^{t_{\mathrm{dec}}} \mathrm{d}t \frac{\langle v \rangle^2}{a^2 n \langle \sigma v \rangle}. \tag{1.31}$$

where v is the particle velocity, σ is the relevant self-interaction cross-section, the brackets indicate thermal averaging, t_0 is the time the diffusion begins, and t_{dec} is when the interactions decouple (become inefficient).

Provided the DM remains relativistic until after collisions become inefficient, the particles then free stream over some further length scale l_{FS}, given by

$$l_{\mathrm{FS}} = \int_{t_{\mathrm{dec}}}^{t_{\mathrm{EQ}}} \mathrm{d}t \frac{v}{a} = \int_{t_{\mathrm{dec}}}^{t_{\mathrm{EQ}}} \mathrm{d}t \frac{a_{\mathrm{dec}}}{a^2}. \tag{1.32}$$

1.4 Axions

Axions are theoretical light pseudoscalar particles which first appeared in a solution to the Strong CP problem of the SM, but have now been generalised to other scenarios and are an attractive DM candidate. For reviews see [13, 29, 47]. They also arise as a generic prediction of compactified string theories, which we will explore in section 1.6.

1.4.1 The Strong CP problem

The Strong CP problem refers to the lack of CP[21] violation in the strong (QCD) sector of the SM. Since we observe CP violation in the weak sector (for example in kaon decay [48]), we seek an explanation of why it is absent in the strong. Formally, there is a term in the QCD Lagrangian of the form

$$\mathcal{L} \supset \frac{g_s^2}{32\pi^2}\theta_0 F \wedge F = \frac{g_s^2}{32\pi^2}\theta_0 \epsilon^{\mu\nu\rho\sigma} F_{\mu\nu} F_{\rho\sigma}, \tag{1.33}$$

where F is the field strength of the gluon field $F = dA + A \wedge A$, g_s is the $SU(3)_{QCD}$ gauge coupling, θ_0 is some real parameter and a trace over $SU(3)$ generators is understood. This 'theta term' would lead to P- and CP-violating non-perturbative QCD processes[22] for nonzero θ; our current experiments (in particular the measurement of the neutron electic dipole moment [49]) put $\theta_0 < 10^{-10}$ [29] but we lack a natural explanation for its smallness.

In fact, the situation is even worse than that just described - it turns out that there is an additional contribution to the QCD Lagrangian of the same form as eq. (1.33) arising from the phases of quark masses, which are encoded in a matrix M_q; rotating these away by chiral rotations to give real quark masses produces a second term in the Lagrangian of the form of eq. (1.34). We therefore have an effective theta term

$$\theta = \theta_0 + \arg\det M_q. \tag{1.35}$$

It is this θ which is measured to be $< 10^{-10}$. It defies the imagination that these two terms should cancel so exactly as to render $\theta < 10^{-10}$ since their origins within the SM are completely unrelated.

The Peccei-Quinn solution [50] to this problem involves introducing a new global symmetry $U(1)_{PQ}$ under which the SM quarks transform axially. This symmetry is both spontaneously broken and anomalous, the latter due to QCD instanton effects. We write the field which leads to the spontaneous breaking as $\Phi(x) = |\Phi| e^{ia(x)/f_a}$, such that, after spontaneous symmetry breaking (SSB), $\langle|\Phi(x)|\rangle = f_a/\sqrt{2}$, where f_a is the SSB scale and is known as the *axion decay constant*[23]. We find:

[21] C: charge conjugation; P: parity/spatial inversion.

[22] The theta term is a total derivative:

$$\epsilon^{\mu\nu\rho\sigma} F_{\mu\nu} F_{\rho\sigma} = \partial^\mu \left(\epsilon_{\mu\nu\alpha\beta} A^\nu (F^{\alpha\beta} + \frac{1}{3} i g A^\alpha A^\beta) \right), \tag{1.34}$$

and so will not alter the equations of motion or appear in perturbation theory - its existence will manifest purely in non-perturbative effects.

[23] The axion field $a(x)$ here should not be confused with the scale factor $a(t)$.

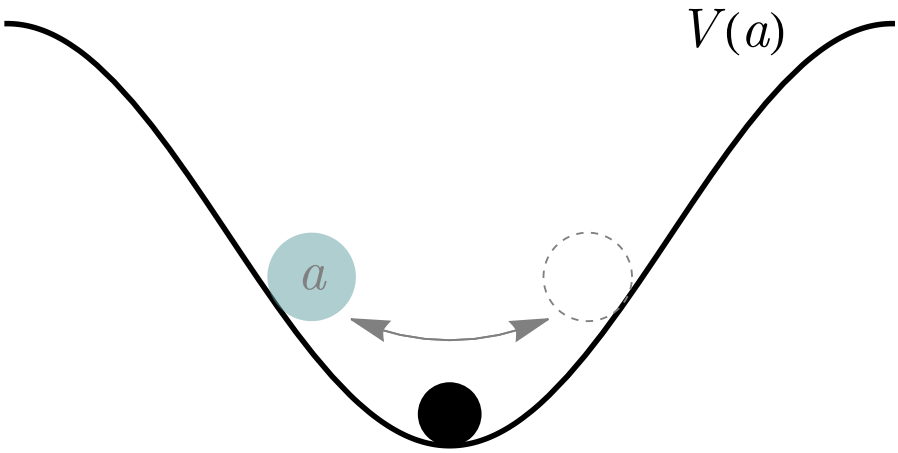


Figure 1.8: Potential for $a = (\overline{\theta} - \theta) f_a$ after QCD instanton effects. The axion a is the physical excitation around the minimum at $-\theta f_a$.

- A new $F \wedge F$ term in the Lagrangian is generated by the anomaly, effectively shifting

$$\theta \rightarrow \overline{\theta}(x) = \theta + \frac{a(x)}{f_a}. \tag{1.36}$$

- A potential is generated for the axion by QCD instantons, with a minimum at $\langle a \rangle = -\theta f_a$, so that the *vacuum expectation value* (vev) of the total coefficient of the CP-violating term vanishes, $\langle \overline{\theta} \rangle = 0$. This also gives the axion a mass m_a.

In this way Peccei and Quinn solved the Strong CP problem by making the total $\overline{\theta}$ dynamically driven to zero. The existence of $a(x)$ as the pseudo Nambu-Goldstone boson of the spontaneous symmetry breaking was in fact absent in the original paper, being pointed out by Wilczek and Weinberg later the same year [51, 52].

Strictly speaking, the axion is the excitation around $\langle a \rangle$ - see fig. 1.8. It's important to note that for the term $aF \wedge F$ to be parity-invariant, this excitation must be a pseudoscalar - it is the vacuum $\langle a \rangle$ which, being a number, is a scalar and therefore $\langle a \rangle F \wedge F$ is parity-violating, but this exactly cancels the parity-violation from $\theta F \wedge F$.

1.4.2 Axion-like particles

In general, a field $a(x)$ is called an *axion-like particle* (ALP) if it is a light pseudoscalar field with a continuous shift symmetry broken explicitly down to a discrete shift symmetry. Such fields usually arise as the angular part of an order parameter Φ that spontaneously breaks an anomalous global $U(1)$ symmetry. The SSB breaking scale is denoted f_a, the axion mass m_a. The effects of the anomalous breaking are considered to become important

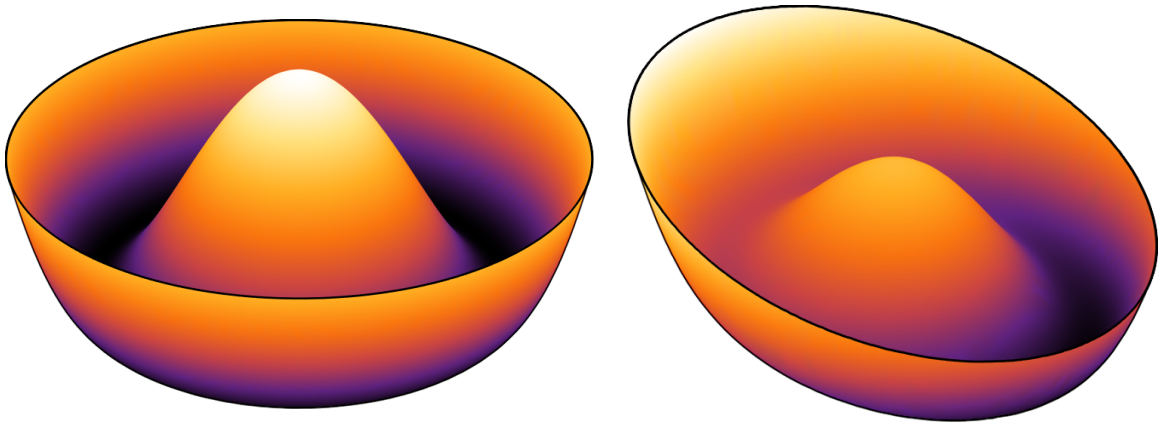


Figure 1.9: The 'Mexican hat' potential (eq. (1.40)) before (left) and after (right) explicit breaking, with the vacuum indicated by the darkest purple region.

at some scale[24] Λ and explicitly break the continuous shift symmetry down to $a(x) \to a(x) + 2\pi n$; the potential which is generated by the anomaly

$$V(a) \sim m_a^2 f_a^2 \left(1 - \cos\left(\frac{a}{f_a}\right)\right) \approx \frac{1}{2} m_a^2 a^2 + \dots \tag{1.37}$$

leads to the relationship

$$m_a \sim \frac{\Lambda^2}{f_a}. \tag{1.38}$$

Note that the middle expression of eq. (1.37) is correct if other non-perturbative effects are small, which is not true for the QCD axion or ALPs whose potential arises from QCD-like instantons - however, the final expression is always a valid approximation for small enough a (simply the parabolic local behaviour of any minimum).

Heuristically (see fig. 1.9), the spontaneous breaking produces the Mexican hat potential, which has a degenerate vacuum, and the explicit breaking tilts the hat, breaking the vacuum degeneracy and giving the angular mode a mass.

The particle solving the strong CP problem is the unique ALP with its mass set by $\Lambda = \Lambda_{QCD}$, strictly the name *axion* is reserved for this state, but in practice ALPs are usually referred to as axions, and the CP-problem-solving axion receives the backronym *QCD axion*.

In the case of the QCD axion, if it is to solve the Strong CP problem, the QCD contribution must dominate all sources of explicit breaking by $\gtrsim 10^{10}$ [53–55]. This *axion quality problem* is non-trivial in quantum gravity theories where there is strong evidence that global symmetries are necessarily explicitly broken [56–61].

[24] Not to be confused with vacuum energy.

Axion production mechanisms

Axions may be produced thermally from the SM in the freeze-out mechanism, but they also have access to two new non-thermal production processes - those of vacuum misalignment production and cosmic string decay.

Consider the universe at temperature $T \gg \Lambda$, the explicit breaking scale. The Mexican hat is untilted and the axion vev $\langle a \rangle$ has no favoured value. It can therefore select random values in different parts of the universe. Suppose SSB takes place before inflation, so that the vev is homogenised over the Hubble volume at $\langle \overline{\theta} \rangle \neq 0$. Turning on the axion potential and tilting the hat causes the axion to roll towards $\langle a \rangle = -\theta$; it will overshoot past its minimum and begin to oscillate coherently, corresponding to a condensate of axions at rest ('zero-modes').

If instead SSB takes place after inflation, a single Hubble patch can start with many different $\langle a \rangle$ domains, which can lead to axionic cosmic strings, domain walls and non-zero momentum modes. The non-zero modes also contribute non-relativistic energy density. The discussion of the third production mechanism, topological defect decay, we postpone until after our discussion on cosmic strings (section 1.5).

Axions as DM

Axions are attractive DM candidates. First, their tiny couplings to the SM satisfy the experimental upper bounds on DM-SM coupling. Second, the total axions produced by the active mechanisms discussed above can form the entirety of the DM, and are non-relativistic ('cold'), as is desirable.

Axion mass ranges

Models of QCD axion include a relation between the axion mass and its coupling to the photon. This is a source of powerful constraint on the QCD axion mass by observations of stellar cooling - while photons produced in a star take a long time to escape to the surface because of the high strength of electromagnetic scattering, if they could turn into axions these could much more easily stream out of the star, carrying away energy and reducing the stellar lifetime. Other mass limits on ALPs coupled to the SM come from searches at the LHC focusing on resonances from photon collisions and Higgs decays [62], cosmological requirements for BBN and ΔN_{eff}, and photon-to-axion conversion in the laboratory - for a review see [29]. While model-dependent, such ALP masses are expected to lie below $\sim 10\,\text{keV}$ - see fig. 1.10.

A very general ALP, which may be secluded from the SM entirely and only be subject to constraints arising from gravitational interactions, can have an almost unbounded mass. However, since the mass is set by the anomaly scale Λ, if the explicit breaking is too drastic the particle may be argued to cease to spiritually be axion-like. On the other end, we can bound the mass from below by a requirement that the axion field is dynamical by the present day (otherwise it is a static background of little phenomenological interest). The evolution of a (pseudo)scalar field in an expanding universe is governed by the differential equation

$$\ddot{a} + 3H\dot{a} = -\frac{\partial V}{\partial a} \approx -m_a^2 a + \ldots, \tag{1.39}$$

where the second term is sometimes called *Hubble friction* - when $H \gg m$, the system is overdamped and doesn't evolve. H was larger in the past than it is today. Since the system will only begin to oscillate around the potential minimum when the mass term becomes important, we require that $m_a \gtrsim H_0$, the value of the Hubble parameter today, which implies $m_a \gtrsim 10^{-33}$ eV for current evolution.

More important for us are the constraints which arise if we consider ALPs to form the majority of the DM. Requiring that the de Broglie wavelength is less than the size of dwarf galaxies we know to have DM halos puts a lower bound on the mass of $\sim 10^{-20}$ eV (if ALPs are 100% of the DM - the bound lowers for lower percentages demanded). We also have the fact that for masses greater than around an electron volt the nature of the axion changes from that of a classical wave-like oscillation to a particle-like model, which is hardly prohibitive but does alter the phenomenology.

1.5 Cosmic strings

A cosmic string is a one-dimensional topological defect which can arise during SSB, when the first homotopy group of the vacuum manifold is nontrivial - for reviews see [64, 65]. To understand why, we consider a simple case - that of a theory with a $U(1)$ symmetry broken when a complex scalar field $\Phi(x) = |\Phi(x)|e^{ia(x)/f}$ develops a nonzero expectation value at some scale f. This is modelled by the Mexican hat Lagrangian (see fig. 1.12):

$$\begin{aligned} \mathcal{L} &= (\partial_\mu \Phi)^\dagger \partial^\mu \Phi - V(|\Phi|) \\ V(|\Phi|) &= \lambda \left(|\Phi|^2 - \frac{f^2}{2} \right)^2, \end{aligned} \tag{1.40}$$

where λ is a dimensionless characterisation of the height of the potential at the origin, $V_{max} = \lambda f^4/4$, and $f/\sqrt{2}$ is the vev of $|\Phi|$ (its value in the valley of the Mexican hat)[25].

[25] The various numerical factors have been chosen so as to yield properly normalised kinetic terms for the local degrees of freedom in the true vacuum away from the string.

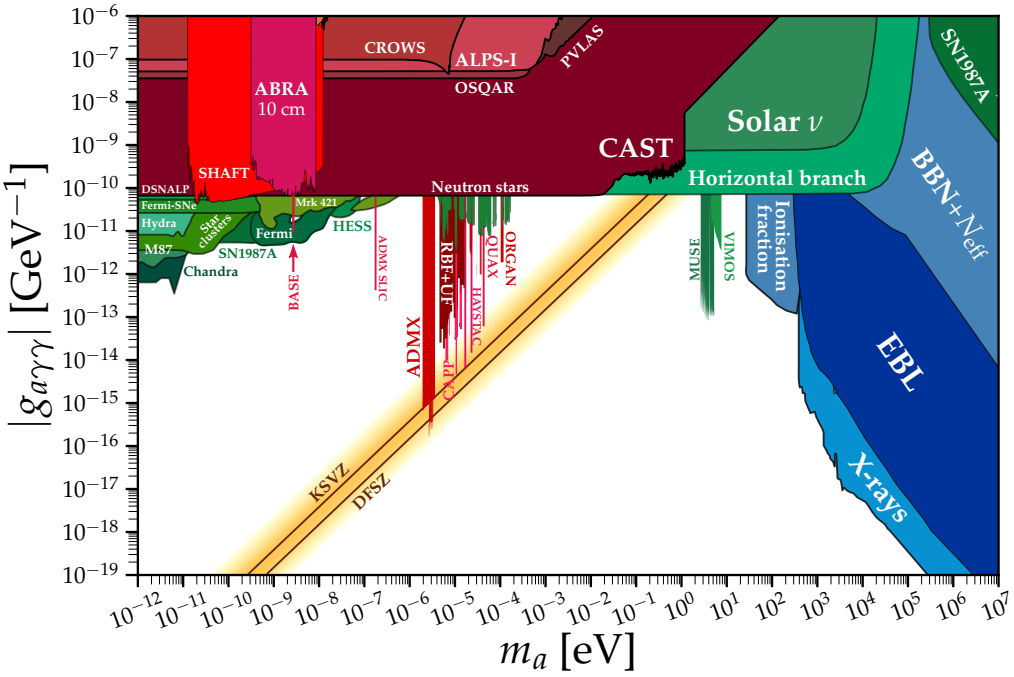


Figure 1.10: Current exclusion ranges for the axion mass, against the axion-photon coupling. The fuzzy orange line indicates the range of QCD axion models. Taken from [63].

Consider the $x-y$ plane, a two-dimensional slice of four-dimensional spacetime. In a configuration with a cosmic string at the origin, an observer with a field-o-meter walking around a closed curve γ encircling the origin at sufficient distance might measure the radial $|\Phi| = \langle\Phi\rangle$ at a constant value $f/\sqrt{2}$, and the angular field $a(x)$ varying from 0 to $2\pi w f$, with $w \in \mathbb{Z}$ called the *winding number*.

Recall that in the first (spontaneous) stage of symmetry breaking of $U(1)_{PQ}$, illustrated in fig. 1.9, the locus of Φ field values which remained in the vacuum (called the *vacuum manifold*) is a circle. Therefore what our observer is measuring is the map from a spatial S^1 to the field-space S^1 of vacuum configurations. Such a map is classified by its winding number, also known as the fundamental homotopy class of the circle, $\pi_1(S^1)$.

The first or fundamental homotopy group of a manifold characterises the possible inequivalent loops which may be embedded within it. More technically, we consider smooth maps from S^1 to a manifold M. Two maps $f_1, f_2 : S^1 \to M$ are said to be *homotopic* if they are 'smoothly deformable' into each other - that is, if there exists a smooth map $H : S^1 \times [0,1] \to M$ such that $H(\theta,0) = f_1(\theta), H(\theta,1) = f_2(\theta)$. Homotopy is an equivalence relation on curves whose equivalence classes form a group under concatenation of loops: $[\gamma] \circ [\gamma'] = [\gamma \circ \gamma']$. For example, consider the torus T^2. The first homotopy group $\pi_1(T^2) \cong \mathbb{Z} \times \mathbb{Z}$, each $\mathbb{Z}$ counting the number of times a curve winds around either the

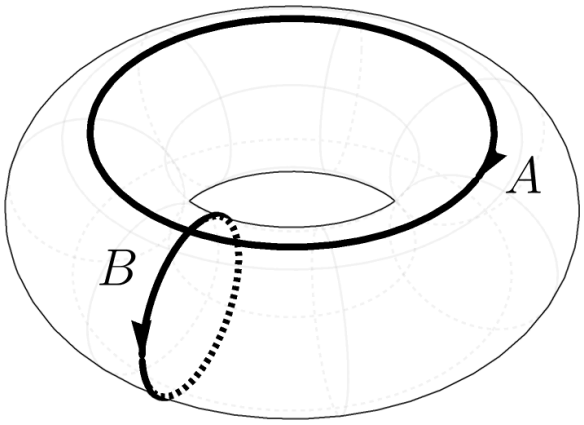


Figure 1.11: The 2-torus showing curves of homotopy classes $(0, 1)$ and $(1, 0)$.

handle or the equator of the doughnut's surface. A curve A which winds once around the equator (in equivalence class $(0, 1)$) cannot be smoothly deformed into a curve B in equivalence class $(1, 0)$, which winds once around the handle - see fig. 1.11. The concatenation of these two gives a curve which winds once around the equator and twice around the handle: $(0, 1) \circ (1, 0) = (1, 1)$.

We will be concerned here with $\pi_1(S_1) \cong \mathbb{Z}$ - the homotopy classes of maps $S^1 \to S^1$, which as mentioned are indexed by an integer, the winding number w; maps of different winding number cannot be smoothly deformed into each other (without cutting).

Now consider again our friend the observer treading the circle γ in the $x - y$ plane, concentric on the origin, and for the sake of argument take the $w = 1$ scenario. If the observer wanders over to the origin and takes a field reading, they will measure some value $\Phi(0)$. Let's assume at first that $\Phi(0)$ is in our vacuum manifold. Then it is a map from a spatial point (the origin) to a field space point ($\Phi(0)$). Viewing the origin as a zero-radius circle, you could see this as a winding number zero map - all points on the first 'circle' (i.e. the single point at the origin) are mapped to a single point on the second circle. However, if we consider a series of interpolating circles between γ and the origin, each slightly smaller than the last, we see that there is no smooth way to pass from a $w = 1$ to a $w = 0$ scenario - at least, not while remaining inside the vacuum manifold.

It is this final point that is crucial. What actually happens (for a theorist's definition of 'happens') is that, at some γ' of smaller radius than γ, the image of the field map starts to lift out of the vacuum and tighten on the centre - see fig. 1.12. At spatial zero, the field maps to field space zero. That means that there is some region close to the origin where the field has come out of its minimum energy configuration, forming a little lump of energy density, called the *core* of the cosmic string.

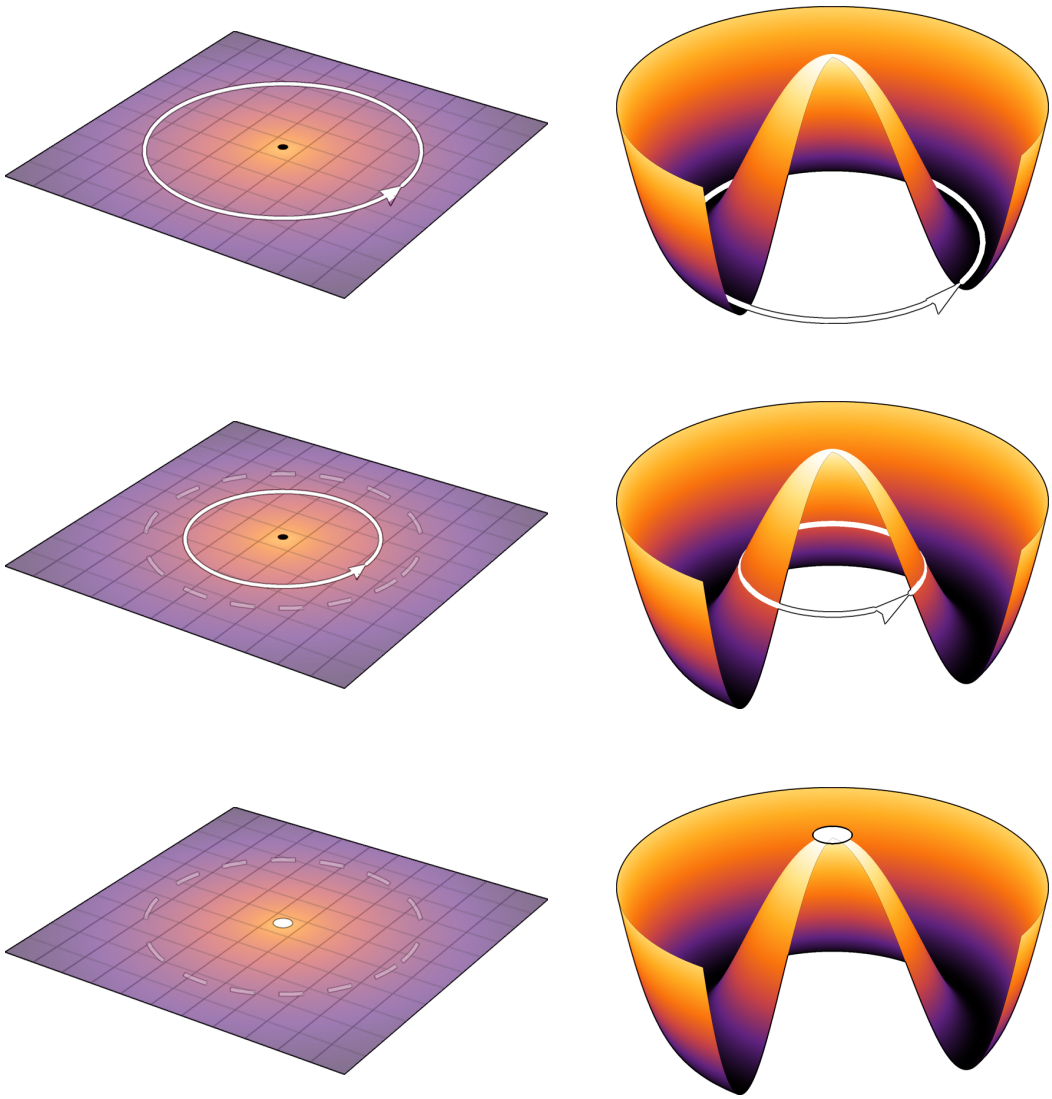


Figure 1.12: Map from the plane to field space for a $U(1)$ cosmic string of winding number $w = 1$.

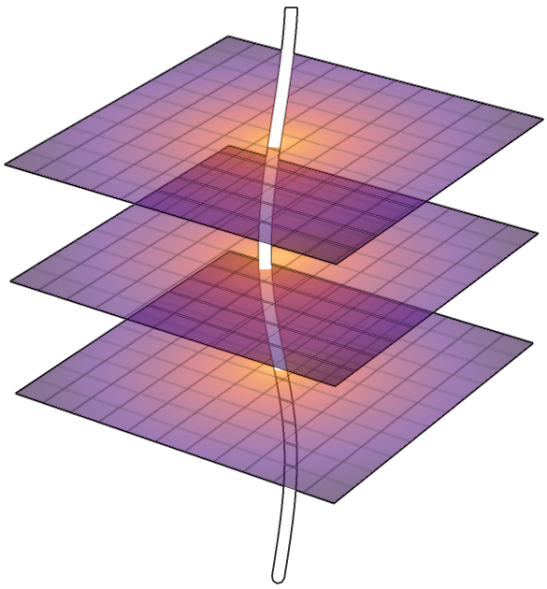


Figure 1.13: Stacking of spatial planes to create a cosmic string solution.

Finally we remember we were considering only a spatial slice, and stack the slices up again (fig. 1.13), so that the cores trace out a one-dimensional locus of energy density in three spatial dimensions - a string.

We believe that our universe underwent a series of phase transitions at early times. As Φ passes its phase transition, it may well select different equivalent vacuum values in different parts of space such that distinct regions meet in winding configurations - see fig. 1.14 - with a typical region size set by the correlation length of Φ; this is known as the Kibble-Zurek mechanism [66, 67]. Simulations (e.g. [68, 69]) generically predict the production of cosmic string networks which evolve dynamically, including annihilation events and the creation and decay of loops of string (see section 1.5.2).

The nature of a given cosmic string is set by the symmetry group G and the spectrum of states charged under it, including its anomalies and breaking. In particular, if G is a global symmetry, the energy per unit length (called the *tension* T) of the string configuration is logarithmically divergent. To see this, we consider the theory eq. (1.40) in the case that $a(x) = wf\theta$. The solution for $|\Phi(r)|$ generally requires numerical treatment, but for parametric estimates we can roughly approximate it by $\langle|\Phi(r < r_c)|\rangle = fr/(\sqrt{2}r_c)$, $\langle|\Phi(r > r_c)|\rangle = f/\sqrt{2}$, rising linearly from 0 to $f/\sqrt{2}$ over the interval $r \in (0, r_c)$, and a constant thereafter - this models the 'thick wall' limit, where the transition region is much

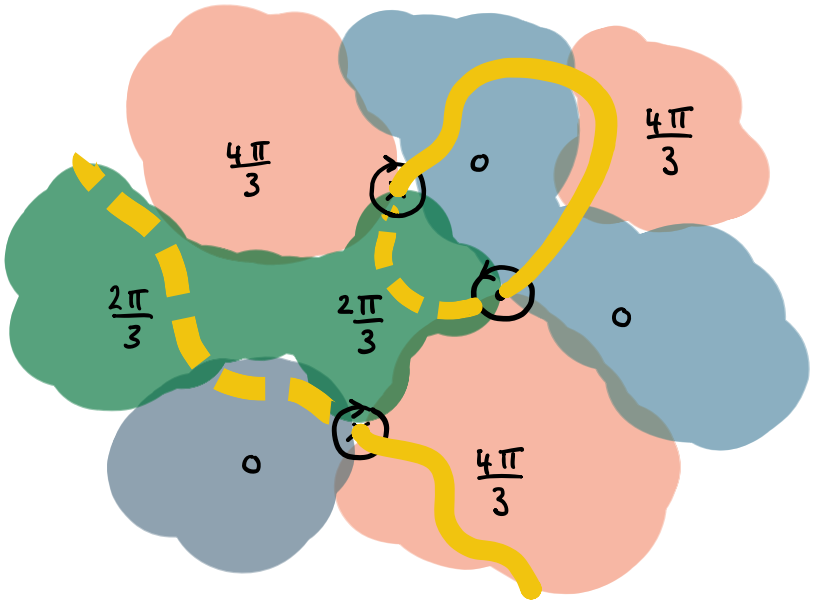


Figure 1.14: An axion field configuration in the plane containing several domains such that three vortex solutions occur - one with $w = 1$, two with $w = -1$. A possible cosmic string network which might penetrate the plane in such a way is shown in yellow.

larger than the region where $\langle|\Phi|\rangle = 0$. Then the tension is

$$\begin{aligned} T &= 2\pi \int_0^{r_c} dr\, r \left((\partial_r |\Phi|)^2 + \frac{1}{r^2} w^2 |\Phi|^2 + V(|\Phi|) \right) + \int_{r_c}^{L} \frac{1}{r^2} w^2 \langle|\Phi|\rangle^2 \\ &= \frac{\pi f^2}{2}(1 + w^2) + \frac{\pi}{3} V_{max} r_c^2 + \pi w^2 f^2 \log\left[\frac{L}{r_c}\right], \end{aligned} \tag{1.41}$$

where we have introduced a radial cutoff L. In physical scenarios there is a natural cutoff, given either by the inter-string distance within a network, or at worst by the Hubble distance; the realistic energy density is therefore finite[26]. The tension is minimised for a core radius

$$r_c \sim \frac{w}{f\sqrt{\lambda}}. \tag{1.42}$$

This result also holds in the 'thin wall' limit.

In contrast, if G is gauged, the associated gauge field will also display winding behaviour in step with the SSB order parameter Φ, such that the tension is finite at large r.

[26] It is also worth noting that the string core gives a finite contribution to the tension in the thin wall case.

1.5.1 Axionic cosmic strings

An *axionic cosmic string* is one in which G is an anomalous global $U(1)$ as described in section 1.4, spontaneously broken at scale f_a by the vev of $\Phi = |\Phi|e^{ia(x)/f_a}$, and the axion $a(x)$ the field which winds around the origin, forming the cosmic string. Because G is anomalous, the degeneracy of the vacuum is broken (i.e. the axion picks up a mass) and this leads to the presence of *domain walls* attached to the cosmic string. In this context, domain walls refer to a wall-like regions ending on the string with some associated wall tension.

To see why domain walls arise, consider again the two stages of the axion potential depicted in fig. 1.9. After SSB the vacuum is degenerate with $G/H \cong S^1$, and the axion field can fall into winding configurations via the Kibble-Zurek mechanism. Then at some lower scale Λ, the hat is tilted, breaking the degeneracy. However, the axion is already stuck in its winding configuration - it cannot simply unwind, it is forced to pass through the regions of non-minimum energy at some point around the spatial circle concentric on the origin. There is competition now between potential and gradient energy - the axion tries to minimise the time it spends out of the vacuum, without paying too high a kinetic cost by zipping across the hill overly quickly. The region out of the vacuum is the domain wall, and its thickness Δ is set by the relative sizes of the potential height ($\sim \Lambda^4$), and the axion decay constant, $\Delta \sim 1/m_a \sim f_a/\Lambda^2$.

Cosmic strings connected to domain walls are strictly unstable: there is again a competition between the bulk tension of the wall, which favours reduced wall volume, and a sort of inertia of the string that scales with the string tension and resists motion, a situation is somewhat akin to a soap bubble on a flexible wire. Domain walls essentially tug on their bounding strings, encouraging them to move and reduce the volume of the domain wall, eventually annihilating with the opposite boundary string. Given a stretch of domain wall, there is also a nonzero probability of a tunneling event in which a small loop of string is nucleated within the wall - however this is exponentially small unless the wall tension is very close to the string tension. The smaller loop can then expand until it annihilates with the original boundaries of the wall.

Despite this inherent instability, axionic cosmic strings can nevertheless be parametrically long-lived, with their lifetime set by the balance between the string and wall symmetry-breaking scales. The former is set by the scale f_a of SSB which first establishes the Mexican hat and the winding of the axion; the latter by the scale Λ of explicit breaking which tilts it - long life is associated with $f_a \gg \Lambda$. For non-QCD axions, Λ can be far below Λ_{QCD}, and cosmic strings can be present late in the cosmological history, perhaps even through

to the present. Since, as mentioned, in quantum gravity it is believed that all global symmetries are explicitly broken (see e.g. [70]), there may be no truly stable global cosmic strings, though there can be stable gauge strings.

We have here only considered the case where the tilted wine bottle potential has a single minimum - called the $N = 1$ scenario. In fact the axion potential can have multiple ($N > 1$) minima; this leads to each string being the meeting point of N domain walls. However, in this case the domain walls are stable, and their energy density comes to dominate the universe, leading to overclosure - though there are modifications which can alleviate this [71].

1.5.2 Phenomenology

String networks in general evolve dynamically and even in the absence of domain walls will decay: long pieces of string pinch off into loops which then oscillate, emitting their energy into gravitational waves and, in the axionic case, axions – this is a further production mechanism available to ALPs. At the same time, new strings keep entering the horizon. It is believed [64] that a string network without domain walls (with domain walls the evolution is substantially more complicated [71]) will eventually approach a *scaling regime*, after which their contribution to the comoving energy density will be a constant: $\Omega_{\text{string}} \sim T/M_{\text{Pl}}^2$. This can constrain the string tension to avoid overlarge energy density fraction: limits from the Planck collaboration [72] among others have $T/M_{\text{Pl}}^2 \lesssim 10^{-7}$. Networks of strings and domain walls are important for both relic axion DM production [73–77] and the generation of stochastic gravitational wave backgrounds [65, 78–81]. They can lead to a variety of other striking, potentially observable, phenomena [82–87].

The presence of a cosmic string at the origin distorts spacetime, such that away from the string core the metric is that of a conical spacetime with an r-dependent deficit angle and gravitational repulsion [88]:

$$ds^2 \simeq (1-k(r))(dt^2 - dx_3^2) - dr^2 - (1-2k(r))r^2 d\theta^2, \tag{1.43}$$

where $k(r) = 4T/M_{\text{Pl}}^2$. Such distortion leads to potentially-observable gravitational lensing.

1.6 String theory phenomenology

String theory (ST) is a theory of quantum gravity (probably our best-understood candidate) in which the fundamental objects in the simplest versions of ST are tiny one-dimensional strings. One example is that of bosonic ST, which contains only bosonic

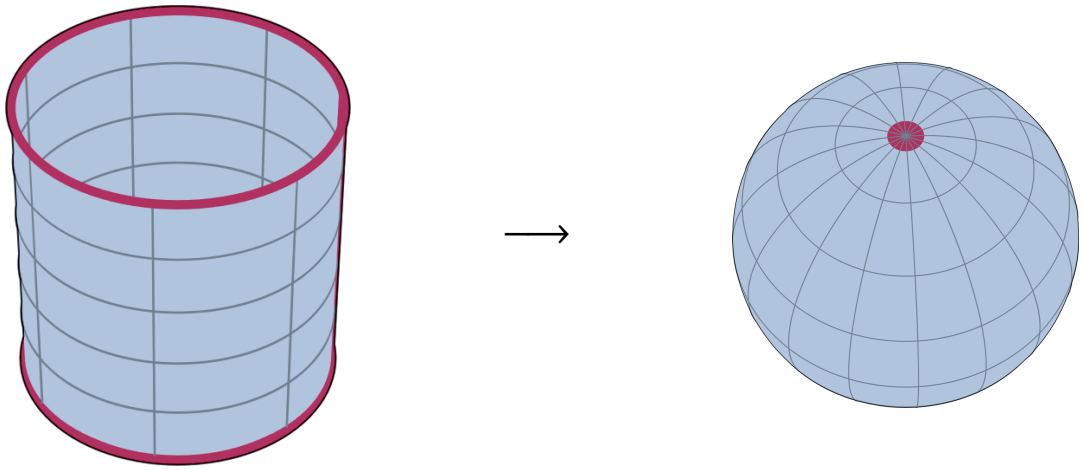


Figure 1.15: Conformal transformation of a cylinder to a Riemann sphere.

modes as the name implies. This ST leads to a tachyonic particle and so must be discarded - however it is often helpful to present in order to minimally illustrate some of the features of ST. Other types of string theory, which include fermionic modes, are Type I, II and heterotic - these all require supersymmetry (SUSY) at the perturbative string level and so are known as 'superstring theories'. We shall refer to the non-bosonic fundamental strings of ST as 'superstrings', to avoid any confusion with cosmic strings.

Bosonic strings can only consistently propagate[27] in 26 dimensions, superstrings in 10, and we shall assume we are starting with $d = 10$ here unless otherwise stated. The degrees of freedom in an uncompactified UV-complete string theory are the excitations of the superstring, relating both to centre-of-mass motion and vibration (as well as those of higher-dimensional objects called branes, discussed below). A one-dimensional string sweeps out a two-dimensional *worldsheet* in its ambient space. An alternative way to look at this is to express the spacetime coordinates of any point (σ, τ) on the worldsheet as a ten-dimensional field $X^i(\sigma, \tau)$, $i = 1, \ldots 10$ taking values in a *target space* (spacetime), whose harmonic oscillators are the modes of the string. This turns out to form a $2d$ conformal field theory on the worldsheet.

Calculating cross-sections in ST involves a *double expansion.* The first is topological - for closed string theories for example, the tree-level amplitude between two closed string states looks like a cylinder. The conformal symmetry of the theory allows us to shrink the two boundaries of the cylinder (the closed string insertions) to points (see fig. 1.15), making a 2-sphere. Performing this procedure at one loop, one finds a torus; at 2 loops, a 2-handled torus and so on. The 'loop expansion' of the string worldsheet is therefore a sum over topologies of different Euler characteristic χ – see fig. 1.16 – each with a weight

[27] The 'critical dimensions' quoted here come from requirements of anomaly cancellation.

of $g_s^{-\chi}$, where g_s is the string coupling constant[28]. On the other hand, the field theory on each worldsheet can have interactions (in the presence of nontrivial background fields), which are expanded in the parameter α'/R^2, where $\alpha' \simeq 2\pi M_s^2$ with M_s the string tension, and R a typical scale of variation of a spacetime field, for example the curvature scale of any compactified direction of our manifold. In what follows we will work purely to leading order in α'/R^2 - this implies low energies and compactification curvature radii that are not too small.

The supergravity

At lower energies[29] the superstring action gives rise to an effective theory called the'$10d$ supergravity'[30], whose degrees of freedom are various massless local fields. The bosonic field content generally includes a metric g, a dilaton ϕ, and some number of antisymmetric tensor fields; the number and type of these tensor fields depend on the type of string theory under consideration - see table 1.2. For example, all string theories but Type I come with the *Kalb-Ramond field* B_2, while Type I and II have *Ramond-Ramond fields* C_i of various degree.

For illustration, the bosonic ST (which requires 26 dimensions) has an effective action to leading order in α'

$$S_{26}^{\text{bos}} = \frac{1}{2\kappa}\int d^{26}x\sqrt{-\det g}e^{-2\phi}\left[\mathcal{R} - \frac{1}{2}|H_3|^2 + 4(\partial\phi)^2\right], \tag{1.44}$$

where H_3 is the field strength tensor of the B_2 field, κ is a constant $\kappa \sim \alpha'^6$, ϕ is the dilaton, g the 26-dimensional metric and $\mathcal{R}$ the Ricci scalar. The superstring theories will have a similar ($10d$) supergravity actions with extra bosonic terms for the other antisymmetric tensor fields, as well as fermionic fields.

We emphasise that everything in this thesis is discussed and calculated at the level of the leading order effective theory, not in the UV-complete full string theory.

Compactification

Of course, we observe rather fewer than 10 dimensions in our own experiments. The extra 6 dimensions are taken to be compact and very small to explain why we do not observe them. We will assume we live in a 10-dimensional manifold which decomposes as a direct

[28] g_s is related to the dilaton field ϕ, which we shall meet just below, by $g_s = e^{\langle\phi\rangle}$, $\langle\phi\rangle$ the vev of ϕ.

[29] I.e. at distances much larger than l_s, the string scale, which is the natural length scale inversely related to the superstring tension.

[30] The mapping of a full ST onto a supergravity action is a subtle business involving matching amplitudes.

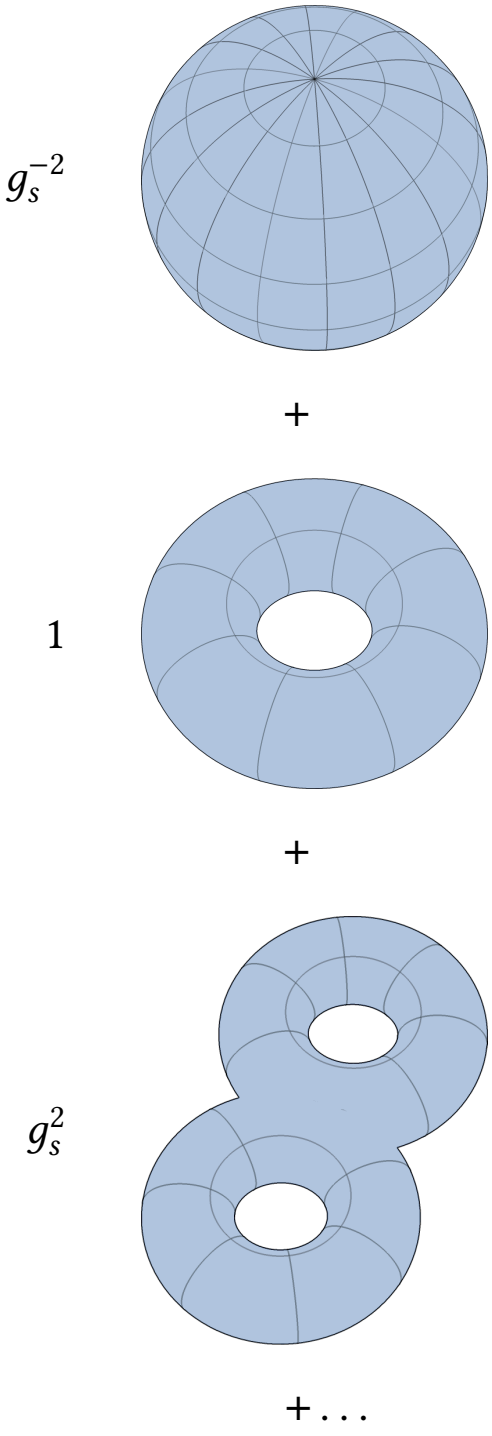


Figure 1.16: The diagrams of a genus expansion of a closed string amplitude to second 'loop' order, with their weighting $g_s^{-\chi}$.

Type	Tensor fields
Bosonic	B_2
Type I	C_2
Type IIA	B_2, C_1, C_3
Type IIB	B_2, C_0, C_2, C_4
Heterotic	B_2

Table 1.2: List of the massless antisymmetric tensor fields appearing in the low energy supergravity field theory of string theory, by Type; the subscript indicates the degree of the form.

product $X_{10} = M_4 \times X_6$, where M_4 is four-dimensional Minkowski space and X_6 is the compact manifold. The choice of X_6 affects the amount of SUSY which is preserved in 4 dimensions; for example, a six-torus T^6 preserves all SUSY[31]. It is usually desirable from a computational standpoint to preserve some SUSY, which for realistic models can then be broken by the insertion of branes (see below), fluxes and non-perturbative effects like instantons.

The amount of SUSY preserved by the compactification depends on the holonomy of the manifold - the transformation picked up by local operators when parallel transported around some loop. A general 6-dimensional manifold will have holonomy transformations in $SO(6)$, and this will break all supercharges; if the holonomy is instead restricted to a subgroup, some SUSY can be preserved. A Calabi-Yau N-fold is defined to be an N-complex-dimensional Kähler manifold[32] with vanishing first Chern class (which implies it is Ricci flat), and automatically has holonomy in $SU(N)$. In fact we will adopt the definition here that a CY has holonomy strictly equal to $SU(N)$, so that, for example, toroidal compactifications (which have trivial holonomy) are not classified as CY. Of particular interest to ST models are *Calabi-Yau threefolds*, to which we will frequently specialise in the examples below.

Toroidal compactifications break no supercharges; if instead X_6 is a CY threefold, the holonomy is $SU(3)$. There is also a unique 2-complex-dimensional CY called $K3$ with $SU(2)$ holonomy - we could then have $X_6 = T^2 \times K3$. Table 1.3 sets out the amount of lower-dimensional SUSY in each case.

In the full string theory after compactification, the momentum modes of the superstrings become quantised along the periodic dimensions; they are joined by 'winding

[31]The level of the supersymmetry, i.e. $\mathcal{N}$, is different however - for example, $\mathcal{N} = 1$ supersymmetry in 10 dimensions has 16 supercharges, while in 4 dimensions 16 unbroken supercharges corresponds to $\mathcal{N} = 4$.

[32]An N-complex-dimensional Kähler manifold is one whose holonomy does not mix holomorphic and antiholomorphic indices, so that the holonomy is at most $U(N)$.

Type	$D = 10$	$X_6 = T^6$	$T^2 \times K3$	$X_6 = CY$
Type I and heterotic	$\mathcal{N} = 1$	$\mathcal{N} = 4$	$\mathcal{N} = 2$	$\mathcal{N} = 1$
Type II	$\mathcal{N} = 2$	$\mathcal{N} = 8$	$\mathcal{N} = 4$	$\mathcal{N} = 2$

Table 1.3: The starting 10-dimensional supersymmetry for each Type against the amount of 4-dimensional supersymmetry after toroidal and CY compactification.

modes' which count how many times a superstring encircles a compact dimension. However, modes of nonzero winding number are extremely heavy[33] (for compactifications not too small) and so may be ignored in the effective field theory.

Superstrings are not the only extended objects which exist in string theories. *Branes*, whose existence in ST was only noticed in the very late eighties [89, 90], are structures of higher dimension which solve the equations of motion of string theory, A p-brane is a brane whose worldvolume is of spacetime dimension $(p + 1)$. Dp-branes are so called because they are the locus of points upon which open strings, which require Dirichlet boundary conditions, can end. These open strings interact with the closed strings away from the brane, and this creates a background source of various fields in the supergravity theory, which is another way of saying the branes are charged objects under those fields. A field-brane coupling is implemented by integrating the field in question over the worldvolume of the brane - this restricts the possible couplings by dimensionality.

To leading order the action of a Dp-brane in the low-energy theory is [91]

$$S_{Dp} = -T_{Dp} \int_{\Sigma_{p+1}} \left(e^{-\phi} \sqrt{-\det(G + H)} + iC_{p+1} \right), \tag{1.45}$$

where $T_{Dp} \sim e^{-\langle\phi\rangle} = 1/g_s$ is the tension of the brane, Σ_{p+1} is the brane's worldvolume, G and H are the metric and B_2 field strength induced on the worldvolume, and C_{p+1} is the RR field of appropriate degree. Branes are therefore very heavy at weak ($g_s \to 0$) coupling, which is one of the reasons they were not detected in the perturbative expansion.

One can also find brane solutions in the low-energy action which do not correspond to a known microscopic description in terms of strings. In particular the NS5 brane appears in bosonic, Type II and heterotic low-energy theories, and is charged under the B_2 field[34]. The tension of the NS5 brane goes as $T_{NS5} \sim 1/g_s^2$.

The insertion of a brane into the background of a theory is one way to spontaneously break supersymmetry, analogous to the SSB of a gauge group by a field vev. For example,

[33] In fact, there can exist special ('self-dual') points in moduli space where winding modes become light - however, this thesis is not concerned with theories near those points.

[34] The action of a single NS5 brane is known, but is subtantially more messy than eq. (1.45) [92].

Field	Electric brane	Magnetic brane
B_2	String	NS5
C_2	$D3$	$D5$
C_3	$D4$	$D4$
C_4	$D5$	$D3$

Table 1.4: Electrically- and magnetically charged branes under each KR and RR field.

consider an infinite brane aligned along the $x - y$ plane. The theory will lose invariance in the z direction in the vicinity of the brane. Brane insertions can also generate masses for fields to which they couple.

String theory enjoys 'electric-magnetic duality', in that there is a complete spectrum of objects charged both electrically and magnetically under all the fields of the theory. A magnetic coupling to a field can also be viewed as an electric coupling to its dual, in a sense illustrated in the following example.

Example

The B_2 field can be sourced electrically by the two-dimensional worldsheet Σ_2 of a superstring (a 1-brane) via the following term in the action

$$S \supset \int_{\Sigma_2} B_2. \tag{1.46}$$

The field strength tensor of B_2 is a 3-form H_3. Taking the $10d$ Hodge dual of this field strength yields a 7-form $\tilde{H}_7 = \star_{10} H_3$; by Poincaré's Lemma this can be written locally as the exterior derivative of a 6-form, $\tilde{B}_6$.

Then electric-magnetic duality implies there is an object with a 6-dimensional worldvolume Σ_6 which sources $\tilde{B}_6$. That just so happens to be the $NS5$-brane with 6-dimensional worldsheet Σ_6:

$$S \supset \int_{\Sigma_6} \tilde{B}_6. \tag{1.47}$$

This can be viewed as telling us that the NS5 brane is charged electrically under $\tilde{B}_6$, or instead magnetically under B_2, since the Hodge star $\star_{10}$ involves an antisymmetric tensor. Equally, a superstring is charged magnetically under $\tilde{B}_6$.

The same procedure applies to the RR fields, where a C_{p+1} field couples electrically to a Dp brane and magnetically to a $D(6-p)$ brane, as set out in table 1.4.

Like superstrings, branes can be inserted wrapping compact dimensions. From the perspective of the uncompact dimensions, the brane will appear as a lower-dimensional object with contributions to its energy from the wrapping tension [93, 94].

Returning to the compactification of the $10d$ supergravity, we want to understand what will be our light degrees of freedom appearing to four-dimensional observers. We find that these comprise two broad classes - the compactification manifold parameters and the Kaluza-Klein (KK) modes.

Scalar compactification parameters

A given manifold may possess compact closed submanifolds called *cycles*. The topological invariants of a d-dimensional manifold known as the *homology groups* $\{H_n\}$ consist of the equivalence classes of n-dimensional ($n \leq d$) cycles under the equivalence relation $A \sim A' \iff A_n - A'_n = \partial B_{n+1}$ - i.e. two n-cycles are to be considered equivalent if $A_n \coprod (-A'_n)$ forms the boundary of another submanifold in one dimension higher - see appendix A for a little more elucidation and a colourful diagram.

Each n-cycle Σ^i_n has an associated volume form Ω^i_n (induced from the metric), so that we can obtain

$$\mathrm{Vol}(\Sigma^i_n) = \int_{\Sigma^i_n} \Omega^i_n. \tag{1.48}$$

These volumes are just real numbers that can depend on position in 4-dimensional space - i.e. they are real four-dimensional scalar fields, known as *moduli fields*.

Example

For an illustrative example which we will make much use of in chapter 4, consider the two-torus T^2. This possesses two non-trivial 1-cycles and one non-trivial 2-cycle, which is the entire surface of the torus itself. The *Kähler modulus* of the T^2 is the total volume (labelled here as ρ_2 for later convenience):

$$\rho_2(x) = \int_{\Sigma_2} \Omega_2 = \sqrt{\det h}, \tag{1.49}$$

where h is the metric on the torus.

Dual to its homology groups, a manifold will have topological invariants called *cohomology groups*. There are several types of cohomology theory, but that relevant to us is that of de Rham cohomology – appendix A – groups whose elements are equivalence classes of differential forms under the relation $\eta \sim \omega \iff \eta = \omega + d\lambda$, with λ an $(n-1)$ form and d the exterior derivative. We shall use $H^n(M)$ to denote the de Rham cohomology group of n-forms on X_6. For Kähler manifolds with complex coordinates $\{z^i, \overline{z}^i\}$, we have an extension of de Rham to *Dolbeault cohomology*, which differentiates between holomorphic and anti-holomorphic indices. For example, H^2 can be decomposed into $H^{2,0} \oplus H^{1,1} \oplus H^{0,2}$, where $H^{2,0}$ contains forms like $\eta_{ij} dz^i \wedge dz^j$, while $H^{1,1}$ has $\eta_{i\overline{j}} dz^i \wedge d\overline{z}^{\overline{j}}$.

Since the holonomy of a Kähler manifold respects holomorphicity, Dolbeault groups are appropriate invariants.

Specifying a compactification manifold, given a topology, is the specification of the metric. For CY manifolds and tori, this boils down to specifying the *Kähler class* and the *complex structure*; the complex structure controls the sizes of odd-dimensional cycles and the Kähler class those of even. The free parameters correspond to the manifold's *Hodge numbers* $h^{p,q}$, which are the dimensions of the Dolbeault cohomology groups $H^{p,q}$. For Calabi-Yau threefolds, the Kähler class is specified by $h^{1,1}$ real parameters, the complex structure by $h^{2,1}$ complex parameters (see appendix A for details).

Example

For T^2, the Kähler class is a single real number (eq. (1.49)) and the complex structure a single complex number, giving us a real scalar field and a complex scalar field in $4d$.

Pseudoscalars from antisymmetric tensor fields

The massless metric, dilaton and antisymmetric tensor fields each give rise to lower dimensional fields from KK decomposition[35] - we will here focus in particular on the components of the antisymmetric fields with all 'legs'[36] along the compact dimensions. A $10d$ antisymmetric tensor B_n with all legs along the compact directions is the product of a 0-form on M_4 and an n-form on X_6:

$$B_n(x, y) = b(x) \wedge \omega_n(y), \tag{1.52}$$

where x denotes the coordinates of M_4 and y those of X_6, and we have made the ansatz that the dependence on x and y factorises. The equation of motion of the massless $10d$ field

[35] Illustratively: given uncompact dimensions with coordinates x and a single circle dimension of radius R with coordinate y, we can expand the y-dependence of a massless scalar field Φ in terms of Fourier modes:

$$\Phi(x, y) = \sum_n \phi_n(x) e^{iny/R}. \tag{1.50}$$

The $5d$ Klein-Gordon equation $(\partial_x^2 + \partial_y^2)\Phi = 0$ tells us that the mass of each lower-dimensional mode $\phi_n(x)$ is

$$m_\phi^2 = \frac{n^2}{R^2}, \tag{1.51}$$

so we have an infinite tower of lower-dimensional states, with masses $\sim n/R$. The only massless mode is the $n = 0$ mode, i.e. that which is constant in the y direction.

[36] The antisymmetric tensor fields are n-forms on X_{10} in general. An n form with 'all legs along the 6 compact directions' (coordinates y^i) is one with the only nonzero components in the $dy^1 \wedge dy^2 \wedge \cdots \wedge dy^n$ slots.

$\triangle_{10} B_n = 0$ factorises into $(\triangle_4 + \triangle_6) B_n = 0$, where $\triangle_d$ is the Laplacian in d dimensions, so that the lower dimensional field is massless if and only if $\triangle_6 \omega_n(y) = 0$. Forms annihilated by the Laplacian are called 'harmonic forms', and it is a theorem (Hodge's theorem) that there is exactly one harmonic form in each cohomology class of X_6. Thus we can write

$$B_n = \sum_i b^i(x) \omega_n^i(y) + \text{ massive modes}, \tag{1.53}$$

where $\{b^i(x)\}$ are the coefficients of the zero mode along the $\{\omega_i^n\}$ harmonic basis for $H^n(X_6)$.

B_n enjoys a $10d$ gauge symmetry $B_n \longrightarrow B_n + c\eta_n$, where η_n is closed and c is some constant. This (with $\eta_n = \omega_n^i$) is inherited in the $4d$ action as a gauge symmetry of the $4d$ mode $b^i(x) \longrightarrow b^i(x) + c$.

Because the masses of the non-zero modes are separated by $\sim 1/R$ with R the characteristic size of the compactification, we can focus in our low-dimensional low-energy theory purely on the massless modes; we shall ignore the massive entirely from here on. The coefficients $b^i(x)$ are pseudoscalar[37] fields from the perspective of M_4.

The duality between homology and cohomology groups means we can select a basis such that

$$\int_{\Sigma_n^i} \eta_n^j = \delta^{ij}, \tag{1.54}$$

where Σ_n^i is the i^{th} n-cycle of $H_n(X_6)$ and η_n^j is a representative of the j^{th} cohomology class of $H^n(X_6)$. Note that this is well-defined on the cohomology group, since $\int_\Sigma d\lambda = \int_{\partial\Sigma} \lambda = 0$ for closed Σ[38]. This allows us to pick out the coefficient $b^m(x)$ of the expansion eq. (1.53) via integration of B_n over the n-cycle Σ^m:

$$b^m(x) = \int_{\Sigma_n^m} B_n. \tag{1.55}$$

In fact, we can do better on Kähler manifolds - we can subdivide the massless modes by their Dolbeault homology groups. So the 2-form B_2 of Type II and heterotic string theory will have separate contributions in general from $H^{2,0}$, $H^{1,1}$ and $H^{0,2}$. For CY threefolds however, $h^{2,0} = h^{0,2} = 0$, in which case there are only $h^{1,1}$ lower-dimensional fields.

[37] The pseudoscalarity arises from the couplings of the B_n to gauge field strengths up in the $10d$ supergravity which are mandated by anomaly cancellation [95].

[38] Technically this is only true for globally well-defined (single-valued) λ, a subtlety which will interest us here not at all.

Example

Let us now consider compactifying on the 6-manifold $X_6 = T^2 \times Y_4$, where Y_4 is some four-manifold, and consider the lower-dimensional fate of the T^2 parts of the B_2 field.

There is only one non-trivial 2-cycle of the torus, so $H_2(T^2) \cong \mathbb{Z}$, and therefore only one nontrivial 2-form ω_2. The part of the B_2 field with legs along the torus directions is therefore

$$B_2 = b(x)\omega_2. \tag{1.56}$$

Here ω_2 is a constant; this is because the only harmonic 2-forms on a compact 2-manifold are constant multiples of the volume form $dy^1 \wedge dy^2$.

We relabel b as ρ_1, again for later convenience, and note it is given by

$$\rho_1(x) = \int_{T^2} B_2. \tag{1.57}$$

Unlike $\rho_2(x)$, this four-dimensional field is a real pseudoscalar rather than a real scalar. In addition, the B_2 field is invariant under the gauge symmetry $B_2 \to B_2 + c\omega_2$, which is inherited as a shift symmetry of the ρ_1 field:

$$\rho_1(x) \to \rho_1(x) + c, \tag{1.58}$$

with c a constant.

We have obtained a pseudoscalar with a shift symmetry - i.e. an axion-like-particle[39] - though with an origin (and UV physics) quite different to traditional QFT axions. The same procedure can be carried out for the other antisymmetric tensor fields listed in table 1.2, and more axions obtained.

As realistic compactifications are topologically rich, with 10^{few} cycles, there are a similar number of potentially light 4d ALPs. For example, if η_i is a basis for the $h^{1,1}$ complex (1,1) harmonic forms (dual to closed 2-cycles) of X_{10} then B_2 gives $h^{1,1}$ potential 4d ALPs via $B_2 = b^i(x)\omega_i$. Related arguments apply to other k-form fields and k-cycles. The presence of fluxes, orientifolds and branes can lift (make massive) a subset of ALPs at tree level, but those that survive remain massless in perturbation theory. Importantly, solving the quality problem in string theory (keeping the QCD axion light) implies there exist many light ALPs [96][40] - a multiplicity known as the *string axiverse* [96–98]. The ubiquity of ALPs in ST favours the Peccei-Quinn solution to the strong CP problem (section 1.4).

[39] This is what Witten calls the *model-dependent axion* due to its dependence on the homology of the compactification.

[40] This is because the fates of different ALPs are linked. If the QCD instantons are the dominant explicit breaking for the QCD axion, other sources of breaking can be no larger, and this will suppress the explicit breaking (and therefore the masses) for other ALPs in the theory.

The lifting of moduli field masses by some potential is called *moduli stabilisation*. There are strong constraints on the masses of light scalars due to fifth force experiments [99] and so realistic models must include moduli stabilisation; however, pseudoscalars obey a different force law and can be much lighter.

The most attractive compactifications preserve $\mathcal{N} = 1$ supersymmetry (SUSY) before moduli stabilization. In $\mathcal{N} = 1$, the pseudoscalar ALPs a^i combine with scalar 'saxions' t^i (the moduli fields) as the complex scalar fields of SUSY chiral multiplets

$$m^i = a^i(x) + it^i(x). \tag{1.59}$$

Before including the stabilization potential the leading 4d effective action of the m fields is

$$\mathcal{L} = G_{i\bar{j}}(m, \overline{m}) g^{\mu\nu} \partial_\mu m^i \partial_\nu m^{\bar{j}}, \tag{1.60}$$

where $m^{\bar{i}} = (m^i)^*$, $\partial_i = \partial/\partial m^i$ and $G_{i\bar{j}} = \partial_i \partial_{\bar{j}} K(m, \overline{m})$ with K the Kähler potential. The behaviour of $G_{i\bar{j}}$ at moduli space boundaries will be of special interest for the construction of axiverse strings, discussed below and in chapter 4.

A moduli potential vanishing at tree level is protected from loop corrections but generated by non-perturbative effects, which, as seen in realistic stabilisation mechanisms, involve SUSY-breaking dynamics. The scalar t^i receive masses, while the pseudoscalar a^i can be separately protected and often receive hierarchically smaller non-perturbative masses. In fact, this hierarchy in t^j and a^j masses *must* exist if axiverse ALPs are light enough ($\lesssim 10^{-3}$ eV) to be relevant for the strong CP-problem or light 'field' DM.

Example

Returning to our example of the T^2 compactification with a B_2 field, we find that ρ_1 and ρ_2 combine into the complex scalar field

$$\rho(x) = \rho_1 + i\rho_2. \tag{1.61}$$

This is known as the *complex Kähler modulus* (or often, abusing nomenclature, as just the Kähler modulus), and takes values in the upper half complex plane $\mathbb{H}$ (since $\mathrm{Im}(\rho)$ is the volume of the torus and must be positive). In fact, the theory enjoys a discrete $PSL(2, \mathbb{Z})$ symmetry,

$$\rho \to \frac{a\rho + b}{c\rho + d}, \tag{1.62}$$

meaning that actual physical field excitations are valued in some fundamental domain of $\mathbb{H}/PSL(2, \mathbb{Z})$ - a popular choice of this fundamental domain is shown in fig. 1.17.

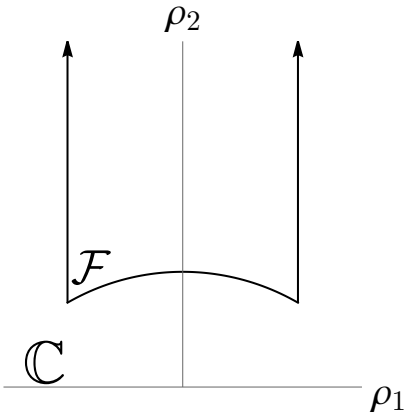


Figure 1.17: A choice of fundamental domain $\mathcal{F} \subset \mathbb{C}$ of the complex Kähler modulus of the torus. The curve is a segment of the unit circle; the vertical lines are at $\rho_1 = \pm 1/2$ and extend to infinity.

1.6.1 Axiverse strings

We shall now pick up in earnest the example we have so far confined to boxes - that of the complex Kähler modulus arising from the torus part of the compactification on $T^2 \times Y_4$, with ALP arising from the 2-form B_2 with legs in the T^2 directions, y^m, $m = 1, 2$ (we do not need to specify Y_4). This simple model can be used to build a cosmic string solution. Here we will outline a basic model of an axiverse cosmic string as presented in [100].

The reduction of the $10d$ string action (eq. (1.60)) in this case gives $K(\rho, \overline{\rho}) \propto \log(\rho_2)$, so $G_{\rho\overline{\rho}} \propto 1/4\rho_2^2$, and the relevant $4d$ effective action of the light fields to leading order in the α' expansion is thus

$$S = M^2 \int d^4x \sqrt{-\det g} g_{\mu\nu} \frac{\partial^\mu \rho \partial^\nu \overline{\rho}}{4\rho_2^2}. \tag{1.63}$$

Here M is some dimensionful scale, g is the $4d$ metric, and the $4d$ dilaton φ does not appear as we assumed it to be stiffly stabilised[41].

A crucial feature of eq. (1.63) is that the decay constant of the axion ρ_1 (which derived from B_2) is set by the vev of the saxion ρ_2 (which is the volume of the internal T^2):

$$f_{\text{eff}} = M/(\sqrt{2}\,\langle \rho_2 \rangle). \tag{1.64}$$

Thus, by analogy with usual QFT axion strings where $f_{\text{eff}}(x) = \sqrt{2}\,\langle |\Phi(x)| \rangle$ has a zero at the string core, we expect axiverse cosmic strings to have cores where $\rho_2 \to \infty$ or, more generally, to a suitable boundary of the moduli space. This expectation is correct, and generalises to axiverse strings arising from compactifications other than a simple T^2, as we will see in chapter 4.

[41] I.e. for simplicity it is assumed to have received a mass at a much higher scale and is thus non-dynamical.

To explicitly exhibit this, we now consider the $x-y$ plane, and go to complex coordinates $\{z, \overline{z}\}$, $\partial = \partial/\partial_z$ etc. The equation of motion derived from eq. (1.63) is

$$\partial\overline{\partial}\rho - \frac{2\partial\rho\overline{\partial}\rho}{\rho - \overline{\rho}} = 0 \ . \tag{1.65}$$

This is solved by any meromorphic or anti-meromorphic function of z, in particular, by the solution

$$\rho = -\frac{i}{2\pi}\log cz, \tag{1.66}$$

with c a dimensionful constant, which corresponds to

$$\begin{aligned} \rho_1 &= \theta/2\pi \\ \rho_2 &= \frac{1}{2\pi}\log\left(\frac{c}{r}\right). \end{aligned} \tag{1.67}$$

The axionic part, ρ_1 (which derived from B_2) winds once around the origin - in other words, it indicates an axionic cosmic string with winding number $w = 1$. On the other hand, ρ_2 diverges logarithmically at the origin.

Of course, this is a solution to the effective theory eq. (1.63), which is valid when the size of the compactification ρ_2 is negligible, and in addition does not take into account the dynamics of fields stabilised at higher scales which would become important very close to the core. In chapter 4 we discuss the UV origin of the cosmic string, as well as its generalisation to more general compactifications and to the rest of the axiverse.

Chapter 2
Production of secluded sectors by Primordial Black Holes

2.1 Introduction

The most studied production mechanism for a relic abundance of particle-DM, thermal freeze-out (section 1.3.4), assumes that the DM in the early Universe was in equilibrium with the hot SM plasma due to much-stronger-than-gravitational DM-SM interactions, but later fell out of equilibrium when annihilation rates failed to keep up with Hubble expansion. This mechanism depends on, at minimum, the mass and couplings of the DM and the number of degrees of freedom. For suitably chosen values, often taken at the weak scale, freeze-out reproduces the relic abundance of the DM. This mechanism, however, is now under strain from a combination of DM direct- and indirect-detection searches (see section section 1.3), and LHC bounds on new physics. Thus it is of great importance to investigate other possible calculable production mechanisms that do not rely on close-to-weak-scale interactions with the SM, such as freeze-in production (section 1.3.5) of feebly-interacting DM from an initial state with negligible DM density.

In this chapter we present a calculable, infra-red mechanism for DM production utilising only the mandatory coupling of DM to gravity. Specifically, we show that both the DM abundance and the hot-Big-Bang SM plasma can result from an initial density of primordial black holes (PBHs).

We will argue that a simple set of assumptions results in uncomplicated (and often largely initial-state independent) expressions for the final DM yield, and thus for $Y_\infty m_{\rm dm}$. Our starting hypotheses are:

1. There exists a population of micro PBHs with mean initial number density, n_0, with overlaid fluctuations. We take the PBH masses to be narrowly peaked around an initial mass, M_0 (the generalisation of our results to somewhat broader initial mass

distributions is straightforward). Here we do *not* seek to justify or provide a detailed mechanism for the existence of this population.

2. On large scales the initial energy density of BHs, $\rho_{\rm BH} = M_0 n_0$, inherits the approximately scale-invariant spectrum of density fluctuations, $\delta\rho/\rho \simeq 10^{-5}$, seen by cosmic microwave background and large-scale structure observations (see section 1.3.1). On tiny scales there can be significant departures from this fluctuation spectrum, e.g., due to Poisson variations in the number of BHs per initial Hubble patch.

3. Any remaining initial energy density not in the form of PBHs is in the form of a SM radiation component. Similarly to freeze-in production, we assume an initially negligible number density of DM particles.

4. The DM is in the form of cosmologically long-lived massive particles with sub-Planckian mass and spin ≤ 2 which, further, have sufficiently small self- and DM-SM interactions that neither the freeze-out nor freeze-in processes are operative (we will see this is often automatic as the DM mass giving the correct $Y_\infty m_{\rm dm}$ can be parametrically large).

5. Stable Planckian-mass BH relics do not exist. From these assumptions a successful mechanism of DM production follows, with noteworthy observational signatures in some cases.

In detail, in section 2.2 we calculate the DM yield and SM 'reheat' temperature, T_{RH}, at the end of PBH evaporation.[1] We present analytic expressions in the four qualitatively different regimes: 'fast' or 'slow' decay of the PBHs (with the general case being solved numerically) in both 'light' and 'heavy' DM scenarios. The observational constraints are applied in section 2.3, allowing us to find the acceptable parameter ranges of our mechanism. In section 2.4, we consider variations of our basic mechanism with additional possible signatures and discuss future directions.

2.2 Dark Matter Yield

We recall from section 1.3.6.1 that the temperature of a Schwarzschild BH of mass M is given by $T_{\rm BH} = M_{\rm Pl}^2/(8\pi M)$ (we work in units where $\hbar = c = k_{\rm B} = 1$) [34]. As the BH evaporates, $T_{\rm BH}$ scans all temperatures from an initial $T_0 = M_{\rm Pl}^2/(8\pi M_0)$ up to $T \sim M_{\rm Pl}$

[1] This is similar to a scenario discussed in [101], wherein the early Universe is reheated via Hawking emission of BHs post-inflation.

where Hawking's calculation breaks down. In what follows we always assume that $T_0 > v_{\rm EW} = 246\text{GeV}$, corresponding to an initial mass of $M_0 < 10^{15} M_{\rm Pl}$. In this limit, all states in the SM are created ultra-relativistically throughout the BH's lifetime and so we need not consider mass thresholds or the physics of crossing through the weak or QCD scales[2]. Thus, during the entire evaporation process, the SM states can be well approximated as massless[3]. Taking, then, effectively massless final states, the total rate of BH mass-loss is (see eq. (1.28))

$$\frac{\mathrm{d}M}{\mathrm{d}t} = -\frac{M_{\rm Pl}^4}{M^2} \sum_{s,i} e_{s,i} g_{s,i} \equiv -e_{\rm T} \frac{M_{\rm Pl}^4}{M^2}, \tag{2.1}$$

where i labels a state of spin s, $g_{s,i}$ is the associated number of degrees of freedom (dof), $e_{s,i}$ are the dimensionless grey-body 'power-factors', given in table 2.1, and $e_{\rm T}$ is the total emission coefficient, which does not depend upon the mass of the BH. The grey-body factors appear due to a spin-dependent (and mass-dependent for particles of mass $m \not\ll T$) potential barrier outside of the horizon, which causes back-scattering into the BH. For Hawking emission dominated by radiation into effectively massless SM states plus gravitons,

$$e_{\rm T} \approx e_{\rm T,SM} \simeq 4.38 \times 10^{-3}. \tag{2.2}$$

This is a good approximation up to small corrections due the existence of the DM sector with small total dof $g_{\rm DM} \ll g_{\rm SM} \simeq 10^2$. Thus the BH mass evolves as

$$M^3(t) = M_0^3 - 3 e_{\rm T} M_{\rm Pl}^4 \, (t - t_0) \,, \tag{2.3}$$

where M_0 is the BH mass at initial time, t_0.

We consider two broad cases with regards to the production of DM particles by Hawking radiation: the first, where the initial temperature of the BH is greater than all mass scales–the 'light' DM case–and the second, where it is below the DM mass, $m_{\rm dm}$. In the latter 'heavy' case, creation of DM particles effectively only takes place after the BH has decayed sufficiently that $T \gtrsim m_{\rm dm}$.

The emission rate of a species i of spin s, and mass m, and with energy in a range $(\omega, \omega + \mathrm{d}\omega)$ is given by eq. (1.29). The total rate of emission, integrated over all final state energies $\omega = \sqrt{p^2 + m^2}$, with $p \in [0, \infty]$, is, for our purposes, well approximated by

$$\frac{\mathrm{d}N_{s,i}}{\mathrm{d}t} \approx \frac{M_{\rm Pl}^2}{M} f_{s,i} g_{s,i} \Theta\left(d_s \frac{M_{\rm Pl}^2}{8\pi M} - m \right) \tag{2.4}$$

[2]The case of an initial temperature below some SM particle mass threshold would follow exactly the adjustments implemented in the 'heavy DM' case discussed below, i.e. particle emission would only begin around the time that the temperature passed through the threshold, affecting the final SM abundance.

[3]Our results generalise naturally to the case where T_0 is less than some SM masses.

Spin	e_s	f_s
0	7.24×10^{-5}	6.66×10^{-4}
1/2	4.09×10^{-5}	2.43×10^{-4}
1	1.68×10^{-5}	7.40×10^{-5}
3/2	5.5×10^{-6}	2.1×10^{-5}
2	1.92×10^{-6}	5.53×10^{-6}

Table 2.1: The numerical power, e_s, and rate, f_s, greybody factors per degree of freedom for neutral particles of given spin s, extracted from [41,102,103]. These have been summed over the dominant angular momentum emission modes [104]. For spin 3/2 we have estimated the coefficients. There is a small, sub-dominant correction to e_s and f_s if particles are charged.

where the coefficients $f_{s,i}$ are dimensionless greybody 'rate-factors', with values given in table 2.1, Θ is the Heaviside step-function, and d_s is a spin-dependent dimensionless coefficient we have found from numerical and semi-analytic solutions of the exact Hawking emission equations. To a sufficient approximation[4] $d_{\text{bosons}} \simeq 3.2$, while $d_{\text{fermions}} \simeq 3.6$. Equations (2.1) and (2.4) imply that the total number of particles, per species, emitted over the BH's life is

$$N_{s,i} \simeq \frac{f_{s,i} g_{s,i}}{2 e_{\text{T}}} \left(\frac{M_0}{M_{\text{Pl}}}\right)^2 \begin{cases} 1 & (T_0 > m/d_s) \\ d_s^2 T_0^2/m^2 & (T_0 < m/d_s) \end{cases} . \tag{2.5}$$

2.2.1 Light Dark Matter

Consider, first, the case where the DM mass is less than the initial effective BH temperature $m_{\text{dm}} < d_s T_0$. The evolution equations of the energy densities of the PBHs, $\rho_{\text{BH}} = M(t)n(t)$, and the SM radiation, ρ_{rad}, in the early Universe are:

$$\frac{\mathrm{d}\rho_{\text{BH}}}{\mathrm{d}t} + 3H\rho_{\text{BH}} = -e_{\text{T}} \frac{M_{\text{Pl}}^4}{M^2} n \; ; \tag{2.6}$$

$$\frac{\mathrm{d}\rho_{\text{rad}}}{\mathrm{d}t} + 4H\rho_{\text{rad}} = +e_{\text{T}} \frac{M_{\text{Pl}}^4}{M^2} n \; . \tag{2.7}$$

We solve these equations together with eq. (2.1) and the Friedmann equation, eq. (1.3), subject to $M_0 > M_{\text{Pl}}$ and $\rho_{\text{BH}}(0) = M_0 n_0 < M_{\text{Pl}}^4$. We also assume that the process begins in a PBH-matter-dominated universe with $\rho_{\text{rad}}(0) \approx 0$ – in section 2.4 we discuss the (in)sensitivity of our results to the relaxation of this assumption. It should be noted that a number of studies into formation process for PBHs give the number of BHs per

[4] This simple parametrisation ignores some sub-leading residual dependence on spin, $s = 0, 1, 2$ in the boson case, and $s = 1/2, 3/2$ in the fermion case, arising from the differing energy dependence of the greybody factors.

initial Hubble patch, $4\pi n_0/3H_0^3 \sim 1$ (e.g., [33, 101, 105, 106]), though we do not impose this constraint here.

The resulting solution is well described by one of two analytic limits, here denoted as 'fast' and 'slow' decay. These limits are characterised by the ratio of timescales of the system: the characteristic BH decay time, $\tau_{\rm decay}(M(t))$, and the Hubble time, $t_H(t) = 3/2H(t)$. We define $B(t) \equiv t_H/\tau_{\rm decay}$, with initial value

$$(B_0)^2 = e_{\rm T}^2 \frac{3}{2\pi} \frac{M_{\rm Pl}^3}{n_0} \left(\frac{M_{\rm Pl}}{M_0}\right)^7 . \tag{2.8}$$

When $B_0 \gg 1$ we have fast decay, while for $B_0 \ll 1$ the decay is initially slow. Note that all decays become fast towards the end of the BH lifetime.

The SM interactions are sufficiently strong that $\rho_{\rm rad}$ thermalises quickly, while, as stated in the above (assumption 4), the DM does not interact significantly with either itself or the SM, so that no other processes affect the DM yield. The two important calculable quantities from these analytic cases are the temperature of the SM radiation bath at the end PBH decay – the 'reheat' temperature, $T_{\rm RH}$ – and the yield of the DM. We will minimally impose that $T_{\rm RH} > 3\,{\rm MeV}$, the starting temperature of Big Bang Nucleosynthesis (BBN) [107, 108], and that the DM yield and mass satisfy $m_{\rm dm} Y = 0.43\,{\rm eV}$, ensuring, respectively, that BBN is standard and $\Omega_{\rm DM} h^2 = 0.11$ today, as observed [5].

From our analytic solution we find, in the case of slow initial decay, $B_0 \ll 1$,

$$T_{\rm RH}^{\rm slow} \simeq 1.09 \frac{e_{\rm T}^{1/2}}{g_*^{1/4}} M_{\rm Pl} \left(\frac{M_{\rm Pl}}{M_0}\right)^{3/2} , \tag{2.9}$$

where g_* is the effective number of SM dof at $T_{\rm RH}$. From the ensuing total entropy density, $s_{\rm tot}$ (well approximated by that in the SM radiation bath in our limit $g_{\rm DM} \ll g_{\rm SM}$), and using eq. (2.5), the yield of species i with spin s at the end of the decay process is then given by

$$Y^{\rm slow} \equiv \frac{n_{s,i}}{s_{\rm tot}} \simeq 0.49 \frac{f_{s,i} g_{s,i}}{g_*^{1/4} e_{\rm T}^{1/2}} \left(\frac{M_{\rm Pl}}{M_0}\right)^{1/2} . \tag{2.10}$$

Notice that both of these expressions are *independent* of the initial PBH number density.

In the fast case, $B_0 \gg 1$, the PBHs effectively dump all of their energy into radiation instantaneously without significant Hubble red-shifting. Thus,

$$T_{\rm RH}^{\rm fast} \simeq \left(\frac{30 n_0 M_0}{\pi^2 g_*}\right)^{1/4} , \tag{2.11}$$

with corresponding particle yield

$$Y^{\rm fast} \simeq 0.50 \frac{f_{s,i} g_{s,i}}{g_*^{1/4} e_{\rm T}} \left(\frac{n_0}{M_{\rm Pl}^3}\right)^{1/4} \left(\frac{M_0}{M_{\rm Pl}}\right)^{5/4} . \tag{2.12}$$

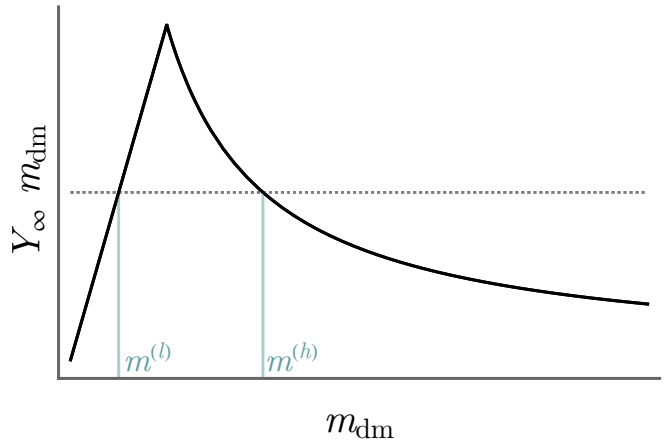


Figure 2.1: Schematic behaviour of $Y_\infty m_{\rm dm}$ as a function of DM mass $m_{\rm dm}$, here given in arbitrary units, with initial PBH properties M_0 and n_0 held fixed. The grey dashed line represents the observed value of $Y_\infty m_{\rm dm}$. The blue lines denote the 'light' ($m^{(l)}_{\rm dm}$) and 'heavy' ($m^{(h)}_{\rm dm}$) DM masses that are consistent with the observed relic abundance.

2.2.2 Heavy Dark Matter

We now consider the case $m_{\rm dm} > d_s T_0$. The reheat temperature remains, in both slow and fast cases, of the form given in eqs. (2.9) and (2.11), up to small corrections of $O(g_{\rm DM}/g_{\rm SM})$. From eq. (2.5), we can then write the yield in this scenario as

$$Y_h = Y_l \frac{T_0^2}{m_{\rm dm}^2} d_s^2, \tag{2.13}$$

where the subscripts h and l refer, respectively, to the heavy and light cases. In fig. 2.1, we see that the observable quantity, $m_{\rm dm} Y$ (equivalently $\Omega_{\rm DM} h^2$), exhibits two contrasting behaviours as a function of the DM mass $m_{\rm dm}$, namely linearly rising for small $m_{\rm dm}$, while decreasing as $1/m_{\rm dm}$ for large values. Thus, for any value of $m_{\rm dm} Y$ lower than the maximum (we find that $m_{\rm dm} Y = 0.43\,\text{eV}$ always satisfies this), *two* solutions for $m_{\rm dm}$ exist – one in each regime. The two solutions satisfy $m^{(h)}_{\rm dm} m^{(l)}_{\rm dm} = T_0^2 d_s^2$.

2.2.2.1 Numerics

We have numerically solved the full set of coupled equations, eqs. (2.1), (2.6) and (2.7) and the Friedmann equation. Our results, shown in fig. 2.2, confirm our limiting approximations are excellent over the majority of parameter space. The line $B_0 = 1$ is also confirmed to be a good discriminant, marking a quick but smooth transition between the two regimes. The plots also make obvious the different behaviour of $m^{(l)}_{\rm dm}$ and $m^{(h)}_{\rm dm}$ over the parameter space, i.e. whether they increase or decrease towards the origin in the upper left corner where M_0 is small and n_0 large.

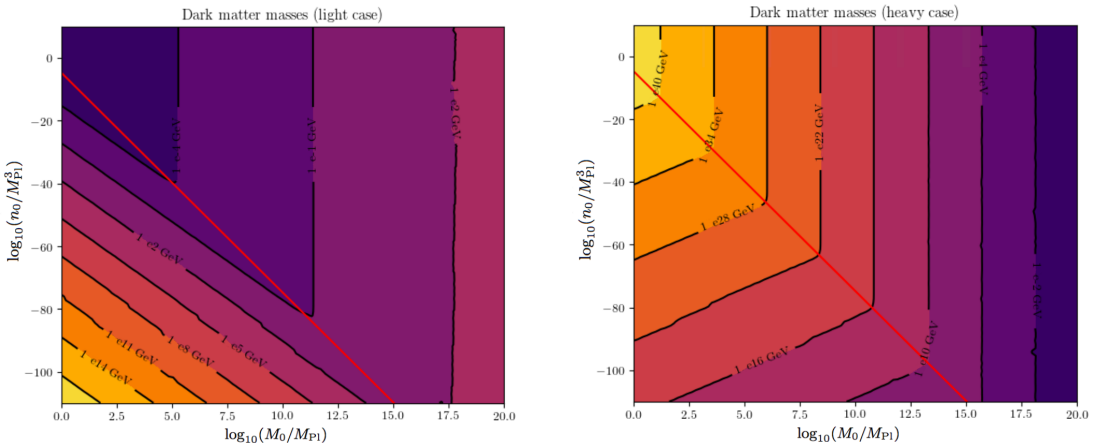


Figure 2.2: Contours of DM mass $m_{\rm dm}$ giving observed $Y_\infty m_{\rm dm}$, for the 'light' and 'heavy' DM cases, as a function of $\log_{10}(M_0/M_{\rm Pl})$ and $\log_{10}(n_0/M_{\rm Pl}^3)$ across the *a priori* allowed parameter space before constraints are imposed - see fig. 2.3 for the relevant constraints. The red line is $B_0 = 1$.

s	g_s	$m_{\rm dm}^{(l)}$/GeV (slow)	$m_{\rm dm}^{(h)}$/GeV (slow)	$m_{\rm dm}^{(l)}$/GeV (fast)	$m_{\rm dm}^{(h)}$/GeV (fast)
0	1	$[2.6\times10^{-7}, 0.80]$	$[3.4\times10^{9}, M_{\rm Pl}]$	$[3.1\times10^{-7}, 2.8\times10^{13}]$	$[2.9\times10^{9}, M_{\rm Pl}]$
1/2	2	$[3.6\times10^{-7}, 1.1]$	$[3.1\times10^{9}, M_{\rm Pl}]$	$[4.2\times10^{-7}, 3.9\times10^{13}]$	$[2.6\times10^{9}, M_{\rm Pl}]$
1	3	$[7.8\times10^{-7}, 2.4]$	$[1.1\times10^{9}, M_{\rm Pl}]$	$[9.2\times10^{-7}, 8.5\times10^{13}]$	$[9.6\times10^{8}, M_{\rm Pl}]$
3/2	4	$[2\times10^{-6}, 6]$	$[5\times10^{8}, M_{\rm Pl}]$	$[2\times10^{-6}, 2\times10^{14}]$	$[5\times10^{8}, M_{\rm Pl}]$
2	5	$[6.3\times10^{-6}, 19]$	$[1.4\times10^{8}, M_{\rm Pl}]$	$[7.4\times10^{-6}, 6.8\times10^{14}]$	$[1.2\times10^{8}, M_{\rm Pl}]$

Table 2.2: Limits on DM mass giving the correct relic abundance in the four regimes of 'light' and 'heavy' DM mass and 'slow' and 'fast' BH decay, which satisfy our observational and theoretical constraints (except free-streaming in 'light' case – see text). A single DM particle of given spin is assumed. In particular, given the large masses allowed above, this mechanism provides a new way for producing so-called 'WIMPzillas' [109] in the early Universe.

2.3 Observational Constraints and Possible Signatures

In order for our model to follow standard cosmological results from BBN onwards, we minimally require that $T_{\rm RH} > 3\,\text{MeV}$ [107, 108]. This constraint, along with $M_0 > M_{\rm Pl}$ and $\rho_{\rm BH}(0) = M_0 n_0 < M_{\rm Pl}^4$, is shown in fig. 2.3 in the 'light' DM mass (left) and 'heavy' DM mass (right) cases. We show only constraint plots for a single real $s = 0$ dof as other spins display precisely the same features, differing only in numerical values. These, together with the DM mass contour plots given in fig. 2.2, lead to the maximally allowed ranges for the DM mass in table 2.2 in each of the four regimes, and for DM spins $0 \leq s \leq 2$ (these are calculated *before* imposition of the additional, strong constraint coming from free-streaming).

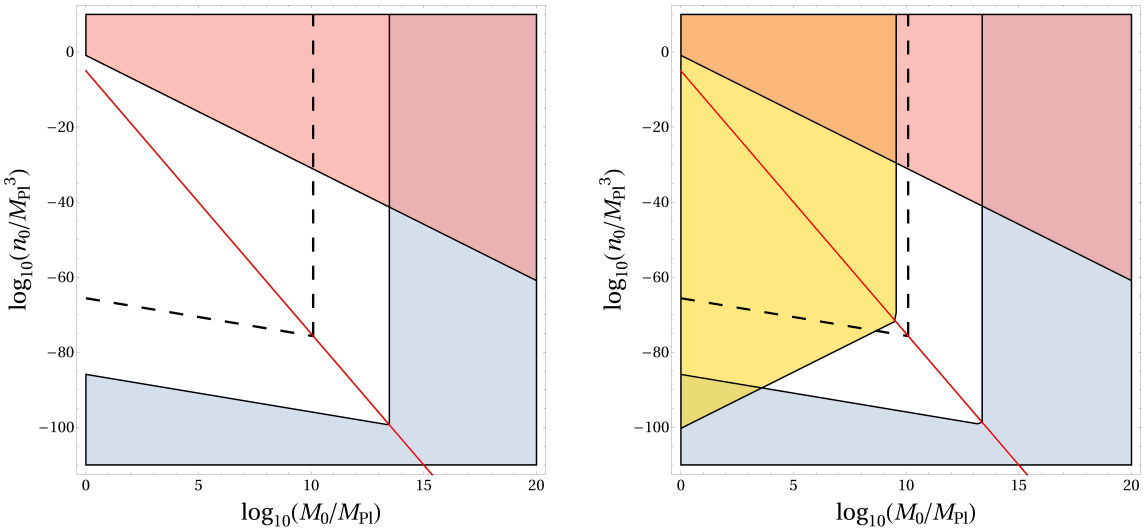


Figure 2.3: Constraints in the $\log_{10}(M_0/M_{\rm Pl})$–$\log_{10}(n_0/M_{\rm Pl}^3)$ plane for 'light' and 'heavy' DM cases (left and right panels), for a single real $s = 0$ dof (other spins display precisely the same features, differing only in numerical values) *before* the additional, strong constraint coming from free-streaming is imposed. (In the case of 'light' DM this strongly DM-spin-dependent constraint excludes DM spin $s \leq 1$, marginally excludes $s = 3/2$, and allows a region of the spin $s = 2$ case to survive. There are no significant constraints on the 'heavy' DM case from free-streaming. See text for more details.) The red line ($B_0 = 1$) marks the boundary between the 'fast' and 'slow' regimes. The blue shaded regions are disallowed as $T_{RH} < 3\,\text{MeV}$. The dashed line is $T_{RH} = 200\,\text{GeV}$. The upper pink shaded regions are excluded as the PBH radius exceeds the inter-PBH spacing, and, in the 'heavy' case, the yellow region by $m_{\rm dm} > M_{\rm Pl}$.

In the slow regime, $T_{\rm RH}$ and Y (eqs. (2.9) and (2.10)) are independent of n_0, and iso-contours of $T_{\rm RH}$, $m_{\rm dm}$ giving the observed $Y_\infty m_{\rm dm}$ and M_0 will all be parallel. Thus, constraining the reheat temperature and the initial BH mass will provide constraints on the DM mass. Since, in the light (respectively, heavy) case, the DM mass contours increase (decrease) with increasing M_0, we find that $T_{\rm RH} \lesssim 3\,\text{MeV}$ sets an upper (lower) bound on $m_{\rm dm}$, while $M_0 > M_{\rm Pl}$ sets a lower (upper) bound. However, in the heavy case, we must exclude the region where $m_{\rm dm} > M_{\rm Pl}$. This then leads to an upper bound on the reheat temperature in the heavy case ranging from $T_{\rm RH} \lesssim 1.3\,\text{TeV}$ for $s = 0$ up to $T_{\rm RH} \lesssim 8.5\,\text{TeV}$ for $s = 2$.

In the fast regime, the mass contours are of differing gradients for the light and heavy cases, setting different locations for the bounds on the DM mass. For the light (heavy) case, the crossover point from the fast to the slow regime at low M_0 and high n_0 provides a lower (upper) bound on the DM mass. As this point is a crossover between regimes, by continuity, we must find that the bounds are parametrically similar. This can indeed be seen in table 2.2. Excluding super-Planckian DM masses we again obtain a maximum $T_{\rm RH}$ in the heavy case, which, by continuity, is the same for the slow regime. From the slope

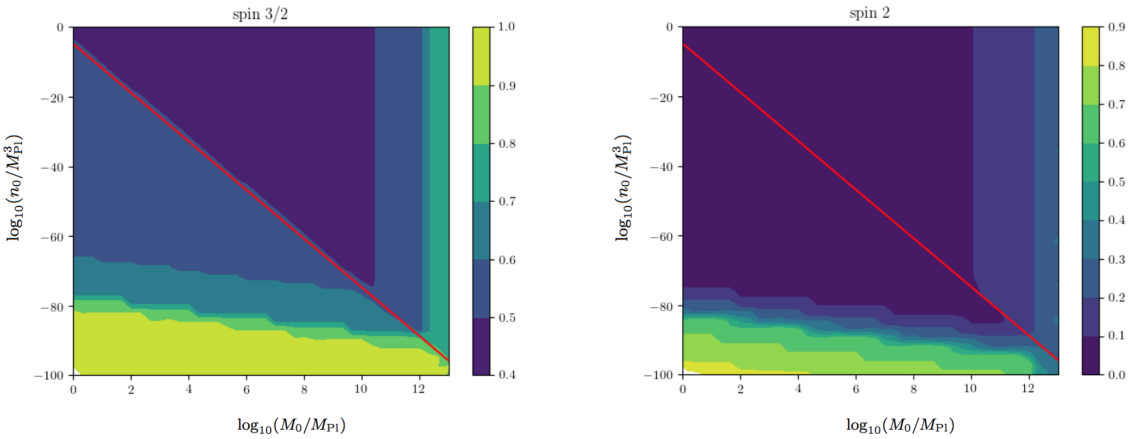


Figure 2.4: Free-streaming constraints in the 'light' DM case for spin 3/2 and 2 (left and right panels), where colour shading shows fraction of DM particles that are still relativistic at $T_{\rm SM} = 1\,\text{keV}$, and we have at every point imposed a 'light' solution DM mass such that the correct $Y_\infty m_{\rm dm}$ is reproduced. Note the differing colour scales in the two cases with the spin 3/2 case having more than $\sim 40\%$ of particles relativistic over the entire plane, while the spin 2 case has substantial regions where less than $\sim 10\%$ of DM particles are relativistic. Red line ($B_0 = 1$) marks the boundary between the 'fast' and 'slow' regimes.

of the mass contours, we see that we set an upper bound in the light case for low M_0 and n_0, deep in the fast region. Similarly, in the heavy case, we set a bound at the crossover for low n_0 and high M_0.

If electroweak baryogenesis is to be accommodated in our model, then we further require that $T_{\rm RH} \gtrsim 200\,\text{GeV}$. We include a contour for this reheat temperature in fig. 2.3. This contour is particularly constraining in the heavy case, yielding, for example, a revised range for the DM mass of $5.5 \times 10^{17}\,\text{GeV} \lesssim m_{\rm dm} \lesssim M_{\rm Pl}$ for a real scalar.

Free-Streaming

The 'light' DM mass case is significantly constrained by the free streaming of the ultra-relativistically-emitted DM particles. Results due to R. Petrossian-Byrne and J. March-Russell (presented in [110]) exhibit the DM momentum distribution function after the end of PBH decay for a single DM species without non-gravitational self- or SM-interactions. It was found that the lower the spin, the higher the proportion of relativistic particles. Imposing a rough criterion that less than 10% of the DM is relativistic when $T_{\rm SM} = 1\,\text{keV}$, it was found that for the 'light' DM mass solution the parameter space is almost entirely excluded for spins $s \leq 1$, but feasible for higher spins - see fig. 2.4. However, for the 'heavy' DM mass solution, it was found that the entirety of parameter space survives.

Dark Radiation

An unavoidable contribution to dark radiation comes from gravitons emitted from the BHs at a rate which is only suppressed compared to SM radiation by the smaller grey-body power coefficient, $e_2 \simeq 1.92\times10^{-6} \ll e_{\rm T,SM} \simeq 4.38\times10^{-3}$ (for related earlier work see [111]). Specifically at the end of PBH decay $\Delta\rho_{\rm grav}/\rho_{\rm rad} = 2e_2/e_{\rm T,SM} \simeq 8.77\times10^{-4}$. The ratio is then constant up to changes in g_*, which give $\Delta\rho_{\rm grav}/\rho_{\rm rad} \simeq 0.02$, evading the bound in eq. (1.23). This therefore does not place a bound on our mechanism. Nevertheless, it may provide an accessible target for planned future high-precision determinations of $N_{\rm eff}$. In section 2.4 we consider motivated variations of our basic model with additional dark radiation contributions.

Density Perturbations

Limits on the spectrum and form of density perturbations provide another potential source of constraint. We have here taken as a basic hypothesis that on moderate-to-large scales (but not on small scales as we soon quantify) the initial BH number density, and thus the initial energy density, $\rho_{\rm BH}$, inherits the spectrum of Gaussian, almost scale-invariant density perturbations that are the result of, say, an early epoch of inflation[5]. One significant point is that because the evaporation of our PBHs sources all forms of matter (both SM and dark), the perturbations at the end of PBH decay are naturally *adiabatic* and not isocurvature[6].

Nevertheless, many production mechanisms for PBHs, for instance their production in ultra-relativistic bubble collisions following, say, a quantum phase transition (e.g., of the type discussed in [112]), lead to substantial random variation in the number of PBHs produced per initial Hubble volume, and thus to a significant extra source of density perturbations on *small* scales of order H_0^{-1}. To quantify the potential later effect of this on structure formation, consider BHs that are initially distributed at t_0 with density variations $\delta\rho$ between initial Hubble volumes V_{H_0}. This implies at later times $\delta\rho/\rho(t) \approx 1/\sqrt{N} = 1/\sqrt{K(t)n_0V_{H_0}(t)}$, where K is the number of V_{H_0} patches within the horizon at t and N is therefore the total number of BHs within that horizon. If we assume a Poisson distribution

[5]We have nothing new here to say about the origin of these perturbations. Note that we do not necessarily require inflation: any mechanism or dynamics in the very early Universe that gives the approximately scale-invariant spectrum of observed density perturbations is suitable as long as there is a population of micro PBHs produced/present at the end satisfying the conditions set out in the introduction, and discussed further in section 2.4.

[6]Isocurvature perturbations are those for which the overdensities of dark matter and radiation fail to line up, and the effect on spatial curvature is therefore cancelled out.

of BHs, this approximation is very accurate at later times when K is very large. Assuming matter domination during BH decay, and radiation domination thereafter, we require that $\delta\rho/\rho$ at matter-radiation equality be at most of order 10^{-6}. We find that this constraint is very weak and the parameter regions thus excluded lie well within the section of the plane already forbidden by the requirement that $T_{\rm RH} \geq 3$ MeV. Thus no substantial new perturbations exist on length scales of interest for moderate-to-large-scale structure formation.

2.4 Comments, Generalisations, and Future Work

Finally, we make some comments, and briefly discuss some motivated variations of our basic mechanism, as well as directions for future work.

Sensitivity to Initial Conditions

The reader might be concerned that we have so far assumed that the initial condition is one of pure PBH matter domination. However, we have found that our DM yield prediction is insensitive to changes in this assumption over a wide range of parameter space. In the fast BH decay regime, provided any initial SM radiation component satisfies $\rho_{\rm rad,SM}(0) \lesssim 0.1\rho_{\rm BH}(0)$, the predicted SM reheat temperature is unaffected up to $\mathcal{O}(10\%)$ corrections or less. Regarding the DM yield, any primordial DM number density $\Delta n_{\rm DM}(0)$ is unimportant if it is substantially less than that produced by the PBH decay. Given the expression for the total number of DM particles emitted, eq. (2.5), this translates into the requirement

$$\frac{\Delta n_{\rm DM}(0)}{n_0} \ll 2\times 10^{-3}\left(\frac{M_{\rm Pl}^3}{n_0}\right)^{2/7}, \tag{2.14}$$

where for concreteness we have inserted typical values for scalar or spin-1/2 fermion DM in the 'light' case, and used the condition $B_0 \sim 1$ which allows the largest (most restrictive) fast-regime value of the initial PBH number density n_0 for a given value of M_0. Since over much of the allowed parameter space $n_0/M_{\rm Pl}^3$ can be as small as 10^{-80} eq. (2.14) is not a particularly restrictive requirement.

The situation in the slow BH decay regime is even better, as any initial SM radiation component is now substantially red-shifted away during the long period of BH decay. Specifically, we find from our analytic slow-regime solution that, at end of PBH decay, any initial SM radiation has been diluted by a factor

$$\frac{\Delta\rho_{\rm rad,SM}(t_{\rm end})}{\Delta\rho_{\rm rad,SM}(t_0)} \simeq \left(\frac{B_0}{0.928}\right)^{8/3} \ll 1 \tag{2.15}$$

as $B_0 < 1$ in the slow regime, and often $B_0 \ll 1$. This is to be compared to the SM radiation component produced by PBH emission, which is $\rho_{\rm rad,SM}(t_{\rm end}) \simeq 0.965 B_0^2 \rho_{\rm BH}(t_0)$. Thus as long as

$$\rho_{\rm rad,SM}(t_0) \lesssim 0.1 B_0^{-2/3} \rho_{\rm BH}(t_0) \tag{2.16}$$

both the SM reheat temperature and the DM yield are substantially unaffected, up to $O(10\%)$ corrections or less, by the presence of the early SM radiation component. Since, consistent with constraints, we find that in the slow regime $B_0^{-2/3}$ can be as large as

$$B_0^{-2/3} \sim 0.24 (M_{\rm Pl}/T_{\rm RH})^{5/9} \gg 1\,, \tag{2.17}$$

a dominant initial SM radiation component, as big as $\sim 10^{11}$ times larger than the initial PBH energy density can be present without affecting our results[7]. It is clear that the slow region is particularly insensitive to initial conditions, and thus attractive in this regard. In addition the region of parameter space where there is of order one BH per initial horizon patch, and so possibly favoured by BH production mechanisms, is contained within the slow regime.

Other DM Interactions

Although our mechanism requires that the traditional freeze-out and recent freeze-in mechanisms of DM production give sub-dominant effects, this doesn't rule out some small self- or DM-SM-interactions with possibly important observational consequences. We thus now briefly turn to the possibilities for detection of DM through non-gravitational signatures.

One natural possibility is the existence of operators which allow the DM to slowly decay to the SM sector – see, e.g., [113–120] for a selection of earlier work on the topic of decaying heavy DM. This is well motivated if the stabilising symmetry of the DM is global, as, by general arguments, all theories incorporating gravity are widely believed to possess no exact global symmetries[8]. Since our DM, especially in the 'heavy' case, is surprisingly massive, even exponentionally tiny symmetry-violating effects can lead to cosmologically relevant decay times. As a rule of thumb, lifetimes of order $10^{26} - 10^{27}$ s are on the allowed border for decaying DM, depending on exact details on the decay. Since for our mechanism the DM is often very massive, the energy of the SM decay products can be very large, thus leading to ultra-high-energy cosmic rays. If we parameterise the effective dimensionless coupling constant that violates the symmetry as $\lambda \sim \exp(-8\pi^2/g^2)$, as

[7] This ratio is for $T_{\rm RH} = 3\,$MeV. For $T_{\rm RH} = 1\,$TeV, a ratio as large as $\sim 10^8$ is still allowed.

[8] It is not known if the strength of this violation is suppressed by some large mass scale, such as the Planck mass, or is non-perturbatively small in some dimensionless coupling.

might be suitable for a non-perturbative violation, then for a DM mass of order the GUT scale, $\sim 10^{16}$ GeV, the 10^{26} s lifetime constraint translates into $g < 0.8$, a not unreasonable number for a fundamental dimensionless coupling. Of course, such a non-perturbatively determined lifetime is very sensitive to the underlying and unknown coupling g so an observationally interesting lifetime is in no way predicted. An alternative, and less sensitive, possibility exists for a DM mass in the region of 100 TeV, for then dimension-six Planck-suppressed operators lead to a lifetime of order 10^{26} s with only mild polynomial dependence on the mass.

The DM can also have self-interactions as long as they don't lead to a freeze-out process. For example, in the case of a single real massive scalar a quartic interaction will not allow physical, kinematically allowed number-changing interactions, but will lead to elastic scattering which can modify the DM momentum distribution. The evolution of DM with number-changing interactions is explored in chapter 3.

For our heavier mass regions the DM can also have substantial interactions with SM matter. This is because for DM mass $m_{\rm dm} \gg T_{\rm RH}$ the freeze-in process is exponentially suppressed [17] in addition to being down by small couplings, while any potential freeze-out reprocessing via, say, self-annihilations of our DM into SM states is suppressed by the extremely tiny number density of DM that applies in the case that $m_{\rm dm} \gg 1\,\text{TeV}$. Some of these issues have previously been discussed in the context of so-called WIMPzilla DM [109, 116] but, in the context of our production mechanism, deserve a more detailed analysis in the future.

Finally, regarding the identity of the DM, the fact that our allowed 'heavy' DM mass range extends all the way up to $M_{\rm Pl}$, and, moreover, is operative for states of spin $s \geq 3/2$, motivates the intriguing possibility that either GUT, or even higher-spin string Regge excitations, if they are sufficiently stable (say due to a combination of $J^{\rm PC}$ conservation, kinematics, and maybe discrete gauge symmetry quantum numbers), might be the DM.

Additional Dark Radiation

If there are new very light dof in addition to the graviton and SM neutrinos then these will also be produced during the decay of the PBHs and will be an additional dark radiation component beyond that of the gravitons. A particularly well-motivated almost massless dof is the axion (section 1.4), whether the QCD axion or multiple axion-like particles as in the string axiverse scenario (section 1.6). If the number of light axions, N_a, is much less than the number of dof at $T_{\rm RH}$, then the effective change in the number of dof is[9] $\Delta N_{\rm eff} \sim (0.04 - 0.08) N_a$, which evades the Planck bound (section 1.3.3) if $N_a \lesssim (3 - 7)$.

[9] In our original paper, we made an error in this calculation which was noticed and corrected by [121].

Opening the 'Light' DM Window

Another variation of our basic mechanism is to allow the number of dof in the SM sector to be much increased beyond the 106.75 of the SM – for instance, due to TeV-scale (R-parity violating) supersymmetry or strong dynamics. This situation can possibly resurrect some of the low-spin, $s \leq 1$ 'light' DM parameter space from the severe free-streaming constraint. The reason for this is two-fold: a drastic increase in SM dof at high energy leads, to first order, to substantial extra redshift of DM momentum by the time the SM temperature reaches 1 keV, and second, less of the original BH mass is injected into DM – the yield is inversely proportional to the now larger total emission coefficient e_{T}. Thus, all other things kept fixed, the DM must be heavier to satisfy the $Y_{\infty} m_{\mathrm{dm}}$ observation and so becomes non-relativistic earlier.

Statement of Authorship for joint/multi-authored papers for PGR thesis

To appear at the end of each thesis chapter submitted as an article/paper

The statement shall describe the candidate's and co-authors' independent research contributions in the thesis publications. For each publication there should exist a complete statement that is to be filled out and signed by the candidate and supervisor **(only required where there isn't already a statement of contribution within the paper itself).**

Title of Paper	Black Hole Genesis of Dark Matter
Publication Status	☑Published ☐ Accepted for Publication ☐Submitted for Publication ☐Unpublished and unsubmitted work written in a manuscript style
Publication Details	Journal of Cosmology and Astroparticle Physics 04 (2018) 009 O. Lennon, J. March-Russell, R. Petrossian-Byrne, H. Tillim

Student Confirmation

Student Name:	Hannah Tillim		
Contribution to the Paper	Was involved in the development of the ideas and particularly in the analytic calculations and numerical simulations of the fast vs slow, light vs heavy regimes, evaluating the constraints except that of free streaming (as made clear in the text) and discussion of the final phenomenology.		
Signature		Date	8th June 2022

Supervisor Confirmation

By signing the Statement of Authorship, you are certifying that the candidate made a substantial contribution to the publication, and that the description described above is accurate.

Supervisor name and title:	Prof. John March-Russell		
Supervisor comments	Hannah's statement correctly characterises her valuable and fully equal contribution to our research and published paper.		
Signature		Date	8th June 2022

This completed form should be included in the thesis, at the end of the relevant chapter.

Chapter 3
Reproductive Freeze-In

3.1 Introduction

One of the few facts known with certainty about the nature of dark matter is that its non-gravitational interactions with the SM sector are weak. However, as mentioned in section 1.3.6, there is some evidence that certain issues such as the cusp-core problem may be solved by introducing interactions within the dark sector itself. Of particular interest to us is the fact that such self-interactions inevitably lead to both elastic *and* inelastic, number-changing scattering processes. In this chapter, we study a new DM relic density generation mechanism involving such inelastic self-interactions.

Specifically, we show that if the initial state of the DM sector is ultra-relativistic, $\langle E_{\rm dm} \rangle \gg m_{\rm dm}$, but far-underpopulated relative to full thermal equilibrium, a calculable non-linear process, that we refer to as *Reproductive Freeze-In* (RFI), can lead to a DM relic density compatible with current observations, bearing new features of phenomenological import.

During the active phase of the process, the DM yield significantly evolves due to $2 \rightarrow k$ ($k > 2$) processes (for DM without conserved quantum numbers or asymmetry) and the DM sector temperature falls relative to that of the SM bath as DM kinetic energy is converted to DM mass. Thus RFI is effectively the inverse of the recently-discussed 'cannibal DM mechanism' [122–126].

The evolution of a self-interacting DM sector initially possessing a non-zero chemical potential has been studied by a number of groups, [16, 127, 128] with a focus on first finding the conditions under which the initially underpopulated sector fully thermalises and subsequently how this impacts the DM abundance as it freezes out. In this work, we instead focus on the freeze-in case [17, 129, 130] where the DM sector evolution never reaches full equilibrium.

Note that the assumed far-underpopulated, ultra-relativistic DM-sector initial conditions often result from dynamics of the extreme early Universe. Examples include post-inflation inflaton decay and reheating [131–133]; the decay of a population of primordial black holes [110, 121, 134] and the decay of superheavy particles associated with, for instance, neutrino mass generation or Peccei-Quinn symmetry breaking.

As we will discuss, possible signatures of the RFI mechanism include the effects of the associated elastic DM self-interactions in galaxies and galaxy clusters and in structure formation, and the weakening of free-streaming constraints on models that produce an initial ultra-relativistic population of DM particles. Since the RFI mechanism does not require that the DM possesses any exact continuous or discrete stabilising symmetry – just that interactions with the SM are feeble – late-time processes including DM decays occurring in the current universe are a possibility.

3.2 RFI Setup

A starting assumption of RFI is that the dynamics of the very early universe - post-inflationary reheating, the creation of the universe itself, or some other possible scenario such as the decay of a population of superheavy states - populates both the SM and DM sectors with initial energy densities with ratio

$$r \equiv \frac{\rho_{\rm dm}}{\rho_{\rm sm}}. \tag{3.1}$$

In the SM sector, for all particles excepting possibly right-handed neutrinos, the gauge and other interactions are not small, and both kinetic and full species ('chemical') equilibrium are assumed to be achieved rapidly with a 'reheat' temperature T_0.

On the other hand, in the DM sector we assume that the appropriate dimensionless measures of self-interaction strength (which may be a gauge coupling, a quartic scalar self-interaction, or a combination $(E/M)^n$ involving the typical energy E and the scale M of a higher-dimensional interaction) are such that elastic scattering is fast compared to the Hubble time, $1/H(t)$. These interactions quickly establish *kinetic* equilibrium (this simplifying assumption can be relaxed, see section 3.6) with an associated kinetic temperature, $\tilde{T}(t)$, but, in contrast, *number-changing* $2 \longrightarrow k$ $(k > 2)$ processes, which drive the system towards *chemical* equilibrium, are parametrically slower[1].

[1]This is easy to achieve. For example, if the DM sector consists of a single massive Majorana fermion, Ψ, then the leading interactions are of the schematic form $\Psi^4/M^2 + \Psi^6/M^5 + \cdots$, and the ratio of the $2 \longrightarrow 4$ to $2 \longrightarrow 2$ processes is $\sim (E/2\pi M)^4 \times (\text{logs}) \ll 1$ in the energy regime of interest, $m_{\rm dm} \ll E \ll M$. Alternatively, if we consider a single-species scalar model with a perturbative quartic self-coupling $\lambda \lesssim 1$, then the ratio of the rates of the $2 \longrightarrow 4$ to $2 \longrightarrow 2$ processes is $\sim (\lambda a^2/16\pi^4) \times (\text{logs}) \ll 1$, where a is the scale factor.

Recall that the distribution functions of particles in kinetic but not chemical equilibrium are given by

$$f(E,t) = \frac{Z(t)}{\exp[E/\tilde{T}(t)] \mp Z(t)}, \tag{3.2}$$

where we define $Z(t) \equiv e^{\mu/\tilde{T}}$ for convenience, with μ the chemical potential, and $\mp$ apply to the Bose/Fermi DM cases. Recall also from section 1.3.2 that for a species with number-changing interactions, as we care about here, $\mu \neq 0$ is associated with deviation from chemical equilibrium. A second fundamental assumption of RFI is that the DM number density, $n_{\rm dm}$ is significantly *under-occupied* compared to equilibrium during the entire evolution (we will verify that this assumption is self-consistently correct), corresponding to $\mu \ll -\tilde{T}$ and therefore $Z \ll 1$. If, further, the DM is ultra-relativistic, the number and energy densities in the DM sector are well approximated by

$$\begin{aligned} n_{\rm dm}(t) &= \frac{g}{\pi^2} Z(t) \tilde{T}(t)^3 \\ \rho_{\rm dm}(t) &= \frac{3g}{\pi^2} Z(t) \tilde{T}(t)^4, \end{aligned} \tag{3.3}$$

where g is the number of particle degrees of freedom.

We will show that, although the DM number density can significantly evolve, in an expanding universe full equilibrium may never be reached and a non-trivial DM yield can result.

Although self-interactions within each sector are vital, the RFI mechanism does not utilise SM-to-DM-sector interactions in any essential way, so we assume for pedagogical simplicity that any such interactions are strictly absent. The SM and DM sectors are then secluded from each other and have separate dynamics apart from their gravitational effects upon each other[2]. Thus, during a period where both sectors remain relativistic, the energy density ratio, r remains constant up to changes in the number of SM relativistic degrees of freedom g_* upon going through a mass threshold for a SM state, a subtlety which we neglect here. In section 3.6 we will comment on these approximations.

In the DM sector the number-changing processes act to drive $Z(t)$ towards unity, that is, towards chemical equilibrium. Concurrently $\tilde{T}$ will be falling faster than dictated by Hubble expansion as kinetic energy is converted into mass energy. Whether the system reaches chemical equilibrium or not depends on the rate of the $2 \to k$ process and how they depend on temperature. We define the ratio of DM to SM-sector temperatures

$$\Theta(t) \equiv \frac{\tilde{T}(t)}{T_{\rm sm}(t)}\,, \tag{3.4}$$

[2]For previous work on this see, e.g., [135].

which is restricted to lie in the range $\Theta_0 \geq \Theta \geq \Theta_{\rm eq}$, where Θ_0 is the initial ratio and $\Theta_{\rm eq}$ is the ratio when the DM sector reaches chemical equilibrium. As the change in Θ occurs via processes that are increasing the number of DM states with mass $m_{\rm dm}$, as soon as the DM becomes non-relativistic at $\tilde{T} \simeq m_{\rm dm}$ the development of $\Theta(t)$ ceases for kinetic reasons apart from trivial evolution due to possible changes in g_*.

Here we take the DM sector to be comprised of a single type of particle with mass $m_{\rm dm}$. The generalisation to more complicated DM sectors is straightforward. As we discuss in the following, we are for simplicity also assuming that the cannibal mechanism [122–126] is frozen out for $\tilde{T} < m_{\rm dm}$, so the DM density is determined by RFI. It is again straightforward to relax this assumption. Constancy of r in the relativistic regime implies

$$\frac{Z(t)\Theta(t)^4}{g_*(t)} = \frac{\pi^4}{90 g} r \,. \tag{3.5}$$

Note that the ratio of DM-sector to SM-sector entropy densities is *not* constant during the evolution, as the DM sector starts off in a far-from-equilibrium state, and the production of DM particles by the inelastic $2 \to k$ processes increases the DM entropy, with the result that $s_{\rm dm}/s_{\rm sm} \propto 1/\Theta(t)$. Instead, it is the ratio of energy densities r that is approximately constant (up to g_* thresholds as mentioned).

The equilibrium value of Θ is

$$\begin{aligned} \Theta_{\rm eq} &\simeq \left(\frac{\pi^4 r}{90}\frac{g_*}{g}\right)^{1/4} \\ &\simeq 0.3 \, \left(\frac{r}{10^{-4}}\right)^{1/4} \left(\frac{g_*/g}{10^2}\right)^{1/4} , \end{aligned} \tag{3.6}$$

though, in all cases of interest to us, evolution of $\Theta(t)$ will stop well before this value is reached. It is also instructive to estimate the maximum possible size of Θ_0 in order understand the conceivable range over which Θ can vary. As the initial average energy per particle in the DM sector is $\langle E \rangle = \rho^0_{\rm dm}/n^0_{\rm dm}$, one finds $\Theta_0 \lesssim \langle E \rangle / 3T_{\rm sm,0}$ where $T_{\rm sm,0}$ is the initial temperature of the fully-thermalised SM sector. Then the most extreme case with $\langle E \rangle \sim M_{\rm Pl}$ and $T_{\rm sm,0} \sim 3$ MeV would have $\Theta_0^{\rm max} \sim 10^{21}$.

Assuming the DM sector never reaches full chemical equilibrium, and utilising the leading expression for the number density, $n_{\rm dm}$, eq. (3.3), as well as eq. (3.5) and the value of the SM entropy density eq. (1.10), we find the DM yield $Y \equiv n_{\rm dm}/s_{\rm sm}$ is related to Θ by

$$Y = \frac{r}{4\Theta} \,. \tag{3.7}$$

Then, if Θ_f is the value of Θ at which the number-changing processes terminate, the correct DM relic abundance $m_{\rm dm} Y_f \simeq 0.434$ eV implies

$$\Theta_f \simeq 57 \left(\frac{r}{10^{-4}}\right)\left(\frac{m_{\rm dm}}{\rm MeV}\right) \,. \tag{3.8}$$

Using $T_{\rm sm} = \tilde{T}/\Theta$ and eq. (3.7), one finds that for the correct DM density, the SM temperature at the end of DM particle production must satisfy

$$T_f \geq \frac{4 m_{\rm dm} Y_f}{r} \simeq \frac{1.74}{r}\,\text{eV}\,, \tag{3.9}$$

with the inequality being saturated if the yield changes fast compared to Hubble expansion when $\tilde{T} \sim m_{\rm dm}$. Since we are assuming the hidden sector is a small perturbation on the energy density during radiation domination, i.e. $r \lesssim 0.1$, we have $T_f \gtrsim 17$ eV, so that particle production ceases before matter-radiation equality or recombination. Further, by using the constraint on dark radiation (assumed here to be entirely dark sector) at the time of BBN (eq. (1.21)) we get a lower limit $T_f \gtrsim 400\,\text{eV}$. Typically, however, there are other, stronger constraints on r. For example, since there exist strong constraints on either the scales of DM free-streaming (if the DM is collision-less) or diffusion damping (if the DM is elastically scattering and behaving as an adiabatically expanding gas) arising from structure formation, the physics of an initially ultra-relativistic DM sector is constrained. We address this constraint on r, and thus T_f, in section 3.5.

However this analysis hides the fact that eq. (3.9) is only true *if* a suitable Y_f giving the observed DM density is achieved at the conclusion of the mechanism. This requires an analysis of the Boltzmann equation determining the evolution of Y (and Θ via eq. (3.7)).

3.3 The Yield Equations

We are interested in the increase in the DM number density in the presence of number-changing interactions. We focus on the single species case for pedagogical simplicity (the more general case of multiple DM particle species of different masses interacting in number-changing ways is a direct, if messy, generalisation). Then, the evolution of the single relevant phase space distribution function, $f(E,t)$, is governed by the Boltzmann equation (eq. (1.5)), which, once integrated, gives the time derivative of the particle number density:

$$\dot{n}(t) + 3Hn = \frac{g}{(2\pi)^3}\int \mathbf{C}[f]\frac{d^3p}{E} \equiv c_n\,. \tag{3.10}$$

The RHS collision term in our case sums over all number-changing $2 \to k$ and $k \to 2$ interactions involving the particle in question. Since by assumption the elastic interactions are 'fast' and maintain kinetic equilibrium, we do not need to explicitly include the effect of $2 \to 2$ processes once the semi-thermal form of the distribution functions, eq. (3.2), is used. Thus each of the terms is an integral, over external momenta, of the number-changing matrix element and a combination of the phase space distributions of

the external particles. In the ultra-relativistic regime $\tilde{T} \gg m_{\rm dm}$ of interest, the dependence of the collision term on the DM sector temperature, $\tilde{T}$, and the energy-independent under-occupancy factor, Z, can be written as

$$c_n = g\tilde{T}^4 \sum_{k>2} (k-2) Z^2 (1 - Z^{(k-2)})\ \mathcal{I}_k(\tilde{T}/M)\ , \tag{3.11}$$

where the sum on k runs over all number-changing channels, and the functions $\mathcal{I}_k(\tilde{T}/M)$ represent the strength and non-trivial temperature dependence of the $2 \longrightarrow k$ interaction. Here M is a possible energy scale, such as that defining an interaction strength in the effective theory, and the presence of the $Z^{(k-2)}$ term follows from considerations of detailed balance.

The first simplification of eq. (3.11) results from the fact that over the whole range of non-trivial evolution of $n(t)$ the DM state is far under-occupied, with $Z \ll 1$, so we may drop the inverse $k \longrightarrow 2$ process term $Z^{(k-2)}$. Similarly, irrelevantly small $j \leftrightarrow k$ terms with both $j, k > 2$ were already neglected in eq. (3.11). Secondly, we assume that $\tilde{T}/M \ll 1$ for all $\tilde{T}$ of interest so that we may expand the function $\mathcal{I}_k(\tilde{T}/M)$ and keep only the leading term. This is sufficient when the only state with mass below the cutoff of our effective theory is the essentially-massless ($m_{\rm dm} \ll \tilde{T}$) DM particle state itself. Thus we may write

$$\mathcal{I}_k(\tilde{T}/M) = A_k \left(\frac{\tilde{T}}{M}\right)^{\alpha} (1 + \cdots)\ , \tag{3.12}$$

where for each process α is an approximately-constant exponent and A_k a dimensionless pre-factor with an exact value determined by the model-dependent structure of the matrix element[3]. For perturbative DM sectors α is close to an even integer.

As the SM temperature satisfies $\dot{T} = -HT$, eqs. (3.10) to (3.12) imply that the DM yield evolves according to

$$\begin{aligned} \frac{dY}{dT_{\rm sm}} &\simeq -\frac{45g(k-2)A_k}{2\pi^2 g_*} Z^2 \left(\frac{\Theta T_{\rm sm}}{M}\right)^{\alpha} \frac{\Theta^4}{H} \\ &\simeq -\sqrt{\frac{256\pi^9 g_*}{45g^2}} \frac{A_k (k-2) M_{\rm Pl}}{r^2 T_{\rm sm}^2} \left(\frac{rT_{\rm sm}}{4M}\right)^{\alpha} Y^{4-\alpha}\ . \end{aligned} \tag{3.13}$$

Although eq. (3.13) is of the form of a conventional yield evolution equation, it is less immediately useful than usually the case as the boundary conditions on the process are

[3] As discussed in the conclusions the more complicated situation where $\mathcal{I}_k(\tilde{T}/M)$ is not determined by a single power-law over the relevant range of $\tilde{T}$ has a richer range of behaviours, as does the related case where the DM sector has massive states that can go on mass-shell at energies $\widetilde{T_0} > E \gg m_{\rm dm}$. These interesting elaborations go beyond the scope of this thesis.

most naturally expressed in terms of the initial and final *DM sector* temperature, which in our case evolves very differently to the SM temperature. In particular, for purely kinematic reasons, the number-changing $2 \to k$ processes certainly cease when $\tilde{T} \simeq m_{\rm dm}$ (the number-changing mechanism can become ineffective *before* this temperature if the interaction rate satisfies $\Gamma_{2\to k} < H$).

Thus it is better to track the evolution of Y with respect to the DM temperature $\tilde{T}$. We find the rate of change of the yield to be given by

$$\begin{aligned} \frac{dY}{d\tilde{T}} &\simeq -\frac{Y^3}{\tilde{T}}\left[Y^2 + \frac{\tilde{T}}{\beta_k M_{\rm Pl}}\left(\frac{M}{\tilde{T}}\right)^{\alpha}\right]^{-1} , \\ \text{with} \quad \beta_k &\equiv \frac{\sqrt{80\pi^9}A_k(k-2)g_*^{1/2}}{15gr(1+r)^{1/2}} . \end{aligned} \tag{3.14}$$

This equation is correct in the limit where $Z \ll 1$ *during the entire evolution* - in particular, the $k \to 2$ inverse reactions encoded by the $Z^{(k-2)}$ factor inside the brackets in the expression eq. (3.11) for the Boltzmann collision term are unimportant. We must self-consistently check that this assumption holds using eq. (3.23) in section 3.4, as we do for the phenomenological example in section 3.5.

Inspecting this equation clearly shows that the evolution of Y falls into two distinct regimes. For Y sufficiently small, the yield as a function of $\tilde{T}$ evolves as

$$\frac{dY}{d\tilde{T}} \simeq -\beta_k \frac{M_{\rm Pl}}{\tilde{T}^2}\left(\frac{\tilde{T}}{M}\right)^{\alpha} Y^3 , \tag{3.15}$$

while for larger Y we switch over to

$$\frac{dY}{d\tilde{T}} \simeq -\frac{Y}{\tilde{T}} . \tag{3.16}$$

These two limiting forms of the yield equations enable a useful approximate analytic understanding of the evolution of the DM density, as we explain in the next section, while eq. (3.14) can be solved numerically to give an accurate value of the DM yield.

The physical interpretation of the two regimes is as follows: the 'small-Y' limit given by eq. (3.15) corresponds to the case when Y develops *slowly* compared to the Hubble rate, namely $\Gamma_{2\to k} \ll H$, while the 'large-Y' scenario given by eq. (3.16) corresponds to *fast* evolution, $\Gamma_{2\to k} \gg H$. In accord with this, the solution of the fast regime evolution eq. (3.16) is simply

$$\frac{Y_f}{Y_i} = \frac{\tilde{T}_i}{\tilde{T}_f} , \tag{3.17}$$

reflecting the fact that in the fast regime the red-shifting of the DM energy density via Hubble expansion is unimportant; all the available kinetic energy in the sector is efficiently processed into the mass-energy-density of the DM particles, independent of the details of the interaction, finally ceasing when one exits the fast regime (often this is when $\tilde{T} \simeq m_{\rm dm}$ is reached). On the other hand, in the slow regime, Hubble expansion plays the dominant role; both SM and DM temperatures evolve almost perfectly in step, with the DM yield staying essentially constant as the RHS of the relevant evolution equation, eq. (3.15), is parametrically small. Thus, as we will see in detail, and check via a numerical solution of eq. (3.14), the non-trivial evolution of the yield is essentially determined by the switch-over between the fast and slow regimes.

3.4 Essential behaviours

The boundary between the two regimes occurs at the $\tilde{T}$-dependent yield given by

$$Y_* = \beta_k^{-1/2} \left(\frac{\tilde{T}}{M_{\rm Pl}}\right)^{1/2} \left(\frac{\tilde{T}}{M}\right)^{-\alpha/2} . \tag{3.18}$$

For a given value of all the underlying interaction parameters, A_k, α etc, this relation defines a curve in the $\tilde{T}$-Y plane with parametric behaviour determined by the exponent α. We take evolution of the yield to cease when $\tilde{T}$ falls below $m_{\rm dm}$. On a Y-x plot ($x = M_{\rm Pl}/\tilde{T}$), one should view the hidden sector as following the curve with the correct initial conditions (e.g. fig. 3.1) or choice of parameters (e.g. fig. 3.2); the intersection with the red curve gives the point at which evolution ceases, which then determines the corresponding mass. The physics of RFI then depends upon whether evolution ceases in the fast or slow regimes. For a given initial yield, one's designated curve which may never reach the red line - this is then an excluded region of parameter space. We also define m_* as the value of the mass where $Y_* = 0.434\,{\rm eV}/m_{\rm dm}$ - i.e. where the Y_* and red lines cross.

$\alpha \leq 0$

From eq. (3.18) we see that for $\alpha \leq 0$ the boundary curve $Y_*(\tilde{T})$ falls as $\tilde{T}$ itself decreases through either Hubble expansion or conversion of kinetic to mass-energy. This case corresponds to the rate of the $2 \to k$ process increasing relative to the Hubble rate as $\tilde{T}$ drops. Thus for sufficiently small DM mass, one always enters the fast regime where the DM yield is determined by the number-changing processes.

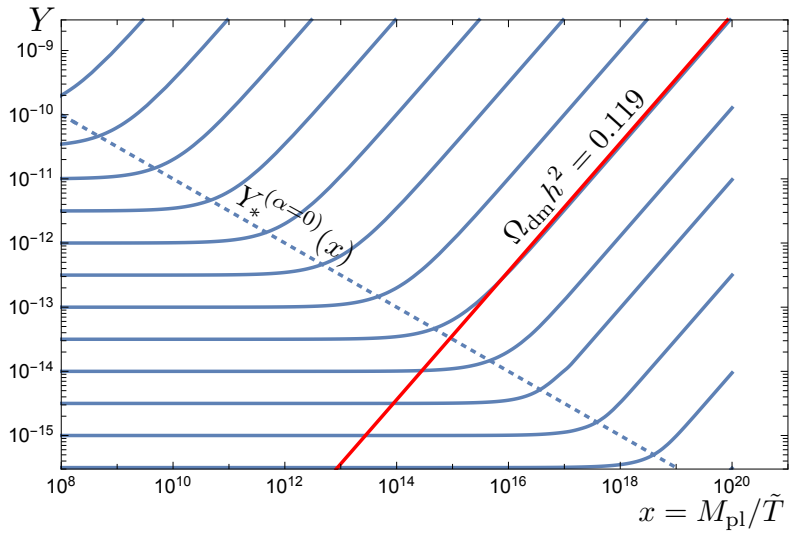


Figure 3.1: Illustration of the DM yield evolution (blue curves) as a function of $x = M_{\rm Pl}/\tilde{T}$ from numerical solution to eq. (3.14), for the case $\alpha = 0$ and fixed interaction strength, starting with varying initial yields at $\tilde{T}_0 = 10^{-8} M_{\rm Pl}$. Y_* (dashed line) delineates the switch-over from slow (below) to fast (above) evolution. The red line corresponds to the observed DM density. Yield evolution terminates when $\tilde{T} \simeq m_{\rm dm}$ (thus $x \simeq M_{\rm Pl}/m_{\rm dm}$). Once evolution passes into the fast regime the yield curves are iso-DM-density-lines, so on the correct yield curve *every* value of the DM mass gives the observed DM density (if assumptions underlying fast evolution hold). The self-consistency and observational constraints discussed in the text have not yet been imposed.

For $\alpha = 0$ and in the regime $m_{\rm dm} < m_*$ an approximate analytical expression relating the final yield to the underlying parameters is simply

$$Y_f \simeq \beta_k \frac{Y_0^3 M_{\rm Pl}}{m_{\rm dm}} \,. \tag{3.19}$$

This shows the automatic $m_{\rm dm}$-independence of the final DM density $m_{\rm dm} Y_f$, but also the fact that the DM density resulting from RFI is sensitive to the initial condition Y_0. This is not such a disadvantage as it may at first seem, either because one has a predictive theory of the initial condition (as, e.g., essentially arises in primordial black hole decay [110, 121, 134]), or because the idealised situation we have so far described, where the DM and SM sectors are completely decoupled from each other, is violated by a feeble coupling which is possibly measurable (e.g. via late-time decays). Moreover, the self-interaction that is key to the DM production is the same interaction that may in favourable cases lead to potentially observable effects in structure formation via elastic scattering.

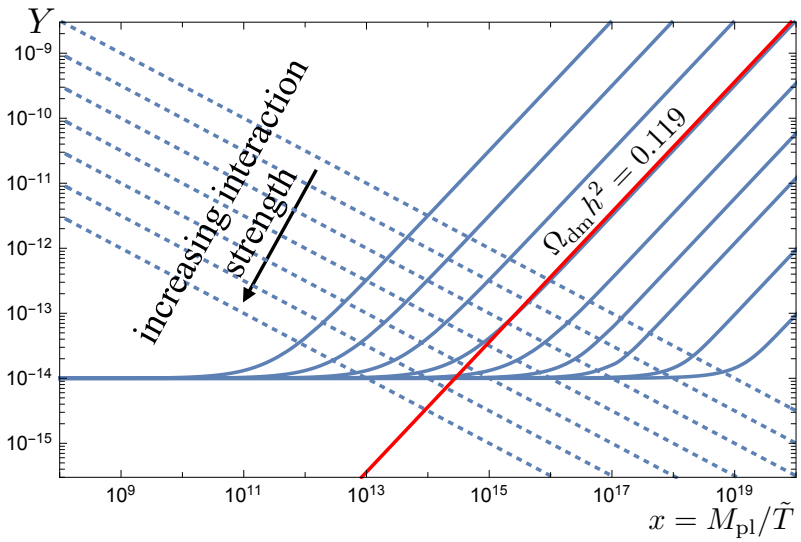


Figure 3.2: Evolution of the DM yield starting with fixed initial value $Y = 10^{-14}$ for varying interaction strengths in the case $\alpha = 0$. Conventions as in fig. 3.1.

In fig. 3.1 we illustrate the behaviour of the yield as a function of $x \equiv M_{\rm Pl}/\tilde{T}$ for the case $\alpha = 0$ as the initial value, Y_0, is varied while keeping the interaction strength fixed. In fig. 3.2 we show the evolution of the yield for fixed $Y_0 = 10^{-14}$ in the case $\alpha = 0$ as the interaction strength is increased.

It is also clear that, while several curves meet the observed DM density curve (red line) in the slow region, due to the parallelism of this line to the yield flows in the fast region, only a single yield flow terminating in the fast region will produce the correct DM density. Having selected this curve, one may choose to terminate at any point after it has joined the red line, and still be confident of producing the correct relic abundance. Put another way, once $m_{\rm dm} < m_*$, DM of *any* lower mass automatically gives the observed DM density if the interaction strength is correctly chosen depending on r and Y_0. This is the region of most interest to us.

$\alpha \geq 4$

Returning to more general behaviour of the yield evolution as a function of α, for values of $\alpha \geq 4$ the Y_* curve increases with x faster than linearly, so one finds that even if Y_0 is large enough so that the initial evolution is in the fast regime where $2 \longrightarrow k$ processes are efficient, the evolution inevitably exits into the slow regime unless the DM mass is such that $m_{\rm dm} > m_*$. This behaviour is illustrated in the case $\alpha = 4$ in fig. 3.3.

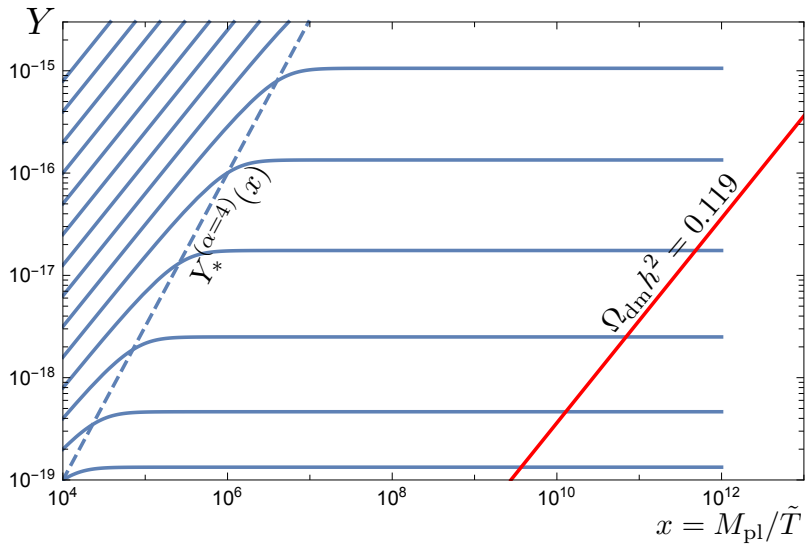


Figure 3.3: Illustration of the evolution of the DM yield for the case $\alpha = 4$. Conventions as in fig. 3.1. The self-consistency and observational constraints discussed in the text have not yet been imposed.

$\alpha = 2$

On the other hand, in the case $\alpha = 2$ the yield evolution is contained fully in either the slow or fast regime (apart from a set of initial conditions of measure zero) depending upon the initial condition for the yield, Y_0 and the strength of the interaction as measured by β_k. This behaviour is illustrated in fig. 3.4.

Finally, we must check that the neglect of the inverse $k \to 2$ processes is correct. First this requires that the under-occupation factor $Z \ll 1$. Since in this limit eq. (3.5) and eq. (3.7) imply the relation

$$Z_f = \frac{128\pi^4 g_* Y_f^4}{45 g r^3}\,, \tag{3.20}$$

we must have the final yield value, Y_f, at which evolution terminates, satisfy

$$Y_f \ll 1 \times 10^{-4} \left(\frac{r}{10^{-4}}\right)^{3/4} \left(\frac{10}{g_*/g}\right)^{1/4}\,, \tag{3.21}$$

implying that the DM mass is bounded below by

$$m_{\rm dm} \gg 3\,\text{keV} \left(\frac{r}{10^{-4}}\right)^{-3/4} \left(\frac{10}{g_*/g}\right)^{-1/4}\,. \tag{3.22}$$

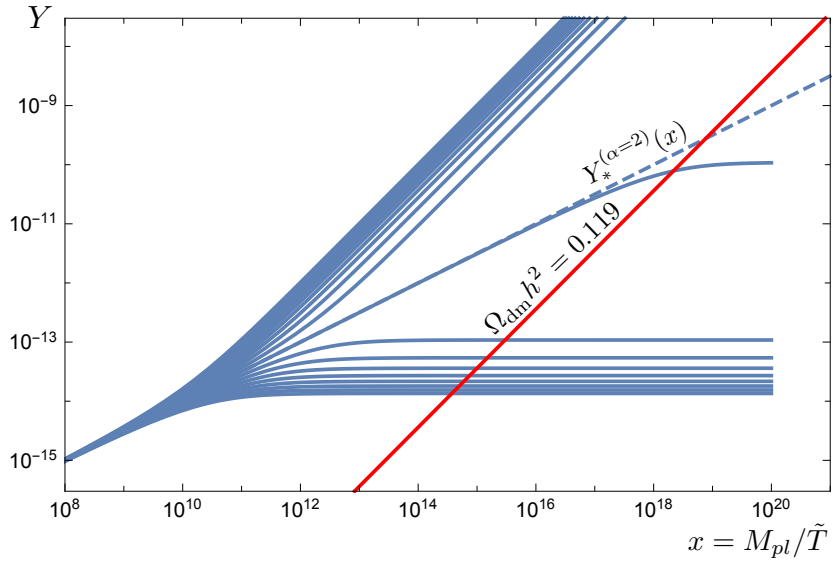


Figure 3.4: Illustration of the yield evolution for the case $\alpha = 2$, for curves of slightly-differing Y_0. In this case the resulting yield curves diverge away from the Y_* line marking the boundary between the fast and slow evolution regimes. The self-consistency and observational constraints discussed in the text have not yet been imposed.

This is a sufficient condition in all cases where the yield evolution terminates in the slow regime.

However this is not the most stringent constraint: In the cases where the evolution of the DM yield terminates (nominally, $\tilde{T} \simeq m_{\rm dm}$) in the regime in which the evolution is fast, then we must require that at $\tilde{T} \simeq m_{\rm dm}$ not only is the rate for $k \to 2$ processes much slower than the rate for $2 \to k$ processes, but that it is much slower than the Hubble rate at this time. If this is not the case then as the DM sector temperature drops well below $\sim m_{\rm dm}$ the exothermic $k \to 2$ processes will still be active and fast relative to the Hubble rate, unlike the endothermic $2 \to k$ interactions which quickly become exponentially suppressed by the tiny Boltzmann factors, and so an epoch of cannibalism of the DM number density will occur[4]. The situation where this more stringent condition can be relevant is when the exponent $\alpha \leq 4$, and is most simply expressed as

$$Z_f^{(k-2)} \left(\frac{\tilde{T}_*}{m_{\rm dm}} \right)^{(3-\alpha)} \ll 1 \,, \tag{3.23}$$

[4]This is, of course, not a problem for the physics - such evolution is perfectly consistent and will occur in a portion of parameter space - rather, the DM density is now set by the freeze-out of the cannibal mechanism, with the RFI mechanism just setting the initial conditions for the later evolution of the DM yield.

where Z_f is given in eq. (3.20) and $\tilde{T}_*$ is the value of $\tilde{T}$ where the yield evolution curves cross the Y_* line de-marking the transition from slow to fast evolution. If eq. (3.23) is satisfied then the DM density is set by RFI and not cannibalism.

3.5 Phenomenology

To see RFI in practice, let us consider a simple example where the hidden sector is described entirely by a $\lambda\phi^4/4!$ model, corresponding to the exponent $\alpha = 0$ at leading order. As discussed in section 3.3, with $\alpha \leq 1$, the number-changing $2 \longrightarrow k$ processes become increasingly efficient as the universe expands, terminating in the fast region when the temperature of the DM sector passes through the DM mass threshold and particle production is kinematically forbidden. The leading-order number-changing process is $2 \longrightarrow 4$, which we estimate to give $A_4 \sim 10^{-11}\lambda^4$, while the elastic process relevant for kinetic equilibrium is $\phi\phi \leftrightarrow \phi\phi$ (see fig. 3.5). For this single scalar, $g = 1$.

Number changing processes may cease due to any of three reasons:

1. the population reaches full chemical equilibrium,
2. Hubble expansion overtakes the cross-section or
3. particle production becomes kinematically forbidden when the temperature falls below the mass required to make a new particle.

Of these, we consider case 3) to be the most interesting. We are therefore considering the scenario with the time ordering

$$t_0 < t_{\rm NR} < t_{\rm dec}$$

where $t_{\rm NR}$ is the time when the hidden sector becomes non-relativistic (before which $2 \longrightarrow 4$ processes are still proceeding), $t_{\rm dec}$ refers to the point at which the $2 \leftrightarrow 2$ processes become inefficient compared to the Hubble expansion, and $t_{\rm EQ}$ (the time of matter-radiation equality) is considered to occur at some point after $t_{\rm NR}$. This last means that the dark sector is nonrelativistic at matter-radiation equality and therefore will not contribute to $\Delta N_{\rm eff}$ at CMB emission. We note that this is guaranteed for $Y_0 \lesssim 10^{-8}$ by the λ perturbativity bound, and indeed is the case for all of the parameter space which we examined.

We will obtain constraints on the $m - \lambda$ parameter space from various sources; in particular we lay out the calculation of the length scales over which the hidden sector will smear out structure during the radiation-domination epoch.

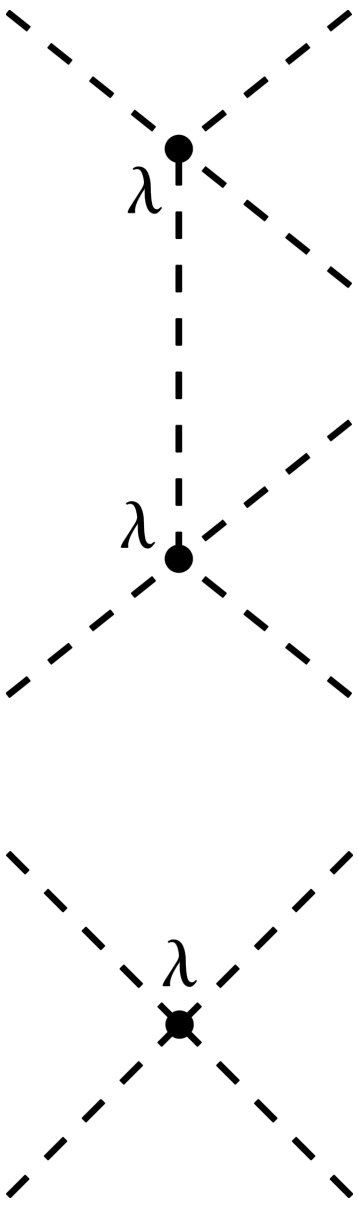


Figure 3.5: Contributions to the inelastic (top) and elastic (bottom) cross-sections in ϕ^4 theory.

3.5.1 Observational constraints

As indicated in section 3.4, we are most interested in the case where the secluded sector evolution enters the fast regime with the DM abundance set by eq. (3.19). Combining this with the requirement that the final relic abundance satisfies $Y_f m_{\rm dm} = 0.434$ eV, we find the useful relation

$$r = 1.8 \times 10^{-8} \left(\frac{\lambda}{0.1}\right)^4 \left(\frac{Y_0}{10^{-8}}\right)^3 . \tag{3.24}$$

This gives us an immediate relationship between λ and Y_0 from the constraint on $\Delta N_{\rm eff}$ at BBN, eq. (1.21).

Insisting that the sector moves into the fast regime means that there is some evolution from the initial yield Y_0, that is $Y_f > Y_0$. Using this condition we find an upper limit on the DM mass given by

$$\frac{m_{\rm dm}}{\rm GeV} \lesssim 0.0434 \left(\frac{10^{-8}}{Y_0}\right). \tag{3.25}$$

Beyond the requirement that the system enters the fast regime, we also insist that the DM states do not reach full chemical equilibrium, that is $\Theta_f > \Theta_{\rm eq}$. Combining this restriction with eq. (3.19) we find a lower limit on the mass

$$\frac{m_{\rm dm}}{\rm GeV} \gtrsim 2.0 \times 10^{-3} \left(\frac{0.1}{\lambda}\right)^3 \left(\frac{10^{-8}}{Y_0}\right)^{9/4} , \tag{3.26}$$

where we have set $g_* = 10$ for simplicity.

The behaviour of this lower limit may initially seem unintuitive; that decreasing λ increases the probability that equilibrium will be reached. This behaviour is, at root, due to the fact that we have imposed the requirement that the system eventually reaches the correct relic abundance: $Y_f m_{\rm dm} = r m_{\rm dm}/4\Theta_f = 0.434$ eV. This means that $\Theta_f \sim r$, while $\Theta_{\rm eq} \sim r^{1/4}$. When we increase λ, because of the relationship in eq. (3.19), this corresponds to an increase in r, which moves Θ_f and $\Theta_{\rm eq}$ further apart.

Recall that we must check eq. (3.23) holds in order to ensure negligible rates of $4 \longrightarrow 2$ reactions. This is not a constraint as such - viable models outside this region are certainly possible - but it will change the prediction for the relic abundance compared with our canonical scenario due to late-time cannibalistic reactions. To avoid this we require

$$\frac{m_{\rm dm}}{\rm GeV} \gg 3 \times 10^{-3} \left(\frac{0.1}{\lambda}\right)^{24/11} \left(\frac{10^{-8}}{Y_0}\right)^{21/11} . \tag{3.27}$$

A constraint may be derived from the bound on DM self-interactions from cluster collisions, e.g. the Bullet Cluster and other collisions, and the observed properties of the

DM halos of galaxies (see section 1.3.3). To be conservative we impose the stronger bound which translates into the constraint

$$\frac{m_{\rm dm}}{\rm GeV} \gtrsim 1.0 \times 10^{-2} \lambda^{2/3} \,. \tag{3.28}$$

It is worth noting that this constraint is independent of Y_0 and, given eq. (3.25), as Y_0 is decreased the impact of the self-interaction limit on the allowed parameter space will become increasingly marginal as the upper limit on the DM mass increases.

3.5.1.1 Bounds on $m_{\rm dm}, \lambda$ and Y_0

We take

$$\begin{aligned} T_{\rm EQ} &= 0.76\,{\rm eV} \\ \Theta_{\rm eq} &= \left(\frac{\pi^4 r g_*}{90}\right)^{1/4} = 8.1 \times 10^4 g_*^{3/8} Y_0^{3/4} \lambda, \end{aligned} \tag{3.29}$$

where EQ refers to matter-radiation equality and eq to equilibrium.

We now synthesise all the constraints above, as well as requiring that the SM temperature when the $2 \leftrightarrow 2$ processes decouple[5] $T_{\rm dec} > T_{\rm EQ}$ and the requirement that the coupling constant λ be less than $\sim 4\pi$ for the validity of the perturbative cross-section, to obtain general absolute bounds on $m_{\rm dm}$, λ and Y_0. It does not follow that any values within these ranges will be viable (it will depend on the values the other parameters take), but rather that anything outside them will be absolutely unviable given our current assumptions. This will be useful to us in determining allowable approximations, as well as knowing which ranges we should be probing with plots.

We find

$$\begin{aligned} 0.27\ {\rm MeV} \lesssim m_{\rm dm} &\lesssim 5.5 \times 10^4\ {\rm GeV} \\ 4.4 \times 10^{-3} \lesssim \lambda &\lesssim 4\pi \\ 7.8 \times 10^{-15} \lesssim Y_0 &\lesssim 1.6 \times 10^{-6}. \end{aligned} \tag{3.30}$$

3.5.2 Damping scales

Recall from section 1.3.6.2 for successful structure formation we must require the damping scale $l_{\rm tot}$ at matter-radiation equality to satisfy $l_{\rm tot}^2 = l_c^2 + l_{\rm FS}^2 \lesssim 100$ kpc, where

$$(l_c)^2 = \int_{t_0}^{t_{\rm dec}} {\rm d}t \frac{\langle v \rangle^2}{a^2 n \langle \sigma_{\rm elast} v \rangle}. \tag{3.31}$$

[5] $T_{\rm dec}$ is calculated below and given in eq. (3.46).

Epoch	Evolution	Damping
$T_0 \to T_*$ (slow regime)	$Y \approx Y_0, \Theta \approx \Theta_0$	relativistic collisional
$\tilde{T}_* \to m$	$\Theta_* \to \Theta_f, Y_* \to Y_f$ (kinematically frozen out after $\tilde{T}$ passes mass threshold). Y_* is calculated by tracing back from Y_f using our knowledge of dynamics in the fast region.	none (no time)
$T_* = T_{\rm NR} \to T_{\rm dec}$	Θ, Y constant.	non-relativistic collisional
$T_{\rm dec} \to T_{\rm EQ}$	Θ, Y constant	free streaming

Table 3.1: Evolution of DM which ends up in the fast regime without thermalising, during the radiation-dominated era.

is the contribution from collisional/diffusion damping and

$$l_{\rm FS} = \int_{t_{\rm dec}}^{t_{\rm EQ}} {\rm d}t \frac{v}{a} = \int_{t_{\rm dec}}^{t_{\rm EQ}} {\rm d}t \frac{a_{\rm dec}}{a^2}. \tag{3.32}$$

that from free streaming. v is the velocity, $\sigma_{\rm elast}$ is the $2 \leftrightarrow 2$ elastic cross-section, and the angular brackets indicate thermal averaging.

The quantities $\langle v \rangle$, n and $\langle \sigma_{\rm elast} v \rangle$ in eq. (3.31) admit tractable relativistic and non-relativistic approximations (see eq. (1.8)), so we divide this integral into two pieces - $t \in (t_0, t_{\rm NR})$ (section 3.5.2.1) and $t \in (t_{\rm NR}, t_{\rm dec})$ (section 3.5.2.2). We refer to these as $(l_{\rm c,R})^2$ and $(l_{\rm c,NR})^2$, though strictly speaking they are not to be considered as the squares of independent lengths. $\sigma_{\rm elast}$ in our case refers to the $2 \leftrightarrow 2$ internal DM scattering processes.

We are in the following assuming that g_* is constant. We also use the expressions valid during radiation domination

$$\begin{aligned} t &= \sqrt{\frac{45}{16\pi^3 g_*}} \frac{M_{\rm Pl}}{T_{\rm sm}^2} \equiv \frac{c_T^2}{g_*^{1/2} T^2} \\ a &= \frac{3.1 \times 10^{-13}}{g_*^{1/4}} \frac{\rm GeV}{T_{\rm sm}}. \end{aligned} \tag{3.33}$$

For most of the calculations we will be using the SM temperature as our clock, so the change in $T_{\rm sm}$ is synonymous with the passage of time. The one exception is during the fast regime, where evolution takes place so quickly that to the level of our approximations they are instantaneous from the perspective of $T_{\rm sm}$ evolution. During that period, therefore, we will monitor events using $\tilde{T}$ - see table 3.1.

Number changing processes cease at $t_{\rm NR}$, or $T_{\rm NR}$, the *Standard Model* temperature at which the *dark matter* becomes non-relativistic. Using eq. (3.9), we have

$$r(t_{\rm NR}) = \frac{1.7\ {\rm eV}}{T_{\rm NR}} \equiv \kappa \frac{\rm GeV}{T_{\rm NR}}, \tag{3.34}$$

which, combined with eq. (3.24), tells us

$$T_* = T_{\rm NR} = \frac{4.41 \times 10^{-20}\ {\rm eV}}{\sqrt{g_*} Y_0^3 \lambda^4}. \tag{3.35}$$

Equation (3.9) with $\Theta_* \approx \Theta_0 = r/4Y_0$ also gives us

$$\tilde{T}_* = \frac{0.434\ {\rm eV}}{Y_0}. \tag{3.36}$$

3.5.2.1 $T_0 \to T_*$

The relativistic damping is in effect during the period $T_0 \to T_* = T_{\rm NR}$. During this time Y and Θ are taken to be about constant, $\Theta \approx \Theta_0$, $Y \approx Y_0$.

We use the relativistic expressions

$$\begin{aligned} n(T_{\rm sm} > T_{\rm NR}) &= \frac{g}{\pi^2} Z \tilde{T}^3 = \frac{\pi^2}{90} r g_* \frac{T^3}{\Theta_0} \\ \langle \sigma^{(R)}_{\rm elast} v \rangle &= \frac{\lambda}{128\pi} \frac{1}{\Theta_0^2 T^2} \end{aligned} \tag{3.37}$$

in eq. (3.38) to obtain

$$\begin{aligned} l^2_{\rm c,R} &= \frac{6.8 \times 10^{84} Y_0^3 \lambda^6}{\rm GeV} \left(\frac{1}{T_*} - \frac{1}{T_0} \right) \\ &= 2.7 \times 10^8\ {\rm Mpc}^2 Y_0^3 \lambda^6 \left(2.3 \times 10^{28} \sqrt{g_*} Y_0^3 \lambda^4 - \frac{\rm GeV}{T_0} \right). \end{aligned} \tag{3.38}$$

We find that the integrand is dominated by contributions near $T_{\rm NR}$, giving us the approximate expression

$$l^2_{\rm c,R} \approx 6.1 \times 10^{36}\ {\rm Mpc}^2 \sqrt{g_*} Y_0^6 \lambda^{10}. \tag{3.39}$$

3.5.2.2 $T_{\rm NR} \to T_{\rm dec}$

After t_{NR}, number-changing processes cease but elastic processes can continue. These $2 \leftrightarrow 2$ processes only decouple when

$$\Gamma_{\rm elast} = n \langle \sigma^{\rm (NR)}_{\rm elast} v \rangle \approx H = \frac{1}{2t} = \frac{g_*^{1/2} T_{\rm sm}^2}{2 c_T^2}. \tag{3.40}$$

For a decoupled non-relativistic species, $\tilde{T} \sim 1/a^2 \sim T_{\rm sm}^2$, so we find

$$\tilde{T}(T_{\rm sm} < T_{\rm NR}) = m_{\rm dm}\left(\frac{T_{\rm sm}}{T_{\rm NR}}\right)^2. \tag{3.41}$$

The non-relativistic temperature dependence of Z is determined [13] by

$$\begin{aligned} \mu(\tilde{T} < m_{\rm dm}) &= m_{\rm dm} + (\mu(\tilde{T}_{\rm NR}) - m_{\rm dm})\tilde{T}/\tilde{T}_{\rm NR} \\ \implies Z(\tilde{T} < m_{\rm dm}) &= \frac{Z_{\rm NR}}{e} e^{m_{\rm dm}/\tilde{T}}, \end{aligned} \tag{3.42}$$

with

$$Z_{\rm NR} = \frac{\pi^4 g_*}{90 g}\frac{r}{\Theta_f^4} = \frac{\pi^4 \kappa}{90}\frac{g_*}{g}\frac{T_{\rm NR}^3}{m_{\rm dm}^4}, \tag{3.43}$$

so that

$$\begin{aligned} n(T_{\rm sm} < T_{\rm NR}) &= g\left(\frac{m_{\rm dm}\tilde{T}}{2\pi}\right)^{3/2} Z(\tilde{T}) e^{-m_{\rm dm}/\tilde{T}} \\ &= \frac{\pi^{5/2}\kappa}{180\sqrt{2}e} g_* \frac{T_{\rm sm}^3}{m_{\rm dm}}. \end{aligned} \tag{3.44}$$

We also have the non-relativistic elastic cross-section

$$\langle \sigma_{\rm elast}^{\rm (NR)} v\rangle = \frac{\lambda^2}{16\pi^{3/2}}\frac{\tilde{T}^{1/2}}{m_{\rm dm}^{5/2}}. \tag{3.45}$$

Putting this all together, we get the SM temperature when $n\langle \sigma_{\rm elast}^{\rm (NR)} v\rangle = H$:

$$T_{\rm dec} = \frac{3.5\times 10^{-18} m_{\rm dm}^{3/2}}{\lambda^3\sqrt{\rm GeV\, g_* Y_0^3}}. \tag{3.46}$$

The thermally-averaged velocity can be calculated following [43]:

$$\langle v\rangle^2 = \frac{8}{\pi}\frac{\tilde{T}}{m_{\rm dm}} = \frac{8}{\pi}\frac{\Theta_f^2}{m_{\rm dm}^2} T_{\rm sm}^2. \tag{3.47}$$

We plug eqs. (3.44) and (3.47) into eq. (3.48) to obtain

$$l_{\rm c,NR}^2 \approx 1.5\times 10^{43}\ {\rm Mpc}^2 \sqrt{g_*} Y_0^6 \lambda^8. \tag{3.48}$$

where in the approximation we have again taken advantage of the fact that, like $l_{\rm c,R}$ above, $l_{\rm c,NR}$ is dominated by contributions near the integral's lower limit.

3.5.2.3 $T_{\rm dec} \to T_{\rm EQ}$

If elastic decoupling takes place before matter-radiation equality, the particles will then free-stream for some additional distance. The free streaming length scale is given by

$$\begin{aligned} l_{\rm FS} &= \int_{t_{\rm dec}}^{t_{\rm EQ}} {\rm d}t \frac{v}{a} \approx \int_{t_{\rm dec}}^{t_{\rm EQ}} {\rm d}t \frac{a_{\rm NR}}{a^2} \\ &= 1.7 \times 10^{21} g_*^{1/4} Y_0^3 \lambda^4 \left(\log \left[\frac{m_{\rm dm}^3}{{\rm GeV}^3 g_* Y_0^3 \lambda^6} \right] - 38.4 \right) \ {\rm Mpc}. \end{aligned} \tag{3.49}$$

If elastic scattering decouples instead *after* matter-radiation equality, collisional damping runs down to $T_{\rm EQ}$ and free-streaming never contributes.

3.5.2.4 Total length scale

We can see from the approximate expressions for the collisional length scales, eqs. (3.39) and (3.48), that the non-relativistic scale always dominates the relativistic one:

$$\frac{(l_{\rm c,R})^2}{(l_{\rm c,NR})^2} \approx 5 \times 10^4 \left(\frac{m_{\rm dm} Y_0 \lambda a^2}{\rm GeV} \right)^{3/2} < 5 \times 10^{-10} \lambda^3 < 10^{-6}, \tag{3.50}$$

where we have used the ranges set out in section 3.5.1.1. We therefore need just consider $l_{\rm c,NR}$ and $l_{\rm FS}$.

If $t_{\rm dec} < t_{\rm EQ}$, we have free-streaming and

$$\begin{aligned} l_{\rm tot} &\approx \sqrt{(l_{\rm c,NR})^2 + (l_{\rm FS})^2} \\ &\approx 3.8 \times 10^{24} g_*^{1/4} Y_0^3 \lambda^4 \sqrt{1 + 0.2 \left(\log \left[\frac{m_{\rm dm}^3}{{\rm GeV}^3 g_* Y_0^3 \lambda^6} \right] - 38.4 \right)^2} \ {\rm kpc}. \end{aligned} \tag{3.51}$$

On the other hand, if $t_{\rm dec} > t_{\rm EQ}$, we have merely the contribution from diffusion:

$$l_{\rm tot} \simeq 2 \times 10^{-3} \, {\rm kpc} \left(\frac{m_{\rm dm}}{\rm GeV} \right)^{3/2} \left(\frac{Y_0}{10^{-8}} \right)^{3/2} \left(\frac{\lambda}{0.1} \right) . \tag{3.52}$$

It is worthy of note that we find it is only for a subset of Y_0 values that the total length scale can ever exceed 100 kpc. That is to say, outside of this range, there is no choice of $m_{\rm dm}$ and λ consistent with the other constraints which gives an $l_{\rm tot} > 100$ kpc. We thus need only concern ourselves with the damping scales for $Y_0 \in (\sim 7 \times 10^{-10}, \sim 10^{-7})$. This will be evident from the plots we discuss below.

3.5.3 Plots

In figs. 3.6 to 3.8 we summarise the constraints on the $\lambda - m_{\rm dm}$ plane for this particular model of RFI with $\alpha = 0$ for different choices of the initial value of the yield, $Y_0 = 10^{-8}, 10^{-7}, 10^{-12}$ respectively.

In fig. 3.6, with $Y_0 = 10^{-8}$ the λ-independent upper bound on the mass (red region) coming from the requirement that some evolution in the fast region occurs is given by eq. (3.25) to be $m_{\rm dm} < 43.4$ MeV. The exclusion regions corresponding to the self-interaction "Halo Limit" (blue area) and restrictions on the damping scales (beige area) rule out the large λ values apart from a wedge around $m_{\rm dm} \sim 20$ MeV. The requirement that the number-changing $4 \longrightarrow 2$ interactions do not become important (orange area) rules out a slice at small λ.

The sharp corner to the damping-excluded beige-coloured region indicates the crossover at which the elastic-scattering decoupling temperature falls below $T_{\rm EQ}$, which to a first approximation switches the damping off at a relatively earlier scale. Also indicated in fig. 3.6 is a dashed vertical line. This line shows where the damping scale limit would fall, everything to the right being ruled out, if there were no self-interactions, that is, if the DM was able to free stream from early times.

Although in the plot we show the $\lambda - m_{\rm dm}$ plane we can convert easily to limits on r for a given Y_0 by using eq. (3.19). For example, from fig. 3.6 we can deduce that the maximum value of r permitted for $Y_0 = 10^{-8}$ is $r \sim 2 \times 10^{-2}$.

In fig. 3.7, the $\lambda - m_{\rm dm}$ parameter space for $Y_0 = 10^{-7}$ is displayed. As discussed above, the limits from structure formation no longer impinge on the parameter space, nor do those from $\Delta N_{\rm eff}$. This is due to the factor of ten reduction in the upper limit on the DM mass now appearing at $m_{\rm dm} = 4.3$ MeV and the limits from the halo measurements in this mass range being much stronger than those coming from the damping scales or dark radiation. The maximum value for r for $Y_0 = 10^{-7}$ is $r \sim 10^{-3}$.

In fig. 3.8 we show the $\lambda - m_{\rm dm}$ parameter space for $Y_0 = 10^{-10}$. With Y_0 being small the upper limit on the DM mass increases to $m_{\rm dm} = 4.3$ GeV. The constraints from structure formation are not relevant in this case due to the small Y_0 and the halo limit is only relevant for a very tiny slice at low masses not visible in the plot. There are two limits on the maximum value of λ, one coming from BBN (combining eqs. (1.21) and (3.24)) and the second from the perturbativity of λ. The perturbativity limit (not displayed in fig. 3.8) is the strongest of these two with the maximum value for r in this case being $r \sim 5 \times 10^{-6}$.

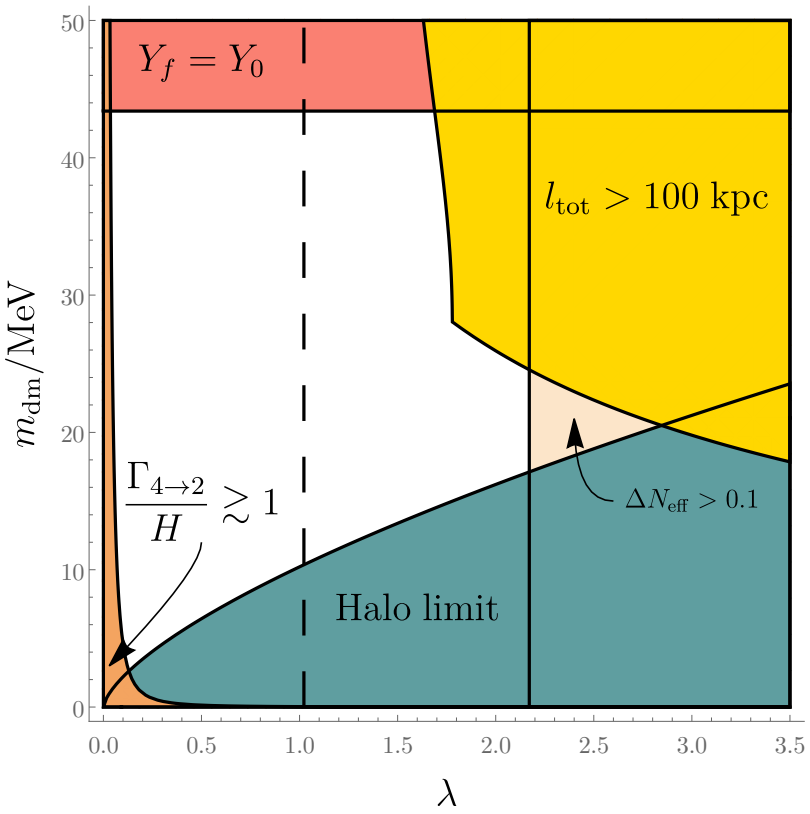


Figure 3.6: The $\lambda - m_{\rm dm}$ parameter space for $Y_0 = 10^{-8}$. The red region eliminates those points for which $Y_0 = Y_f$, the blue those which violate the bound in eq. (3.28), the yellow those for which $l_{\rm tot} > 100$ kpc, the orange those for which cannibalistic processes may occur and the beige those for which $\Delta N_{\rm eff}(t_{\rm BBN}) > 0.1$. The region to the right of the light vertical dotted line would be excluded in the case of no self-interactions, see text for details.

3.6 Remarks

In this chapter we have presented the RFI mechanism for DM production. DM resides in an initially ultra-relativistic, far under-populated secluded sector and undergoes a period of rapid number density increase via $2 \to k$ processes. This converts the initially large DM kinetic energy to mass, in the form of additional DM states. The relic abundance is set by the point at which the DM temperature drops below its mass, at which stage the $2 \to k$ ($k > 2$) processes become inefficient.

We have made some simplifying assumptions that have allowed us to present a straightforward analytic understanding of the mechanism. Most fundamentally, we have so far assumed that *kinetic* equilibrium is quickly established in the secluded sector by elastic interactions, so that the distribution functions are determined solely by an evolving temperature and chemical potential. This enabled us to write down a simple evolution equation for the DM yield, eq. (3.14). However, the RFI mechanism does *not* require that

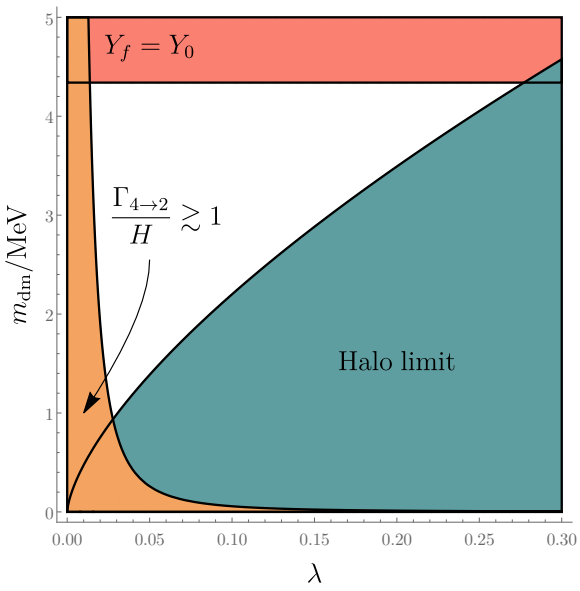


Figure 3.7: The $\lambda - m_{\rm dm}$ parameter space for $Y_0 = 10^{-7}$. Conventions as described in fig. 3.6.

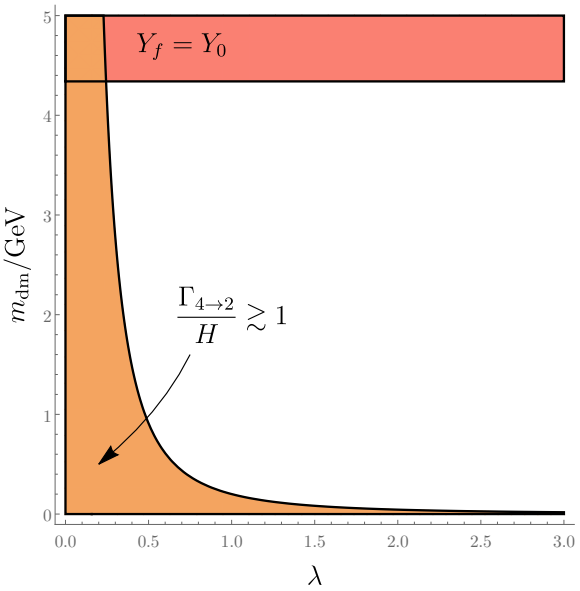


Figure 3.8: The $\lambda - m_{\rm dm}$ parameter space for $Y_0 = 10^{-10}$. Conventions as described in fig. 3.6.

full kinetic equilibrium is established. The distribution functions could have significant non-thermal 'tails' or other features which change the resulting DM yield, or alter the astrophysical and cosmological signatures in interesting ways (for instance there could remain a small ultra-relativistic sub-component of the DM until late times), though such an investigation goes beyond the scope of this thesis. Even if our simplifying assumption of kinetic equilibrium is a good approximation, there are a number of issues that deserve investigation. Important aspects to follow up on include the thermal corrections to the DM masses and couplings. Although these considerations will not modify the general picture of the mechanism, they may change some of the detailed behaviour, in particular where the evolution tracks the ultra-relativistic secluded sector. Late-time exothermic 'cannibal' interactions are also a natural possibility in this class of models. In this treatment we have assumed that g_* and thus r are constant all the way down to $T_{\rm EQ}$. The formalism of RFI freely admits a more detailed approach in which g_* and thus r vary over time.

Again for simplicity we have assumed that there is one dominant number-changing interaction, with one fixed temperature dependence, that is, one particular value of α. Often this will not be the case. For example, if the secluded sector consists of multiple particles the temperature dependence of the collision term, eq. (3.12), may change dramatically as the DM temperature drops below mass thresholds of states involved in the number-changing interactions driving RFI. Resonance effects may also play a material role.

Since this chapter was concerned with exploring the general features of the RFI mechanism, we haven't studied specific implementations beyond the $\lambda\phi^4$ model examined in section 3.5. However we emphasise that many models previously considered in the context of self-interacting or cannibal DM, such as hidden-sector 'pion' DM [136–138] and possibly glueball DM [138–142], also have a regime of parameter space where the RFI mechanism determines the DM density. The confinement transition, though, must be carefully examined in the non-equilibrium case of a far-under-populated, high-temperature sector.

The DM self-interactions studied in this paper could also play a role in alleviating the present σ_8 and Hubble tensions [143–145], due to such effects as a DM viscosity [146], or due to the collisional-damping/free-streaming studied in section 3.5, and/or a possible sub-component of the DM (which could either be the non-thermalised 'tail' mentioned above, or a new light state mediating the elastic and inelastic interactions) acting as dark radiation (see e.g., [147]).

Finally we note that in this paper we have strictly forbidden any SM-DM interactions. As we discussed, the mechanism is still testable by virtue of the fact that the same self-interaction is responsible for the DM number-changing interactions that determine the relic abundance and the elastic scattering processes that may be potentially observable in, or at least constrained by, structure formation. If, however, we relax this restriction on SM-DM interaction it may be possible for this mechanism to admit decaying DM signals [148][6], or other interesting effects.

[6]Note the DM can be superheavy $m_{\rm dm} \gg$ TeV as long as it was also initially ultra-relativistic

Statement of Authorship for joint/multi-authored papers for PGR thesis

To appear at the end of each thesis chapter submitted as an article/paper

The statement shall describe the candidate's and co-authors' independent research contributions in the thesis publications. For each publication there should exist a complete statement that is to be filled out and signed by the candidate and supervisor **(only required where there isn't already a statement of contribution within the paper itself).**

Title of Paper	Reproductive Freeze-In of Self-Interacting Dark Matter
Publication Status	☑ Published ☐ Accepted for Publication ☐ Submitted for Publication ☐ Unpublished and unsubmitted work written in a manuscript style
Publication Details	Physical Review D 102 (2020) 8, 083018 J. March-Russell, H. Tillim, S. M. West

Student Confirmation

Student Name:	Hannah Tillim		
Contribution to the Paper	Equal part in generation of ideas and calculations, and took the lead in the phenomenology section.		
Signature		Date	8th June 2022

Supervisor Confirmation

By signing the Statement of Authorship, you are certifying that the candidate made a substantial contribution to the publication, and that the description described above is accurate.

Supervisor name and title:	Prof. John March-Russell		
Supervisor comments	Hannah's statement correctly characterises her valuable and fully equal contribution to our research and published paper.		
Signature		Date	8th June 2022

This completed form should be included in the thesis, at the end of the relevant chapter.

Chapter 4
Axiverse strings

4.1 Introduction

In section 1.4 we discussed the Strong CP problem and its solution, with associated axion excitation, as well as axion-like particles. In addition to particle excitations of $a(x)$, we also considered topologically non-trivial axion cosmic string solutions (see section 1.5) where $a(x)$ winds as some loop in physical space is traversed [65, 149]. Then, for QFT axions, $|\Phi(x)|$ necessarily has a zero at some location, and this core region explores and is sensitive to UV physics.

The tension, $T \sim f_a^2 \log(Lf_a)$, with f_a the axion decay constant, of such global strings IR diverges with the system size L, and moreover they become the boundaries of axion domain walls once $a(x)$ acquires a mass, and are thus formally "confined". Cosmologically, however, the inter-string separation provides an IR cutoff, and as discussed in section 1.5, long-lived domain walls are physically feasible and responsible for interesting phenomenological signatures.

We here consider the physics of cosmic strings built from the axions which are expected to be ubiquitous in string theory (section 1.6), which we call *axiverse strings*. While aspects of string axions and of axiverse cosmic strings have been explored, to the best of our knowledge none have touched on the physics of solutions in the presence of moduli stabilisation. Yet we know that such stabilisation is vital for physical models. Below we will present such a model which stabilises the scalar saxionic partner of a winding axionic field.

4.2 Basics

As in the examples we presented in section 1.6, we are considering the simple case of compactification on a 6-manifold $Y_4 \times T^2$, the ALP arising from the 2-form B_2 with legs in the T^2 directions (coordinates y_i, $i = 1, 2$). We do not need to specify Y_4 for this treatment.

If h_{ij} is the T^2 internal metric, then

$$\rho(x) \equiv B_{12} + i\sqrt{\det h} \equiv \rho_1 + i\rho_2 \tag{4.1}$$

is the dimensionless complexified Kähler 'size' modulus, and ρ_1 is our ALP of period 1. The domain, $\mathcal{F}$, of inequivalent ρ fields is the upper-half $\mathbb{C}$-plane modulo $SL(2,\mathbb{Z})$, as we displayed in fig. 1.17.

We modify the $4d$ action[1] of the light fields (eq. (1.63)) by the addition of a potential term that depends only on ρ_2:

$$S = M^2 \int d^4x\sqrt{-\det g}\left\{g_{\mu\nu}\frac{\partial^\mu\rho\partial^\nu\overline{\rho}}{4\rho_2^2} - V(\rho_2)\right\} . \tag{4.2}$$

In section 4.6 the effect of an additional non-perturbative potential for the axion is explored, assuming a well-separated hierarchy of scales $V(\rho_2) \gg \tilde{V}(\rho_1)$, so ρ_2 is much heavier than ρ_1.

We can make certain model-independent statements about the potential $V(\rho_2)$:

1. It must go to zero in the 'decompactification limit' $\rho_2 \to \infty$ [150–154].

2. It must have a local minimum at some $\rho_2 = b > 0$, with $V(b) \simeq 0$, for stabilisation.

3. We require $b \gg 1$ so that the stabilizing T^2 is large and the leading-order action, eq. (1.60), is appropriate. This is also necessary to sufficiently suppress the non-perturbative effects that would otherwise lift all ALP masses and eliminate the axiverse [96].

We thus take $V(\rho_2)$ to be of the form shown in fig. 4.1. A toy-model potential with these properties is

$$V(\rho_2) = \mu^2 e^{-a\rho_2}(\rho_2 - b)^2 , \tag{4.3}$$

where $\mu^2 e^{-ab} \ll M^2$ sets the scale. The canonical modulus mass is

$$m_c = \sqrt{2}\mu e^{-ab/2} \tag{4.4}$$

at $\langle\rho_2\rangle = b$.

The solution is indifferent to the shape of V for $\rho_2 < b$ as long as b is a minimum, while the exponential decline of $V(\rho_2 \to \infty)$ in eq. (4.3) is for convenience - all results are qualitatively unaffected as long as $V(\rho_2 \to \infty) \sim 1/\rho_2^n$ for $n > 0$.

To proceed, we initially freeze the metric $g_{\mu\nu}(x) = \eta_{\mu\nu}$. For an infinite string along the x_3-axis the solution depends only on the transverse coordinates $z \equiv x_1 + ix_2 \equiv r\exp(i\theta)$. In

[1] In section 4.4. we return to this and discuss the physics that sets the scale M.

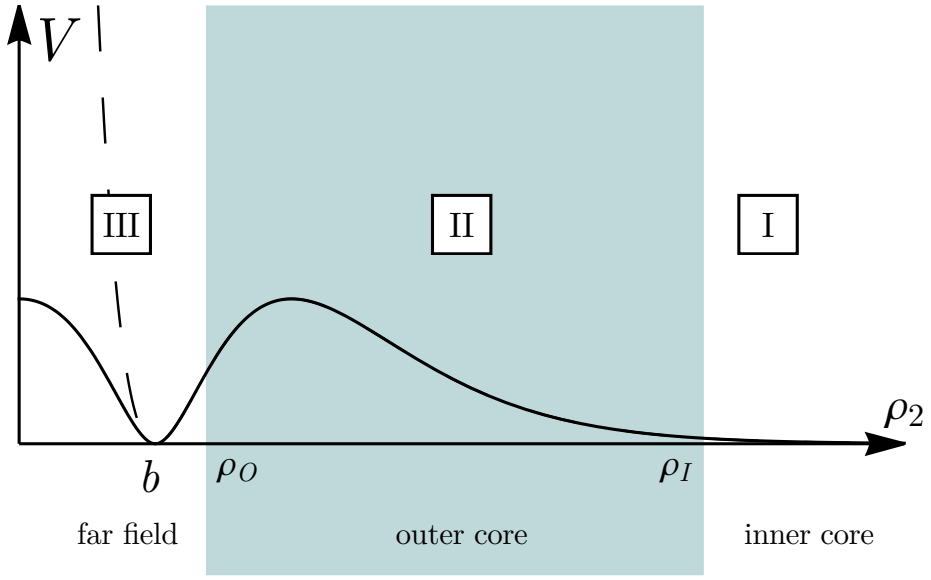


Figure 4.1: General shape of $V(\rho_2)$, with the three regions delineated.

the absence of V, the equation following from eq. (4.2) is solved by any (anti)meromorphic ρ (section 1.6.1). However, these solutions are not directly physically relevant as they are greatly altered by the potential. Thus consider the ansatz

$$\rho_1 = \theta/2\pi,\ \rho_2 = \rho_2(r) \tag{4.5}$$

for the elementary winding number $w = 1$ string. This leads to

$$\frac{d^2\rho_2}{dr^2} + \frac{1}{r}\frac{d\rho_2}{dr} - \frac{1}{\rho_2}\left(\frac{d\rho_2}{dr}\right)^2 + \frac{1}{4\pi^2 r^2 \rho_2} = 2\rho_2^2 \frac{dV}{d\rho_2}\,, \tag{4.6}$$

with $\rho_2(r \to 0) \to \infty$, and $\rho_2(r \to \infty) \to b$. The solution is then found by stitching three regions - see figs. 4.1 and 4.2:

Region I (inner core):	$0 < r < r_I$	$\infty > \rho_2 > \rho_I$
Region II (outer core):	$r_I \le r \le r_O$	$\rho_I \ge \rho_2 \ge \rho_O$
Region III (far field):	$r_O < r < \infty$	$\rho_O > \rho_2 > b$

The boundaries of Region II are set by the point at which the approximations of Regions I and III fail at the 10% level. For $V(\rho_2)$ of eq. (4.3) we take matching values $\rho_O \equiv b + 1/a$ and $\rho_I \equiv b + 8/a \gg 1$. The features of the string solution do not depend on these specific choices.

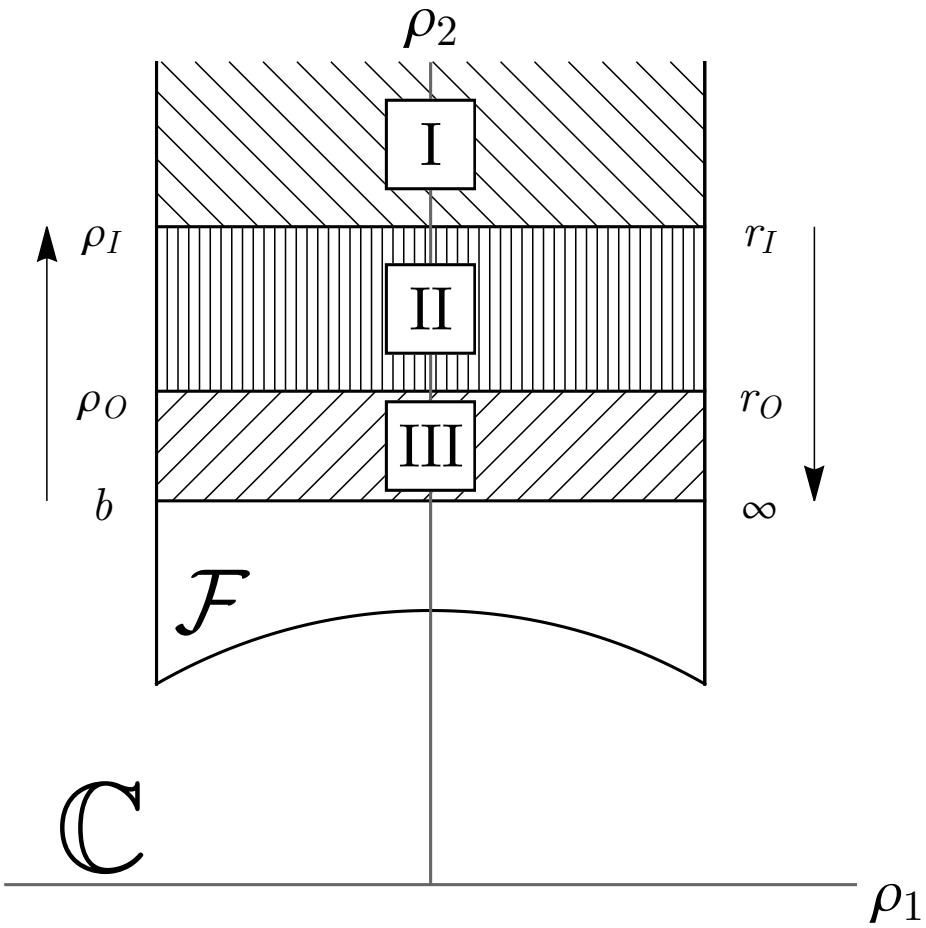


Figure 4.2: Domain $\mathcal{F}$ of T^2 Kähler moduli space with regions explored by I) inner core ($r < r_I$), II) outer core ($r_I \leq r \leq r_O$), III) far field ($r > r_O$), indicated.

Region I

In the inner-core, where $\rho_2 \to \infty$, V can be neglected, giving an approximate solution[2] valid for $\rho > \rho_I \gg 1$,

$$\rho(z,\overline{z}) \simeq -\frac{i}{2\pi}\log(cz), \quad c = \frac{\exp(-2\pi\rho_I)}{r_I} \,. \tag{4.7}$$

Region III

In Region III, V is important, and the solution asymptotes to $\langle\rho_2\rangle = b$. The solution in the $r > r_O$ region is

$$\rho_2 = b + \frac{b}{(2\pi b\, m_c r)^2} + \dots \,, \tag{4.8}$$

with $1/r^2$ behaviour characteristic of global cosmic strings. Given $\rho_O = b + 1/a$ the outer core radius is then $r_O \simeq (a/b)^{1/2}/2\pi m_c$.

Region II

In between there is an 'outer core' transition region, either 'thick' or 'thin'. The numerically-derived, non-universal, outer-core solution stitches Region I and III together.

4.3 The axiverse string tension

The action, eq. (4.2), implies the $w = 1$ total tension is

$$\begin{aligned} T &= 2\pi M^2 \int dr r \left[\frac{(\partial_r \rho_2)^2}{\rho_2^2} + \frac{1}{4\pi^2 r^2 \rho_2^2} + \mu^2 e^{-a\rho_2} (\rho_2 - b)^2 \right] \\ &\equiv T_I + T_{II} + T_{III}, \end{aligned} \tag{4.9}$$

where we have split into contributions $T_{I,II,III}$ from the three regions.

In Region I, the holomorphicity of the solution, eq. (4.7), allows one to pull back the non-potential parts of the integral in the first line of eq. (4.9) to the domain of ρ:

$$T_I = -i2\pi M^2 \int_{\mathcal{F}} d\rho d\overline{\rho}\; \partial_\rho \partial_{\overline{\rho}} \log \rho_2 = \frac{\pi M^2}{\rho_I} \,. \tag{4.10}$$

[2] As the ρ domain is $\mathcal{F}$, rather than a strip of $\mathbb{C}$ as naively given by eq. (4.7), in principle a more precise core solution is $j(\rho) = 1/cz$ where Klein's modular j-function maps the fundamental domain, $\mathcal{F}$, to $\mathbb{C}$ [100]. However for realistic strings with moduli stabilised the solution is only needed for $c|z| \ll 1$. In terms of $q \equiv \exp(2\pi i\rho)$, $j(\rho) \simeq q^{-1} + 744 + O(q)$ for $|q| \ll 1$. In this limit $\rho(z) \simeq -i\,(\log cz + 744\, cz + \dots)\,/2\pi$ agreeing with eq. (4.7) up to errors of $< 1\%$ for $\rho_2 > b > 2$ - intriguingly slightly deviating from cylindrical symmetry as $\rho_1 \simeq (\theta + 744\, cr \sin\theta + \dots)/2\pi$.

Here we have used Stokes' theorem to obtain a line integral with only contribution the horizontal line at $\rho_2 = \rho_I$. Note that this contribution does not depend on the physical size of the inner core, and in particular it is *finite* despite the fact that $\rho_2 \to \infty$ ('decompactification') at the origin in the effective theory. The expression for ρ_I will depend on the potential chosen; for eq. (4.3) we find $\rho_I \approx b + 8/a$, so

$$T_I = O(M^2/b). \tag{4.11}$$

In Region III, the kinetic contribution dominates over the potential, giving us

$$T_{III} = \frac{M^2}{8\pi b^2} \log\left[\frac{L}{r_O}\right] + O(M^2/b^6), \tag{4.12}$$

where L is a cutoff given by inter-string separation within a string network, or at worst by the Hubble radius, as discussed in section 1.5.1.

Region II is also dependent on the exact form of the potential. Using eq. (4.3), we find

$$T_{II} \simeq \frac{2M^2}{b} f(r_I/r_O), \tag{4.13}$$

where f is a function of the ratio of inner to outer radii of the inner core. We find that the ratio is typically very small (thick wall, $r_I \ll r_O$) and $f \sim 1$. We therefore have

$$T_{II} = O(M^2/b). \tag{4.14}$$

Putting this all together, we find the tension dominated by the Region III kinetic term, so that the total is of precisely the form of a field theory global cosmic string, logarithmically divergent with radius.

Finally note that the action eq. (4.2) and domain of the T^2 complex structure modulus τ are identical to that for ρ, so these results apply to T^2 complex structure strings too.

4.4 Gravity and the core

For $r > r_O$ the tension of an axiverse string goes as a conventional global string, naively IR-divergent, eq. (4.12). For an isolated infinitely long static string this leads to a metric singularity at large distances [155], but for the realistic situation of a string network the inter-string separation gives a finite effective L, and the metric is smooth. At intermediate distances, $r_O < r < L$, and the 4d metric is well approximated by eq. (1.43) in the observationally-required limit $k(r) \equiv 4G_N T_1(r) \ll 1$, with a $V(\rho_2)$-dependent constant k_0 determined by numerically matching to the core solution

$$ds^2 \simeq (1-k(r)+k_0)(dt^2 - dx_3^2) - dr^2 - (1-2k(r))r^2 d\theta^2. \tag{4.15}$$

The mass scale, M, of the action eq. (4.2), equivalently the axion decay constant $f_{\rm eff} = M/(\sqrt{2}\,\langle\rho_2\rangle)$, may be greatly reduced compared to $M_{\rm pl}$ if warped compactifications [98, 156, 157] are considered[3] with the cycle on which the ALP is defined localised in the IR region with warp factor $e^{-w_0} \ll 1$. M may also be lowered in SM-on-a-brane large volume compactifications with large string length $\ell_s \equiv 2\pi\sqrt{\alpha'}$ [98]. Both constructions allow $4G_N T_1(r) \ll 1$ consistent with the gravitational constraints on cosmic strings (see e.g. [158]).

In the inner core the ansatz $ds_4^2 = dt^2 - dx_3^2 - p(z,\overline{z})dzd\overline{z}$ does not alter eq. (1.65), so eq. (4.7) is still a solution [100]. Analysis of the 4d Einstein equations shows that $p(z,\overline{z}) \sim -\log(r)$ as $r \to 0$. Importantly, since the decompactification is localised in 4d, $M_{\rm pl}$ remains finite, set by the asymptotic $\langle\rho_2\rangle = b$.

Strictly, though, the 4d effective theory breaks down for *local* experiments in the inner core as $r \to 0$. A better description follows from a 6d theory with ρ_1, ρ_2 replaced by B_2, h_{mn}. One then sees that the B_2 and metric configuration is due to an effective string in 6d oriented along the x^3 axis that magnetically sources B_2 – the NS5-brane[4] of heterotic or type II theories (see section 1.6) wrapped on the Y_4 part of $Y_4 \times T^2$. Such an effective string is well known [93, 94].

We can measure the magnetic charge of the NS5 by integrating the $B_2 = \rho_1(x)\omega_2$ (see eq. (1.56)) flux over the boundary at $r \to \infty$, which is a product of an S^1 in the $x-y$ plane with the internal T^2, and find it is equal to the winding number of the string:

$$\begin{aligned}\int_{S^1\times T^2} H_3 &= \int dB_2 = \int_{S^1} d\rho_1 \int_{T^2} \omega_2 \\ &= \int_{S^2} d\rho_1 \equiv w,\end{aligned} \tag{4.16}$$

where we have used the definition of the cycle/cocycle dual basis of the torus $\int_{T^2}\omega_2 = 1$, and w is exactly the winding number of the cosmic string.

The dilaton becomes dynamical at scales $r \lesssim 1/m_\varphi$, and the physics deviates from the inner-core solution as presented in section 4.2. The full 10d NS5-brane solution [93] becomes asymptotically operative as $r \lesssim \min(1/m_\varphi, R_4)$ where R_4 is the linear size of Y_4. The connection of such wrapped brane sources with axionic cosmic string solutions has also been recently noted [159, 160].

[3] Our calculations remain valid provided all the cycles giving rise to our ALPs are at the same level of the warped throat and thus equally warped.

[4] In other cases, involving ALPs from RR k-forms the effective string at the core of the solution is a suitable wrapped D-brane.

4.5 General axiverse strings

We can generalise this analysis to large classes of axiverse strings. The solution depends on the $G_{i\bar{j}}(m,\overline{m})$ metric behaviour in the limit $G_{i\bar{j}} \to 0$, as well as the potential $V(m,\overline{m})$. As before, we assume V has three properties: a) There is a local minimum with $V \simeq 0$ at which all non-ALP saxion moduli, $\mathrm{Im}(m^i)$, are stabilised; b) stabilisation occurs at $\langle \mathrm{Im}(m^i) \rangle = b^i \gg 1$ to have control over the 4d effective action; c) For $\mathrm{Im}(m^i) \to \infty$, $V \to 0$.

The string solution is then a semi-geodesic "force-modified-motion" on the moduli space found by solving

$$\boldsymbol{\nabla}^2 m^i + \Gamma^i_{jk}(m)(\boldsymbol{\nabla} m^j).(\boldsymbol{\nabla} m^k) = \partial_i V(m)\,, \tag{4.17}$$

subject to appropriate boundary conditions. Here Γ is the connection derived from G. The metric is most important in the core where the effects of V are small.

In addition to the heterotic and type II ALPs arising from B_2, type II strings on a CY orientifold Z also have ALPs arising from RR k-forms C_k (see section 1.6). As orientifolds now have fields and basis forms split into even/odd sectors, for IIA the result is $h^{1,1}_-$ complex Kähler moduli T^i defined by expanding $B_2 + iJ = T^i\omega_i = (b^i + it^i)\omega_i$ where ω_i is a basis of $h^{1,1}_-$ odd (1,1)-forms and J is the Kähler (1,1)-form of Z. The saxion components t^i measure the (dimensionless) size of 2-cycles of Z. These are accompanied by $h^{2,1}+1$ CS moduli, including the axio-dilaton, with ALPs β^a defined by $C_3 = \beta^a(x)\alpha_a$. Here α_a are a basis of even harmonic 3-forms on Z [98, 161].

For IIB, there are $h^{1,1}_+$ Kähler moduli with ALPs c^i defined by $C_4 = c^i(x)\tilde{\omega}_i$ where $\tilde{\omega}_i$ are a basis of even $(2,2)$ forms dual to the even (1,1)-forms. The associated saxion components $\tau^i(x)$ measure the size of 4-cycles of Z. In addition there are $h^{1,1}_-$ ALPs d^i arising from $C_2 = d^i(x)\omega_i$, and also the 4d axio-dilaton field S [161, 162].

All the above are 'closed-string' axions, but a wide variety of ALPs exist in Type I string theory and M-theory, and there often arise other potential axions. A fraction of these ALPs can be made massive at tree level by a variety of mechanisms, but some remain massless before non-perturbative lifting, and are candidates for associated axiverse strings.

Turning to the kinetic metric, consider, eg heterotic and IIA Kähler $T^i = b^i + it^i$ moduli. Since for a 6d CY its volume $\mathcal{V}(x) = \kappa_{ijk}t^it^jt^k/6$ where $\kappa_{ijk} = \int_Z \omega_i \wedge \omega_j \wedge \omega_k$ is the integer-valued triple intersection number, and the leading Kähler potential is of form $K = -2\log(\mathcal{V} + \dots)$ one finds for heterotic and IIA cases [163, 164]

$$G^{B_2}_{i\bar{j}}(x) = \frac{\kappa_{ikl}t^kt^l\kappa_{jmn}t^mt^n}{16\mathcal{V}^2} - \frac{\kappa_{ijk}t^k}{4\mathcal{V}} + \dots \tag{4.18}$$

up to corrections which are small if $t^i \gg 1$. Note that $G^{B_2}(t^i \to \infty) \sim 1/t^2$ just like the $1/\rho_2^2$ scaling of the T^2 metric. Up to a factor of the coupling g_s^2 the metric for the C_2 and 2-cycle d^i ALPs in IIB is identical to eq. (4.18), while for the c^i-moduli of IIB arising from C_4 and 4-cycles

$$G^{C_4}_{i\bar{j}}(x) = g_s^2 \left(\frac{t^i t^j}{8\mathcal{V}^2} - \frac{(\kappa_{ijk} t^k)^{-1}}{2\mathcal{V}} \right) + \ldots , \tag{4.19}$$

an implicit function of the 4-cycle (strictly, divisor) volumes $\tau_i = \kappa_{ijk} t^j t^k/2$. As $\tau^i \to \infty$, $G^{C_4} \sim 1/\tau^2$.

A simple two Kähler moduli example is the IIB orientifold of a degree-18 hypersurface in $\mathbb{P}^4_{(1,1,1,6,9)}$ with $\mathcal{V} = (3t_1^2 t_5 + 18 t_1 t_5^2 + 36 t_5^3)/6$ where t_1, t_5 are the 2-cycle volumes (in the notation of [165] where it was argued that all CS and dilaton moduli can be stabilised by fluxes, and later successful Kähler moduli stabilisation [166]). The 4-cycle volumes, the partners of the $c^{4,5}$ ALPs from C_4, are $\tau_4 = t_1^2/2$ and $\tau_5 = (t_1 + 6t_5)^2/2$ giving $\mathcal{V} = (\tau_5^{3/2} - \tau_4^{3/2})/9\sqrt{2}$. The G^{C_4} metric is thus

$$\frac{g_s^2}{36\mathcal{V}^2} \begin{pmatrix} [2\tau_4 + \tau_5^{3/2}/\tau_4^{1/2}]/3 & -(\tau_4\tau_5)^{1/2} \\ -(\tau_4\tau_5)^{1/2} & [2\tau_5 + \tau_4^{3/2}/\tau_5^{1/2}]/3 \end{pmatrix}. \tag{4.20}$$

Now consider a string formed by the winding of c^5. The inner core behaviour is found by expanding the metric in the limit $\tau_5 \to \infty$, $\tau_4 =$ fixed, giving a diagonal metric with $G_{55} \simeq 3/\tau_5^2$.

As this is the same $1/\rho_2^2$ scaling as for T^2, and by definition the potential is unimportant in the inner core, the inner core behaviour of $m^5 \equiv c^5 + i\tau^5$ derived from eq. (4.17) is identical to crefeq:innercoresol except the decompactification is to 8d!

In Region III the metric is effectively frozen at its asymptotic value, so one again finds a $1/r^2$ dependence in the appropriate combination of moduli (upon diagonalising the asymptotic metric) as in eq. (4.8), and a tension of the same form as eq. (4.12). Only for the detailed matching in the outer-core region does the full kinetic metric (and potential) need to be kept.

As emphasised in section 4.4, in the deep inner core the axiverse string fields are sourced by an effective 'magnetic' string in the decompactified 8d theory. In the case of an ALP from the RR C_4 this string in 8d arises from a $D3$ brane wrapped over the dual 2-cycle to τ_5 (see also [159, 160]).

In all cases we have examined we have found qualitatively similar behaviour to that of sections 4.2 and 4.4, though we do not know if this covers all axiverse string possibilities.

4.6 Phenomenology

We now briefly discuss aspects of axiverse string phenomenology. The non-perturbative potential for the ALP itself will give it a tiny mass and it is energetically favourable for the ALP winding to fall into a domain-wall configuration (see section 1.5.1). String-derived axion cosmic strings were excluded from consideration in [167] as domain walls make the overall network unstable to decay. Nevertheless the presence of the decaying string network can lead to important physical effects in the expanding universe. In particular, as some of the axiverse ALP masses can be as small as 10^{-20} eV or even $H_0 \sim 10^{-33}$ eV [96], the network can survive to the post-recombination epoch, or even the present. If the axion couples to electromagnetism, strings can give rise to quantised polarisation rotation of CMB photons, as well as zero modes mandated by index theorems and associated forms of superconductivity [82–85, 168–172].

As striking, the *long-distance* $1/r^2$ variation, eq. (4.8), of the associated non-ALP modulus $\mathrm{Im}(m^i)$ leads to new effects characteristic of axiverse strings. One variation that is essentially guaranteed is the mass of the ALP itself, as almost always the non-perturbative effects that set the potential $|\tilde{V}| \sim \exp(-S[\mathrm{Im}(m^i)])$ depend exponentially on $\mathrm{Im}(m^i)$; here S is a suitable instanton action. Moreover SM Yukawa couplings of the light quarks and leptons in string theory also often depend exponentially on moduli as they too are generated non-perturbatively [173–175], so masses and mixings of the light SM fermions can vary strongly in the vicinity of the string. These changes are typically equivalence principle violating.

Finally, we believe that our axiverse cosmic strings will be formed in the early universe by similar physics to that of the D-brane inflation production mechanisms of macroscopic cosmic F- and D-strings [167, 176–178] - however, this requires more careful study.

Statement of Authorship for joint/multi-authored papers for PGR thesis

To appear at the end of each thesis chapter submitted as an article/paper

The statement shall describe the candidate's and co-authors' independent research contributions in the thesis publications. For each publication there should exist a complete statement that is to be filled out and signed by the candidate and supervisor **(only required where there isn't already a statement of contribution within the paper itself).**

Title of Paper	On the Nature of Axiverse Cosmic Strings
Publication Status	☐Published ☐ Accepted for Publication ☑Submitted for Publication ☐Unpublished and unsubmitted work written in a manuscript style
Publication Details	Submitted to Physical Review Letters ArXiv preprint 2109.14637 J. March-Russell, H. Tillim

Student Confirmation

Student Name:	Hannah Tillim		
Contribution to the Paper	Equal collaboration with supervisor, he leading on string theory side and I on construction and investigation of cosmic string solution resulting in analysis presented in sections 4.1 and 4.2.		
Signature		Date	8th June 2022

Supervisor Confirmation

By signing the Statement of Authorship, you are certifying that the candidate made a substantial contribution to the publication, and that the description described above is accurate.

Supervisor name and title:	Prof. John March-Russell		
Supervisor comments	Hannah's statement correctly characterises her valuable and fully equal contribution to our research and published paper.		
Signature		Date	8th June 2022

This completed form should be included in the thesis, at the end of the relevant chapter.

Appendix A
Homology and cohomology

Given a manifold M of dimension m, one is interested in various quantities which characterise its topology. Two of the most important are the homology and cohomology groups - H_i and H^i respectively.

There are many flavours of both homology and cohomology theories, almost all of which we will blithely ignore here - for rigorous and comprehensive treatment see e.g. [161, 179, 180]. The setups we describe here correspond to simplicial homology and de Rham cohomology, and we shall assume we are dealing with connected, path-connected and oriented manifolds M.

Homology

Heuristically[1], homology counts equivalence classes of closed oriented submanifolds of M which are not themselves boundaries of higher-dimensional submanifolds. Given a manifold N of dimension n, called an *n-chain*, define the operator ∂_n from n-dimensional manifolds to $(n-1)$-dimensional manifolds as that which sends $N \to \partial N$, the boundary of N. If $\partial N = \emptyset$, N is *closed* and is called an *n-cycle*; the set of all such is labelled Z_n. If $N = \partial \tilde{N}_{n+1}$, where $\tilde{N}$ is a manifold of dimension $(n+1)$, then N is called a *boundary*; the set of all boundaries is labelled B_n and it is a subset of Z_n (since the boundary of a boundary is empty). Both Z_n and B_n form abelian groups under disjoint union of manifolds $\coprod$.

A homology complex of a manifold M with dimension m is

$$C_m \xrightarrow{\partial_m} C_{m-1} \xrightarrow{\partial_{m-1}} \cdots \xrightarrow{\partial_2} C_1 \xrightarrow{\partial_1} C_0, \tag{A.1}$$

where C_m is the set of m-chains (C_0 is the set of points). The boundary of a boundary is empty, so $\mathrm{im}\partial_n \subset \ker\partial_{n-1}$. We define the n^{th} *homology group* H_n as the quotient (abelian)

[1] In practice the procedure requires a more technical approach involving triangulation of the space to obtain simplices.

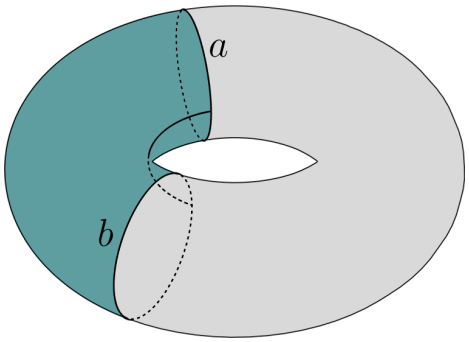


Figure A.1: Two 1-cycles form the boundary of a two-dimensional subsurface of the torus.

group Z_n/B_n:

$$H_n(M) \equiv \frac{\mathrm{im}\partial_{n+1}}{\ker\partial_n}. \tag{A.2}$$

Its elements are n-cycles identified if they differ by a boundary: $N_n \sim N_n' \iff N_n \coprod (-N_n') = \partial\tilde{N}_{n+1}$, where the negative sign indicates opposite orientation. In particular, any boundary belongs to the trivial class.

For example, consider the torus (fig. A.1). A single 1-cycle along the handle of the torus does not enclose anything[2], and so it belongs to a nontrivial homology class. However, the two 1-cycles in the figure, each encircling the handle once, are both in the same nontrivial homology class. That is because $c_2 \coprod (-c_1)$ forms the boundary of an oriented tubular section of the torus - a cylinder. It is for this reason that people sometimes say that H_n 'counts the number of $(n+1)$-dimensional holes'.

The homology groups of the torus are[3] $H_0 \cong \mathbb{Z}, H_1 \cong \mathbb{Z} \oplus \mathbb{Z}, H_2 \cong \mathbb{Z}, H_{n\geq 3} \cong 0$. H_2 is generated by the only 2-cycle of the torus, the entire two-dimensional surface itself. Since the space is two-dimensional, there are no submanifolds of dimension $n \geq 3$, and nothing from which to build those homology groups, so they vanish.

There is a very simple relationship between H_1 and π_1 (the first homotopy group discussed in section 1.5) - the first is the 'abelianisation' of the latter. This is because a 1-cycle, the object of interest for the first homology group, is always realisable as a loop, the object of interest for the first homotopy group; the same is not true of higher-dimensional cycles - for example, a T^2 surface is not topologically equivalent to a sphere. However, while π_1 cares about what order you travel along lobes of your loop (e.g. along the handle then along the equator or vice versa), H_1 cares only about the orientation of each lobe.

[2]Except the 'interior of the doughnut' of which the torus forms the boundary, but this interior is not part of the space.

[3]In any path-connected space, any two points (0 cycles) form the boundary of the path between them (a 1-cycle). Therefore there is a single homology class, and the group is generated by this class, over the integers.

The dimensions of the homology groups are called the *Betti numbers* of the manifold, $b^k = \dim H_k$. *Poincaré duality* states that for M with dimension m,

$$H_k(M) \cong H_{m-k}(M). \tag{A.3}$$

This means, among other things, that $b^k = b^{m-k}$. Note in particular that for a connected path-connected manifold $b^0 = b^m = 1$, explained by the facts that

- any two points form the boundary of a path, and
- there is a unique boundary-less m-dimensional manifold - M itself.

and that $b^{k>m} = 0$ (there are no $(k > m)$-dimensional submanifolds of an m-dimensional manifold).

Cohomology

Differential geometry deals with objects called *differential forms* or k-forms, $k \in \mathbb{Z}_{\geq 0}$. Here we present an extremely quick and dirty review to motivate the cohomology of forms (de Rham cohomology).

Differential forms

Given a manifold M of dimension m and coordinates $\{x^\mu\}$ in some chart ϕ, over a field F, a 0-form f is simply a function $f : M \to F$. The space of all functions is called $\mathcal{F}(M)$ or $\Omega^0(M)$.

Consider the set of all possible curves through M passing through point p. There is a *tangent space* at p, T_p formed by the maps $V_p : \Omega^0 \to F$. Each map takes a function f to the derivative (at p) of f along some curve $\gamma(\lambda)$, where λ is the parameter of the curve, $V_p : f \mapsto V_p[f] = df/d\lambda|_p = V_p^\mu \partial_\mu f(p)$, where $V_p^\mu = dx^\mu/d\lambda$. The coordinate basis of T_p in the chart ϕ is $\{\partial_\mu\}$. A *vector field* V is one defined smoothly on all of M, $V(p) \equiv V_p$, the set of vector fields is called $\mathcal{X}(M)$.

A 1-form is a field that takes values in the dual space to T_p, i.e. the space T_p^* of maps $\omega(p) : V_p \to F$. Equivalently, a 1-form is an element of $\mathcal{X}^*$ that reduces to the previous definition at every point p. An example of such a field is ω_f such that $\omega_f[V](p) = V_p[f]$ for some function f. The set of these fields is denoted $\Omega^1(M)$. We define the *exterior derivative* d:

$$d : \Omega^0 \to \Omega^1, \quad f \mapsto df = \omega_f, \tag{A.4}$$

and define the coordinate basis of $\Omega^1(M)$ as $\{dx^\mu \mid dx^\mu[V] = V^\mu\}$.

In coordinates

$$df = \partial_\mu f dx^\mu. \tag{A.5}$$

A $(0,k)$ tensor field is a field taking values in the tensor product $\bigotimes^k T_p^*$, i.e. maps from $\bigotimes^k T_p$ to F. This space is spanned by the elements $dx^{\mu_1} \otimes dx^{\mu_2} \otimes \cdots \otimes dx^{\mu_k}$. A k-form (or k-cochain), $\omega_k \in \Omega^k$, is a totally antisymmetric $(0,k)$ tensor field, and can be expressed in the basis $dx^{\mu_1} \wedge dx^{\mu_2} \wedge \cdots \wedge dx^{\mu_k}$, where $dx^i \wedge dx^j \equiv (dx^i \otimes dx^j - dx^i \otimes dx^j)/2$. We can extend the exterior derivative to a map between spaces of differential forms $d_k : \Omega^k \to \Omega^{k+1}$. For a k-form

$$\omega_k = \frac{1}{k!} \omega_{\mu_1 \cdots \mu_k} dx^{\mu_1} \wedge \cdots \wedge dx^{\mu_k}, \tag{A.6}$$

we have

$$d_k \omega_k = \frac{1}{k!} \partial_\nu \omega_{\mu_1 \cdots \mu_k} dx^\nu \wedge dx^{\mu_1} \wedge \cdots \wedge dx^{\mu_k}. \tag{A.7}$$

The Poincaré duality (see above) of differential forms is the isomorphism

$$\Omega^k(M) \cong \Omega^{m-k}(M). \tag{A.8}$$

We can express this isomorphism using the *Hodge star* $\star : \Omega^k \to \Omega^{m-k}$, such that

$$\star\omega = \frac{\sqrt{g}}{k!(m-k)!} \omega_{\mu_1 \cdots \mu_k} \epsilon^{\mu_1 \cdots \mu_k}_{\nu_{k+1} \cdots \nu_m} dx^{\nu_{k+1}} \wedge \cdots \wedge dx^m, \tag{A.9}$$

where g is the determinant of the metric and ϵ is the totally antisymmetric tensor.

De Rham cohomology

The *de Rham complex* is the chain complex:

$$\Omega^0 \xrightarrow{d_0} \Omega^i \xrightarrow{d_1} \cdots \xrightarrow{d_{m-2}} \Omega^{m-1} \xrightarrow{d_{m-1}} \Omega^m. \tag{A.10}$$

Since $\partial_\mu \partial_\nu = \partial_\nu \partial_\mu$, by antisymmetry $d^2 \omega_k = 0$ for any k. An *exact k-form* is one which can be written $\omega_k = d_{k-1} \lambda_{k-1}$ for some $\lambda \in \Omega^{k-1}$, i.e. $\omega_k \in \text{im } d_{k-1}$. A *closed k-form* (also called a *k-cocycle*) is one which obeys $d_k \omega_k = 0$, i.e. $\omega_k \in \ker d_k$. All exact forms are closed but not all closed forms are exact (just as, above, all boundaries have no boundary, but not all boundary-less manifolds form the boundary of a higher-dimensional manifold). We define the k^{th} *de Rham cohomology group* as

$$H^k_{\text{dR}}(M) \equiv \frac{\text{im} d_{k-1}}{\ker d_k}. \tag{A.11}$$

The identification of the quotient is $\omega_k \sim \omega_k' \iff \omega_k' = \omega_k + d\lambda_{k-1}$.

It turns out that[4] elements of H^k (equivalence classes of closed k-forms) are dual to those of H_k (equivalence classes of boundary-less k-cycles):

$$H^k_{\mathrm{dR}}(M) \cong H_k(M), \tag{A.12}$$

so that, given a basis $\{[\Sigma^j_k]\}$ of H_k, one can define the dual basis $\{[\omega^i_k]\}$ of H^k_{dR} such that

$$\int_{[\Sigma^j_k]} [\omega^i_k] \equiv \int_{\Sigma^j_k} \omega^i_k = \delta^i_j, \tag{A.13}$$

where Σ^j_k (ω^i_k) is any representative of the j^{th} homology class of k-cycles (i^{th} cohomology class of k-cocycles). The integral doesn't depend on the exact representative, since (using Stokes' theorem) $\int_{\partial N} \omega = \int_N d\omega = 0$ ($d\omega = 0$ by definition) and $\int_\Sigma d\lambda = \int_{\partial\Sigma} \lambda = 0$ ($\partial\Sigma = \emptyset$ by definition). This justifies the terminology of cochain, cocycle and so on.

Because of this duality we also have that $\dim H^k = \dim H_k = b^k$. Poincaré duality (see above) also tells us that

$$H^k_{\mathrm{dR}}(M) \cong H^{m-k}_{\mathrm{dR}}(M). \tag{A.14}$$

Note in particular that there is a unique non-trivial m-dimensional cohomology class, with a distinguished element called the *volume form* Ω, defined by

$$\int_M \Omega = \mathrm{Vol}(M). \tag{A.15}$$

The Laplacian

We can define a map $d^\dagger_k : \Omega^k \to \Omega^{k-1}$ called the *adjoint* of the operator $d^\dagger_k : \Omega^{k-1} \to \Omega^k$, such that $d^\dagger \propto \star d \star$ (the exact relationship is metric-signature dependent). This is then used to define the *Laplacian*

$$\triangle \equiv dd^\dagger + d^\dagger d. \tag{A.16}$$

A k-form satisfies $\triangle\omega = 0$ iff $d\omega = d^\dagger\omega$; ω is then called *harmonic*; the set of all such is called $Harm^k(M)$, and *Hodge's theorem* tells us that there is exactly one harmonic form in every cohomology class, so

$$H^k_{\mathrm{dR}} \cong Harm^k(M). \tag{A.17}$$

[4] On smooth manifolds.

Dolbeault cohomology

On a complex manifold (of real dimension $2n$), we have a globally well-defined mixed-index tensor called the *complex structure* I, such that in any local patch I can be put into the form

$$I = \begin{pmatrix} 0 & -1_n \\ 1_n & 0 \end{pmatrix} \tag{A.18}$$

in some coordinate system we label $\{x^i, y^j,\ i, j = 1, \ldots, n\}$.

This tensor is used to define complex coordinates $\{dz^i, d\bar{z}^{\bar{j}}\}$ on each patch, via the prescription $dz^i \equiv dx^i + I^i_j dy^j$, $d\bar{z}^{\bar{i}} \equiv dx^i - I^i_j dy^j$. We define a *holomorphic* k-form as one of the form $\omega^{i_1 \cdots i_k}_k dz^{i_1} \wedge \cdots \wedge dz^{i_k}$ (with no $d\bar{z}^{\bar{j}}$) and vice versa for antiholomorphic k-forms. A k-form with p dzs and q $d\bar{z}$s is said to have p holomorphic indices and q anti-holomorphic indices[5].

In general, it will be impossible to define a k-form globally such that it always has the same number of holomorphic and anti-holomorphic indices. If this is possible, we have a *Kähler manifold* - one where transporting any tensor around the manifold will not mix holomorphic and antiholomorphic indices[6]. In this case, we can happily decompose the space of k-forms Ω^k:

$$\Omega^k = \bigoplus_{p,q \,|\, p+q=k} \Omega^{p,q}_k, \tag{A.21}$$

where $\Omega^{p,1}$ is the space of k-forms with p holomorphic and q antiholomorphic indices. In particular, we can decompose the cohomology groups likewise, obtaining the (p, q)-graded set of *Dolbeault cohomology groups* $H^k_{p,q}$:

$$H^k = \bigoplus_{p,q \,|\, p+q=k} H^k_{p,q}. \tag{A.22}$$

The dimensions of the Dolbeault cohomology groups are called the *Hodge numbers* $h^{p,q}$. They are usually displayed in the *Hodge diamond*; for example, for $n = 3$:

[5] More technically, Dolbeault cohomology is defined using the decomposition of the exterior derivative into the *Dolbeault operators* ∂ and $\bar{\partial}$, but this is the upshot.

[6] This is true iff

$$dJ = 0, \tag{A.19}$$

where

$$J \equiv g_{i\bar{j}} dz^i d\bar{z}^{\bar{j}} \tag{A.20}$$

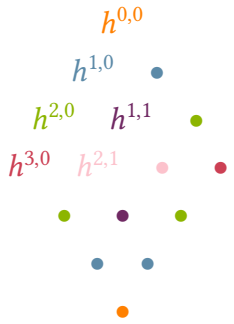
is called the *Kähler form*, and g is the metric.

$$
\begin{array}{ccccccc}
 & & & h^{0,0} & & & \\
 & & h^{1,0} & & h^{0,1} & & \\
 & h^{2,0} & & h^{1,1} & & h^{0,2} & \\
h^{3,0} & & h^{2,1} & & h^{1,2} & & h^{0,3} \\
 & h^{3,1} & & h^{2,2} & & h^{1,3} & \\
 & & h^{3,2} & & h^{2,3} & & \\
 & & & h^{3,3} & & &
\end{array}
$$

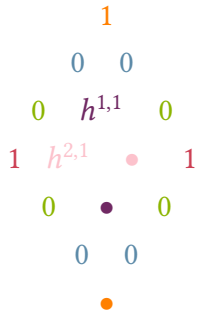
In fact, just as $b^k = b^{m-k}$, we can winnow down the independent Hodge numbers:

$$
\begin{aligned}
h^{p,q} &= h^{q,p} \\
h^{p,q} &= h^{(n-p),(n-q)},
\end{aligned}
\tag{A.23}
$$

so that what we really have is



If we specialise to the case of Calabi-Yau n-folds (Kähler manifolds of real dimension $2n$ with holonomy in $SU(n)$), we get extra relations, meaning for e.g. in the $n = 3$ case,



So for a CY threefold, there are just two independent Hodge numbers. *Yau's theorem* tells us that the metric of a CY is determined uniquely by its choice of complex structure I and its Kähler form J, which are in the threefold case given by $h^{2,1}$ complex and $h^{1,1}$ real parameters respectively.

Bibliography

[1] Gerard 't Hooft. Naturalness, chiral symmetry, and spontaneous chiral symmetry breaking. *NATO Sci. Ser. B*, 59:135–157, 1980.

[2] D.S. Gorbunov and V.A. Rubakov. *Introduction to the Theory of the Early Universe: Hot Big Bang Theory*. World Scientific, 2011.

[3] A. D. Sakharov. Violation of CP Invariance, C asymmetry, and baryon asymmetry of the universe. *Pisma Zh. Eksp. Teor. Fiz.*, 5:32–35, 1967.

[4] Gary Hinshaw, D Larson, Eiichiro Komatsu, David N Spergel, CLaa Bennett, Joanna Dunkley, MR Nolta, M Halpern, RS Hill, N Odegard, et al. Nine-year wilkinson microwave anisotropy probe (wmap) observations: cosmological parameter results. *The Astrophysical Journal Supplement Series*, 208(2):19, 2013.

[5] P. A. R. Ade et al. Planck 2015 results. XIII. Cosmological parameters. 2015.

[6] Gianfranco Bertone and Dan Hooper. History of dark matter. *Rev. Mod. Phys.*, 90(4):045002, 2018.

[7] Heinz Andernach and Fritz Zwicky. English and spanish translation of zwicky's (1933) the redshift of extragalactic nebulae. *arXiv preprint arXiv:1711.01693*, 2017.

[8] V. C. Rubin, J. Burley, A. Kiasatpoor, B. Klock, G. Pease, E. Rutscheidt, and C. Smith. Kinematic studies of early-type stars. I. Photometric survey, space motions, and comparison with radio observations. , 67:491–531, October 1962.

[9] Sloane Digital Sky Survey: Galaxy Map. https://www.sdss.org/science/orangepie/ Accessed on 29 May 2022.

[10] G. Chincarini and H. J. Rood. The Coma supercluster: analysis of Zwicky-Herzog cluster 16 in field 158. , 206:30–37, May 1976.

[11] S. A. Gregory and L. A. Thompson. The Coma/A1367 supercluster and its environs. , 222:784–799, June 1978.

[12] M. Joeveer and J. Einasto. Has the Universe the Cell Structure? In M. S. Longair and J. Einasto, editors, *Large Scale Structures in the Universe*, volume 79, page 241, January 1978.

[13] Edward W Kolb and Michael Stanley Turner. *The Early Universe*. Frontiers in Physics. Westview Press, Boulder, CO, 1990.

[14] Douglas Clowe, Maruša Bradač, Anthony H Gonzalez, Maxim Markevitch, Scott W Randall, Christine Jones, and Dennis Zaritsky. A direct empirical proof of the existence of dark matter. *The Astrophysical Journal*, 648(2):L109, 2006.

[15] Marc Schumann. Direct Detection of WIMP Dark Matter: Concepts and Status. *J. Phys. G*, 46(10):103003, 2019.

[16] Giorgio Arcadi, Oleg Lebedev, Stefan Pokorski, and Takashi Toma. Real Scalar Dark Matter: Relativistic Treatment. *JHEP*, 08:050, 2019.

[17] Lawrence J. Hall, Karsten Jedamzik, John March-Russell, and Stephen M. West. Freeze-In Production of FIMP Dark Matter. *JHEP*, 03:080, 2010.

[18] D. Spergel and P. Steinhardt. Observational evidence for selfinteracting cold dark matter. *Phys. Rev. Lett.*, 84:3760–3763, 2000.

[19] M. Markevitch and etal. Direct constraints on the dark matter self-interaction cross section from the merging galaxy cluster 1e 0657â56. *Astrophys. J.*, 606(2):819â824, May 2004.

[20] Mark Vogelsberger, Jesus Zavala, and Abraham Loeb. Subhaloes in Self-Interacting Galactic Dark Matter Haloes. *Mon. Not. Roy. Astron. Soc.*, 423:3740, 2012.

[21] Miguel Rocha, Annika H.G. Peter, James S. Bullock, Manoj Kaplinghat, Shea Garrison-Kimmel, Jose Onorbe, and Leonidas A. Moustakas. Cosmological Simulations with Self-Interacting Dark Matter I: Constant Density Cores and Substructure. *Mon. Not. Roy. Astron. Soc.*, 430:81–104, 2013.

[22] Annika H.G. Peter, Miguel Rocha, James S. Bullock, and Manoj Kaplinghat. Cosmological Simulations with Self-Interacting Dark Matter II: Halo Shapes vs. Observations. *Mon. Not. Roy. Astron. Soc.*, 430:105, 2013.

[23] Jesus Zavala, Mark Vogelsberger, and Matthew G. Walker. Constraining Self-Interacting Dark Matter with the Milky Way's dwarf spheroidals. *Mon. Not. Roy. Astron. Soc.*, 431:L20–L24, 2013.

[24] Sean Tulin, Hai-Bo Yu, and Kathryn M. Zurek. Beyond collisionless dark matter: Particle physics dynamics for dark matter halo structure. *Phys. Rev. D*, 87(11), Jun 2013.

[25] F. Kahlhoefer and etal. Colliding clusters and dark matter self-interactions. *MNRAS*, 437(3):2865â2881, Nov 2013.

[26] Scott W. Randall, Maxim Markevitch, Douglas Clowe, Anthony H. Gonzalez, and Marusa Bradac. Constraints on the Self-Interaction Cross-Section of Dark Matter from Numerical Simulations of the Merging Galaxy Cluster 1E 0657-56. *Astrophys. J.*, 679:1173–1180, 2008.

[27] Sean Tulin and Hai-Bo Yu. Dark Matter Self-interactions and Small Scale Structure. *Phys. Rept.*, 730:1–57, 2018.

[28] Sacha Davidson and Subir Sarkar. Thermalisation after inflation. *Journal of High Energy Physics*, 2000(11):012, 2000.

[29] P.A. Zyla et al. Review of Particle Physics. *PTEP*, 2020(8):083C01, 2020. and 2021 update.

[30] Ya B Zel'dovich, Lev B Okun', and S B Pikel'ner. Quarks: Astrophysical and physic-ochemical aspects. *Soviet Physics Uspekhi*, 8(5):702, 1966.

[31] Benjamin W. Lee and Steven Weinberg. Cosmological Lower Bound on Heavy Neutrino Masses. *Phys. Rev. Lett.*, 39:165–168, 1977.

[32] Giorgio Arcadi, Maíra Dutra, Pradipta Ghosh, Manfred Lindner, Yann Mambrini, Mathias Pierre, Stefano Profumo, and Farinaldo S. Queiroz. The waning of the WIMP? A review of models, searches, and constraints. *Eur. Phys. J. C*, 78(3):203, 2018.

[33] Bernard J. Carr and S. W. Hawking. Black holes in the early Universe. *Mon. Not. Roy. Astron. Soc.*, 168:399–415, 1974.

[34] S. W. Hawking. Particle Creation by Black Holes. *Commun. Math. Phys.*, 43:199–220, 1975.

[35] G. E. A. Matsas, J. C. Montero, V. Pleitez, and D. A. T. Vanzella. Dark matter: The Top of the iceberg? In *Conference on Topics in Theoretical Physics II: Festschrift for A.H. Zimerman Sao Paulo, Brazil, November 20, 1998*, 1998.

[36] Nicole F. Bell and R. R. Volkas. Mirror matter and primordial black holes. *Phys. Rev.*, D59:107301, 1999.

[37] Anne M. Green. Supersymmetry and primordial black hole abundance constraints. *Phys. Rev.*, D60:063516, 1999.

[38] M. Yu. Khlopov, Aurelien Barrau, and Julien Grain. Gravitino production by primordial black hole evaporation and constraints on the inhomogeneity of the early universe. *Class. Quant. Grav.*, 23:1875–1882, 2006.

[39] Tomohiro Fujita, Masahiro Kawasaki, Keisuke Harigaya, and Ryo Matsuda. Baryon asymmetry, dark matter, and density perturbation from primordial black holes. *Phys. Rev.*, D89(10):103501, 2014.

[40] P. C. W. Davies. Thermodynamics of Black Holes. *Proc. Roy. Soc. Lond.*, A353:499–521, 1977.

[41] Don N. Page. Particle Emission Rates from a Black Hole: Massless Particles from an Uncharged, Nonrotating Hole. *Phys. Rev.*, D13:198–206, 1976.

[42] Benjamin V Lehmann, Christian Johnson, Stefano Profumo, and Thomas Schwemberger. Direct detection of primordial black hole relics as dark matter. *Journal of Cosmology and Astroparticle Physics*, 2019(10):046, 2019.

[43] Xiaoyong Chu, Basudeb Dasgupta, and Joachim Kopp. Sterile neutrinos with secret interactions a lasting friendship with cosmology. *JCAP*, 2015(10):011â011, 2015.

[44] Celine Boehm and Richard Schaeffer. Constraints on dark matter interactions from structure formation: Damping lengths. *Astron. Astrophys.*, 438:419–442, 2005.

[45] C. Boehm et. al. Constraining dark matter candidates from structure formation. In *Dark Matter in Astro- and Particle Physics: Proceedings of the International Conference DARK 2002, Cape Town, South Africa, 4–9 February 2002*. Springer Berlin Heidelberg, 2012.

[46] Saniya Heeba, Felix Kahlhoefer, and Patrick Stöcker. Freeze-in production of decaying dark matter in five steps.

[47] Andreas Ringwald. Axions and axion-like particles. *arXiv preprint arXiv:1407.0546*, 2014.

[48] J. H. Christenson, J. W. Cronin, V. L. Fitch, and R. Turlay. Evidence for the 2π decay of the k_2^0 meson. *Phys. Rev. Lett.*, 13:138–140, Jul 1964.

[49] Shahida Dar. The neutron edm in the sm: A review. *arXiv preprint hep-ph/0008248*, 2000.

[50] R. Peccei and H. Quinn. CP Conservation in the Presence of Instantons. *Phys.Rev.Lett.*, 38:1440–1443, 1977.

[51] Steven Weinberg. A New Light Boson? *Phys.Rev.Lett.*, 40:223–226, 1978.

[52] Frank Wilczek. Problem of Strong P and T Invariance in the Presence of Instantons. *Phys.Rev.Lett.*, 40:279–282, 1978.

[53] Marc Kamionkowski and John March-Russell. Planck scale physics and the Peccei-Quinn mechanism. *Phys.Lett.B*, 282:137–141, 1992.

[54] Richard Holman, Stephen D. H. Hsu, Thomas W. Kephart, Edward W. Kolb, Richard Watkins, and Lawrence M. Widrow. Solutions to the strong CP problem in a world with gravity. *Phys.Lett.B*, 282:132–136, 1992.

[55] Stephen M. Barr and D. Seckel. Planck scale corrections to axion models. *Phys.Rev.D*, 46:539–549, 1992.

[56] Steven Giddings and Andrew Strominger. Axion Induced Topology Change in Quantum Gravity and String Theory. *Nucl.Phys.B*, 306:890–907, 1988.

[57] Tom Banks and Lance J. Dixon. Constraints on String Vacua with Space-Time Supersymmetry. *Nucl.Phys.B*, 307:93–108, 1988.

[58] Sidney Coleman and Ki-Myeong Lee. WORMHOLES MADE WITHOUT MASSLESS MATTER FIELDS. *Nucl.Phys.B*, 329:387–409, 1990.

[59] Tom Banks and Nathan Seiberg. Symmetries and strings in field theory and gravity. *Physical Review D*, 83(8):084019, 2011.

[60] Daniel Harlow and Hirosi Ooguri. Symmetries in quantum field theory and quantum gravity. *Commun.Math.Phys.*, 383(3):1669–1804, 2021.

[61] Tristan Daus, Arthur Hebecker, Sascha Leonhardt, and John March-Russell. Towards a Swampland Global Symmetry Conjecture using weak gravity. *Nucl.Phys.B*, 960:115167, 2020.

[62] Kristof Schmieden. Searches for Axion Like Particles at the LHC. Technical report, CERN, Geneva, Sep 2021.

[63] Ciaran O'Hare. cajohare/axionlimits: Axionlimits, doi.org/10.5281/zenodo.3932430, July 2020.

[64] Tom WB Kibble. Cosmic strings reborn? *arXiv preprint astro-ph/0410073*, 2004.

[65] A. Vilenkin and E. P. S. Shellard. *Cosmic Strings and Other Topological Defects*. CUP, 7 2000.

[66] T. W. B. Kibble. Topology of Cosmic Domains and Strings. *J.Phys.A*, 9:1387–1398, 1976.

[67] W. H. Zurek. Cosmological Experiments in Superfluid Helium? *Nature*, 317:505–508, 1985.

[68] A. Albrecht and N. Turok. Evolution of cosmic strings. *Phys. Rev. Lett.*, 54:1868–1871, Apr 1985.

[69] Marco Gorghetto, Edward Hardy, and Giovanni Villadoro. Axions from strings: the attractive solution. *Journal of High Energy Physics*, 2018(7):1–57, 2018.

[70] Tristan Daus, Arthur Hebecker, Sascha Leonhardt, and John March-Russell. Towards a swampland global symmetry conjecture using weak gravity. *Nuclear Physics B*, 960:115167, 2020.

[71] Takashi Hiramatsu, Masahiro Kawasaki, and Ken'ichi Saikawa. Evolution of string-wall networks and axionic domain wall problem. *Journal of Cosmology and Astroparticle Physics*, 2011(08):030, 2011.

[72] Planck Collaboration. Planck 2013 results. XXV. Searches for cosmic strings and other topological defects. , 571:A25, November 2014.

[73] Richard Lynn Davis. Cosmic Axions from Cosmic Strings. *Phys.Lett.B*, 180:225–230, 1986.

[74] Diego Harari and P. Sikivie. On the Evolution of Global Strings in the Early Universe. *Phys.Lett.B*, 195:361–365, 1987.

[75] R. A. Battye and E. P. S. Shellard. Global string radiation. *Nucl.Phys.B*, 423:260–304, 1994.

[76] Takashi Hiramatsu, Masahiro Kawasaki, Ken'ichi Saikawa, and Toyokazu Sekiguchi. Production of dark matter axions from collapse of string-wall systems. *Phys.Rev.D*, 85:105020, 2012. [Erratum: Phys.Rev.D86, 089902 (2012)].

[77] Marco Gorghetto, Edward Hardy, and Giovanni Villadoro. Axions from Strings: the Attractive Solution. *JHEP*, 07:151, 2018.

[78] M. B. Hindmarsh and T. W. B. Kibble. Cosmic strings. *Rept. Prog. Phys.*, 58:477–562, 1995.

[79] Ken'ichi Saikawa. A review of gravitational waves from cosmic domain walls. *Universe*, 3(2):40, 2017.

[80] Marco Gorghetto, Edward Hardy, and Horia Nicolaescu. Observing invisible axions with gravitational waves. *JCAP*, 06:034, 2021.

[81] Chia-Feng Chang and Yanou Cui. Gravitational Waves from Global Cosmic Strings and Cosmic Archaeology. 6 2021.

[82] Robert H. Brandenberger, Brandon Carter, Anne-Christine Davis, and Mark Trodden. Cosmic vortons and particle physics constraints. *Phys.Rev.D*, 54:6059–6071, 1996.

[83] Prateek Agrawal, Anson Hook, and Junwu Huang. A CMB Millikan experiment with cosmic axiverse strings. *JHEP*, 07:138, 2020.

[84] Hajime Fukuda, Aneesh Manohar, Hitoshi Murayama, and Ofri Telem. Axion strings are superconducting. *JHEP*, 06:052, 2021.

[85] Prateek Agrawal, Anson Hook, Junwu Huang, and Gustavo Marques-Tavares. Axion string signatures II: A cosmological plasma collider. 10 2020.

[86] Mudit Jain, Andrew J. Long, and Mustafa A. Amin. Cmb birefringence from ultralight-axion string networks. *JCAP*, 2021(05):055, May 2021.

[87] Graciela B. Gelmini, Anna Simpson, and Edoardo Vitagliano. Gravitational waves from axionlike particle cosmic string-wall networks. *Physical Review D*, 104(6), Sep 2021.

[88] Diego Harari and P. Sikivie. The Gravitational Field of a Global String. *Phys.Rev.D*, 37:3438, 1988.

[89] Jin Dai, R. G. Leigh, and Joseph Polchinski. New Connections Between String Theories. *Mod. Phys. Lett. A*, 4:2073–2083, 1989.

[90] Joseph Polchinski. Dirichlet branes and ramond-ramond charges. *Physical Review Letters*, 75(26):4724, 1995.

[91] E. Kiritsis. *String Theory in a Nutshell: Second Edition.* In a Nutshell. Princeton University Press, 2019.

[92] Tom Banks and Nathan Seiberg. Symmetries and Strings in Field Theory and Gravity. *Phys.Rev.D*, 83:084019, 2011.

[93] J. Polchinski. *String theory. Vol. 2: Superstring theory and beyond.* CUP, 12 2007.

[94] Jerome P. Gauntlett. Branes, calibrations and supergravity. *Clay Math.Proc.*, 3:79–126, 2004.

[95] Michael B. Green, John H. Schwarz, and Edward Witten. *Superstring Theory Vol. 2: 25th Anniversary Edition.* Cambridge Monographs on Mathematical Physics. Cambridge University Press, 11 2012.

[96] Asimina Arvanitaki, Savas Dimopoulos, Sergei Dubovsky, Nemanja Kaloper, and John March-Russell. String Axiverse. *Phys.Rev.D*, 81:123530, 2010.

[97] Edward Witten. Some Properties of O(32) Superstrings. *Phys.Lett.B*, 149:351–356, 1984.

[98] Peter Svrcek and Edward Witten. Axions In String Theory. *JHEP*, 06:051, 2006.

[99] Daniel J Kapner, Tessa S Cook, Eric George Adelberger, Jens H Gundlach, Blayne R Heckel, CD Hoyle, and H Erik Swanson. Tests of the gravitational inverse-square law below the dark-energy length scale. *Physical review letters*, 98(2):021101, 2007.

[100] Brian R. Greene, Alfred D. Shapere, Cumrun Vafa, and Shing-Tung Yau. Stringy Cosmic Strings and Noncompact Calabi-Yau Manifolds. *Nucl.Phys.B*, 337:1–36, 1990.

[101] Juan Garcia-Bellido, Andrei D. Linde, and David Wands. Density perturbations and black hole formation in hybrid inflation. *Phys. Rev.*, D54:6040–6058, 1996.

[102] J. H. MacGibbon and B. R. Webber. Quark and gluon jet emission from primordial black holes: The instantaneous spectra. *Phys. Rev.*, D41:3052–3079, 1990.

[103] B. J. Carr, Kazunori Kohri, Yuuiti Sendouda, and Jun'ichi Yokoyama. Constraints on primordial black holes from the Galactic gamma-ray background. *Phys. Rev.*, D94(4):044029, 2016.

[104] Norma G. Sanchez. Absorption and Emission Spectra of a Schwarzschild Black Hole. *Phys. Rev.*, D18:1030, 1978.

[105] S. W. Hawking. Black Holes From Cosmic Strings. *Phys. Lett.*, B231:237–239, 1989.

[106] Alexander Polnarev and Robert Zembowicz. Formation of Primordial Black Holes by Cosmic Strings. *Phys. Rev.*, D43:1106–1109, 1991.

[107] M. Kawasaki, Kazunori Kohri, and Naoshi Sugiyama. MeV scale reheating temperature and thermalization of neutrino background. *Phys. Rev.*, D62:023506, 2000.

[108] Karsten Jedamzik and Maxim Pospelov. Big Bang Nucleosynthesis and Particle Dark Matter. *New J. Phys.*, 11:105028, 2009.

[109] Edward W. Kolb, Daniel J. H. Chung, and Antonio Riotto. WIMPzillas! *AIP Conf. Proc.*, 484(1):91–105, 1999.

[110] Olivier Lennon, John March-Russell, Rudin Petrossian-Byrne, and Hannah Tillim. Black Hole Genesis of Dark Matter. *JCAP*, 1804(04):009, 2018.

[111] Alexander D. Dolgov and Damian Ejlli. Relic gravitational waves from light primordial black holes. *Phys. Rev.*, D84:024028, 2011.

[112] Isabel Garcia Garcia, Sven Krippendorf, and John March-Russell. The String Soundscape at Gravitational Wave Detectors. 2016.

[113] John R. Ellis, G. B. Gelmini, Jorge L. Lopez, Dimitri V. Nanopoulos, and Subir Sarkar. Astrophysical constraints on massive unstable neutral relic particles. *Nucl. Phys.*, B373:399–437, 1992.

[114] V. A. Kuzmin and V. A. Rubakov. Ultrahigh-energy cosmic rays: A Window to postinflationary reheating epoch of the universe? *Phys. Atom. Nucl.*, 61:1028, 1998.

[115] Michael Birkel and Subir Sarkar. Extremely high-energy cosmic rays from relic particle decays. *Astropart. Phys.*, 9:297–309, 1998.

[116] Daniel J. H. Chung, Edward W. Kolb, and Antonio Riotto. Superheavy dark matter. *Phys. Rev.*, D59:023501, 1999.

[117] Houri Ziaeepour. Searching the footprint of WIMPZILLAs. *Astropart. Phys.*, 16:101–120, 2001.

[118] Cyrille Barbot and Manuel Drees. Detailed analysis of the decay spectrum of a super heavy X particle. *Astropart. Phys.*, 20:5–44, 2003.

[119] Chung-Hsien Chou and Kin-Wang Ng. Decaying superheavy dark matter and subgalactic structure of the universe. *Phys. Lett.*, B594:1–7, 2004.

[120] Asimina Arvanitaki, Savas Dimopoulos, Sergei Dubovsky, Peter W. Graham, Roni Harnik, and Surjeet Rajendran. Astrophysical Probes of Unification. *Phys. Rev.*, D79:105022, 2009.

[121] Dan Hooper, Gordan Krnjaic, and Samuel D. McDermott. Dark Radiation and Superheavy Dark Matter from Black Hole Domination. *JHEP*, 08:001, 2019.

[122] Eric D. Carlson, Marie E. Machacek, and Lawrence J. Hall. Self-interacting dark matter. *Astrophys. J.*, 398:43–52, 1992.

[123] Yonit Hochberg, Eric Kuflik, Tomer Volansky, and Jay G. Wacker. Mechanism for Thermal Relic Dark Matter of Strongly Interacting Massive Particles. *Phys. Rev. Lett.*, 113:171301, 2014.

[124] Yonit Hochberg and etal. Model for thermal relic dark matter of strongly interacting massive particles. *Phys. Rev. Lett.*, 115(2), Jul 2015.

[125] D. Pappadopulo, J. Ruderman, and G. Trevisan. Dark matter freeze-out in a nonrelativistic sector. *Phys. Rev.*, D94(3):035005, 2016.

[126] M. Farina and etal. Phases of cannibal dark matter. *JHEP*, 2016(12), Dec 2016.

[127] Saniya Heeba, Felix Kahlhoefer, and Patrick Stöcker. Freeze-in production of decaying dark matter in five steps. *JCAP*, 11:048, 2018.

[128] Valentina De Romeri, Dimitrios Karamitros, Oleg Lebedev, and Takashi Toma. Neutrino dark matter and the Higgs portal: improved freeze-in analysis. 3 2020.

[129] John McDonald. Gauge singlet scalars as cold dark matter. *Phys. Rev. D*, 50:3637–3649, 1994.

[130] Lawrence J. Hall, John March-Russell, and Stephen M. West. A Unified Theory of Matter Genesis: Asymmetric Freeze-In. 10 2010.

[131] Lev A. Kofman. The Origin of matter in the universe: Reheating after inflation. 1996.

[132] Daniel J.H. Chung, Edward W. Kolb, and Antonio Riotto. Nonthermal supermassive dark matter. *Phys. Rev. Lett.*, 81:4048–4051, 1998.

[133] Christopher F. Kolda and John March-Russell. Supersymmetric D term inflation, reheating and Affleck-Dine baryogenesis. *Phys. Rev. D*, 60:023504, 1999.

[134] Philip C. Argyres, Savas Dimopoulos, and John March-Russell. Black holes and submillimeter dimensions. *Phys.Lett.B*, 441:96–104, 1998.

[135] P. Adshead, Y. Cui, and J. Shelton. Chilly Dark Sectors and Asymmetric Reheating. *JHEP*, 06:016, 2016.

[136] Yang Bai and Richard J. Hill. Weakly Interacting Stable Pions. *Phys. Rev. D*, 82:111701, 2010.

[137] Subhaditya Bhattacharya, Blaˇ zenka Melić, and Jos Wudka. Pionic Dark Matter. *JHEP*, 02:115, 2014.

[138] Graham D. Kribs and Ethan T. Neil. Review of strongly-coupled composite dark matter models and lattice simulations. *Int. J. Mod. Phys. A*, 31(22):1643004, 2016.

[139] Alon E. Faraggi and Maxim Pospelov. Selfinteracting dark matter from the hidden heterotic string sector. *Astropart. Phys.*, 16:451–461, 2002.

[140] Kimberly K. Boddy, Jonathan L. Feng, Manoj Kaplinghat, and Tim M. P. Tait. Self-Interacting Dark Matter from a Non-Abelian Hidden Sector. *Phys. Rev. D*, 89(11):115017, 2014.

[141] Isabel Garcia Garcia, Robert Lasenby, and John March-Russell. Twin Higgs WIMP Dark Matter. *Phys. Rev. D*, 92(5):055034, 2015.

[142] Amarjit Soni and Yue Zhang. Hidden SU(N) Glueball Dark Matter. *Phys. Rev. D*, 93(11):115025, 2016.

[143] Jose Luis Bernal, Licia Verde, and Adam G. Riess. The trouble with H_0. *JCAP*, 10:019, 2016.

[144] N. Aghanim et al. Planck 2018 results. VI. Cosmological parameters. 7 2018.

[145] Adam G. Riess, Stefano Casertano, Wenlong Yuan, Lucas M. Macri, and Dan Scolnic. Large Magellanic Cloud Cepheid Standards Provide a 1% Foundation for the Determination of the Hubble Constant and Stronger Evidence for Physics beyond ΛCDM. *Astrophys. J.*, 876(1):85, 2019.

[146] Sampurn Anand, Prakrut Chaubal, Arindam Mazumdar, and Subhendra Mohanty. Cosmic viscosity as a remedy for tension between PLANCK and LSS data. *JCAP*, 11:005, 2017.

[147] Christopher Dessert, Can Kilic, Cynthia Trendafilova, and Yuhsin Tsai. Addressing Astrophysical and Cosmological Problems With Secretly Asymmetric Dark Matter. *Phys. Rev. D*, 100(1):015029, 2019.

[148] Jeremy Mardon, Yasunori Nomura, and Jesse Thaler. Cosmic Signals from the Hidden Sector. *Phys. Rev. D*, 80:035013, 2009.

[149] A. Vilenkin and A. Everett. Cosmic Strings and Domain Walls in Models with Goldstone and PseudoGoldstone Bosons. *Phys.Rev.Lett.*, 48:1867–1870, 1982.

[150] Steven Giddings and Robert Myers. Spontaneous decompactification. *Phys.Rev.D*, 70:046005, 2004.

[151] Hirosi Ooguri and Cumrun Vafa. On the Geometry of the String Landscape and the Swampland. *Nucl.Phys.B*, 766:21–33, 2007.

[152] Ralph Blumenhagen, Daniel Kläwer, Lorenz Schlechter, and Florian Wolf. The Refined Swampland Distance Conjecture in Calabi-Yau Moduli Spaces. *JHEP*, 06:052, 2018.

[153] Hirosi Ooguri, Eran Palti, Gary Shiu, and Cumrun Vafa. Distance and de Sitter Conjectures on the Swampland. *Phys.Lett.B*, 788:180–184, 2019.

[154] Arthur Hebecker and Timm Wrase. The Asymptotic dS Swampland Conjecture - a Simplified Derivation and a Potential Loophole. *Fortsch.Phys.*, 67(1-2):1800097, 2019.

[155] Andrew Cohen and David Kaplan. The Exact Metric About Global Cosmic Strings. *Phys.Lett.B*, 215:67–72, 1988.

[156] Thomas Flacke, Ben Gripaios, John March-Russell, and David Maybury. Warped axions. *JHEP*, 01:061, 2007.

[157] Lisa Randall and Raman Sundrum. A Large mass hierarchy from a small extra dimension. *Phys.Rev.Lett.*, 83:3370–3373, 1999.

[158] R. Abbott et al. Constraints on Cosmic Strings Using Data from the Third Advanced LIGO–Virgo Observing Run. *Phys.Rev.Lett.*, 126(24):241102, 2021.

[159] Stefano Lanza, Fernando Marchesano, Luca Martucci, and Irene Valenzuela. Swampland conjectures for strings and membranes. *JHEP*, 2021(2), Feb 2021.

[160] Stefano Lanza, Fernando Marchesano, Luca Martucci, and Irene Valenzuela, 2021.

[161] Luis E. Ibanez and Angel M. Uranga. *String theory and particle physics: An introduction to string phenomenology*. Cambridge University Press, 2 2012.

[162] Michele Cicoli, Mark Goodsell, and Andreas Ringwald. The type IIB string axiverse and its low-energy phenomenology. *JHEP*, 10:146, 2012.

[163] Tom Rudelius. On the possibility of large axion moduli spaces. *Journal of Cosmology and Astroparticle Physics*, 2015(04):049, 2015.

[164] Cody Long, Liam McAllister, and Paul McGuirk. Heavy tails in calabi-yau moduli spaces. *Journal of High Energy Physics*, 2014(10):1–46, 2014.

[165] Frederik Denef, Michael R. Douglas, and Bogdan Florea. Building a better racetrack. *JHEP*, 06:034, 2004.

[166] Vijay Balasubramanian, Per Berglund, Joseph P. Conlon, and Fernando Quevedo. Systematics of moduli stabilisation in Calabi-Yau flux compactifications. *JHEP*, 03:007, 2005.

[167] Edmund Copeland, Robert Myers, and Joseph Polchinski. Cosmic F and D strings. *JHEP*, 06:013, 2004.

[168] Edward Witten. Superconducting Strings. *Nucl.Phys.B*, 249:557–592, 1985.

[169] Curtis Callan and Jeffrey Harvey. Anomalies and Fermion Zero Modes on Strings and Domain Walls. *Nucl.Phys.B*, 250:427–436, 1985.

[170] Aneesh Manohar. Anomalous Vortices and Electromagnetism. 2. *Phys.Lett.B*, 206:276, 1988. [Erratum: Phys.Lett. 209, 543 (1988)].

[171] Mark G. Alford, Katherine Benson, Sidney R. Coleman, John March-Russell, and Frank Wilczek. The Interactions and Excitations of Nonabelian Vortices. *Phys.Rev.Lett.*, 64:1632, 1990. [Erratum: Phys.Rev.Lett. 65, 668 (1990)].

[172] Mark G. Alford, Katherine Benson, Sidney R. Coleman, John March-Russell, and Frank Wilczek. Zero modes of nonabelian vortices. *Nucl.Phys.B*, 349:414–438, 1991.

[173] D. Cremades, L. E. Ibanez, and F. Marchesano. Yukawa couplings in intersecting D-brane models. *JHEP*, 07:038, 2003.

[174] L. E. Ibanez and A. M. Uranga. Neutrino Majorana Masses from String Theory Instanton Effects. *JHEP*, 03:052, 2007.

[175] Ralph Blumenhagen, Mirjam Cvetic, Dieter Lust, Robert Richter, and Timo Weigand. Non-perturbative Yukawa Couplings from String Instantons. *Phys.Rev.Lett.*, 100:061602, 2008.

[176] Gia Dvali and S.-H.Henry Tye. Brane inflation. *Phys.Lett.B*, 450(1-3):72–82, Mar 1999.

[177] Saswat Sarangi and S.-H.Henry Tye. Cosmic string production towards the end of brane inflation. *Phys.Lett.B*, 536(3-4):185–192, Jun 2002.

[178] Nicholas Jones, Horace Stoica, and S.-H.Henry Tye. The production, spectrum and evolution of cosmic strings in brane inflation. *Phys.Lett.B*, 563(1-2):6–14, Jun 2003.

[179] Allen Hatcher. *Algebraic topology*. Cambridge Univ. Press, Cambridge, 2000.

[180] Mikio Nakahara. *Geometry, topology and physics*. Graduate student series in physics. Hilger, Bristol, 1990.